Spring 5-2021

Development of Hybrid Ultra-High Performance Concrete Thermoplastic Composite Panels for Blast and Ballistic Protection

Alyssa M. Libby
University of Maine, alyssa.libby1@maine.edu

DEVELOPMENT OF HYBRID ULTRA-HIGH PERFORMANCE CONCRETE

THERMOPLASTIC COMPOSITE PANELS FOR BLAST

AND BALLISTIC PROTECTION

By

Alyssa M. Libby

B.S. University of Maine, 2019

A THESIS

Submitted in Partial Fulfillment of the

Requirements for the Degree of

Master of Science

(in Civil Engineering)

The Graduate School

The University of Maine

May 2021

Advisory Committee:

Eric N. Landis, Professor of Civil and Environmental Engineering, Advisor

Roberto Lopez-Anido, Professor of Civil and Environmental Engineering

Jameson Shannon, Chief, Concrete and Materials Branch, Geotechnical and Structural Laboratory, Engineer Research and Development Center

DEVELOPMENT OF HYBRID ULTRA-HIGH PERFORMANCE CONCRETE

THERMOPLASTIC COMPOSITE PANELS FOR BLAST

AND BALLISTIC PROTECTION

By Alyssa M. Libby

Thesis Advisor: Dr. Eric N. Landis

An Abstract of the Thesis Presented
in Partial Fulfillment of the Requirements for the
Degree of Master of Science
(in Civil Engineering)
May 2021

In recent years, ultra-high performance concrete (UHPC) has become a material of interest for structures needing resistance to impact and blast loadings. These types of loadings have induced brittle flexural failure in UHPC due to punching shear from the impactor. One way to improve the impact resistance, energy absorption, and ductility of UHPC is by adding fiber-reinforced polymer (FRP) skins to the front and rear faces of the concrete, resulting in a sandwich configuration. In this study, E-glass fiber-reinforced thermoplastic laminates were bonded to UHPC panels using a heated consolidation process known as stamp thermoforming. The bond between the UHPC and thermoplastic laminates was specifically of interest, so two variables, adhesive type and consolidation pressure, were investigated. The adhesives of interest were polyethylene terephthalate glycol (PETG) neat resin and ethylene acrylic acid (EAA), known by the trade name Surlyn by DuPont. PETG neat resin has been used in previous work on this project and has been proven to successfully bond thermoplastic laminates and UHPC. EAA was a new material of interest due to its reputable impact behavior and advantageous self-healing properties. Two pressures of 80 and 100 psi were used to consolidate the sandwich panels during manufacturing.

The impact resistance of the thermoplastic-reinforced UHPC panels was investigated through a combination of quasi-static and low-velocity drop weight impact tests. The bond between the UHPC and thermoplastic laminates was analyzed using both three-point bending tests and direct single-lap shear tests. Preliminary results from these tests showed that EAA performed better under impact and produced a stronger bond between UHPC and the thermoplastic laminates than the PETG neat resin. A consolidation pressure of 100 psi was shown to produce a stronger bond than one of 80 psi. More work must be performed to enhance the impact resistance of the thermoplastic-reinforced UHPC sandwich panels and the bond between UHPC and thermoplastic laminates.

ACKNOWLEDGEMENTS

Foremost, I would like to express my sincere gratitude to my advisor, Eric Landis, for his continuous support not only throughout my graduate studies, but also throughout my undergraduate career. Without his guidance and persistent help, this dissertation would not have been possible. I would also like to thank my committee members, Roberto Lopez-Anido and Jameson Shannon, for their time and involvement in this project.

I would especially like to thank the U.S. Army Engineer Research and Development Center (ERDC) for providing the funding for this study under a contract with the Advanced Structures and Composites Center (ASCC). In addition to financial support, I would like to thank everyone at ERDC for welcoming me when I visited their facility and for being so willing to help me with this project. I would specifically like to thank Todd Rushing and Jedadiah Burroughs for helping me batch UHPC and fabricate some of the concrete panels used in this study.

I would also like to thank the staff at the ASCC for their help with various aspects of this project. Specifically, I would like to thank Cody Sheltra for his active involvement on this project. This work would have been possible without his assistance. I would also like to thank Bill Yori for his help with the thermoplastic laminates used in this study, Walter Morris for his waterjet expertise, and Tom Snape for working with me to develop fixtures for testing.

I also owe a special thank you to fellow graduate students, J.J. Hollstein and Justin Harris, for their help with UHPC batching and material testing. Their company in the lab made onerous tasks much more enjoyable.

Lastly, I would like to thank my family and friends for supporting me and encouraging me to follow my dreams.

TABLE OF CONTENTS

LIST OF TABLES

LIST OF FIGURES

LIST OF ABBREVIATIONS

LIST OF EQUATIONS

CHAPTER 1

INTRODUCTION

Ultra-high-performance concrete (UHPC) has become widely popular in the infrastructure industry in recent decades. The material was first used by the U.S. Army Corps of Engineers in the 1980s and became commercially available in the U.S. in 2000. UHPC is known for its advantageous qualities such as high flexural and compressive strength, durability, and long-term stability compared to conventional concrete. Its high strength and durability can be attributed to the use of densely packed materials combined with small particle size, creating a homogenous and nearly impermeable matrix.

Penetration tests performed in recent decades showed that increasing concrete compressive strength resulted in a decrease of projectile penetration depths (O'Neil, et al., 1999), making UHPC an attractive building material for protective structures needing resistance to impact, blast, and other explosive loadings. The addition of steel fibers increases the appeal of UHPC for these types of structures, as fibers have been shown to decrease the brittleness effect of UHPC and increase resistance against punching action on the front face of an element during impact (Dancygier & Yankelevsky, 1996). Steel fibers enhance the cracking resistance of UHPC through the phenomenon of fiber bridging (Verma, et al., 2016).

Internal steel fiber reinforcement has been shown to reduce brittle failure of UHPC, but it does not eliminate it. In addition to internal fibers, external reinforcement sheets can be added to UHPC cores to increase the element’s flexural strength and improve its resistance to impact. In recent years, two major types of concrete external reinforcement have been investigated: steel plates and fiber-reinforced polymer (FRP) plates. A popular construction that utilizes this type of reinforcement is a sandwich panel system, in which stiff plates are adhesively bonded to both faces of a concrete core. Sandwich panel setups have been shown to significantly improve the impact behavior of UHPC by shear plugging and seizing the concrete debris on the rear face and by providing added resistance on the rear face, which in turn decreases residual velocity and penetration of the projectile (Feng, et al., 2020).

Both steel and FRP plates significantly increase concrete's resistance to impact. However, FRP holds many advantages over steel including its high stiffness to weight ratio, high strength to weight ratio, and structural tailorability. Strength and stiffness of an FRP laminate can be altered by adjusting the stacking sequence of the laminate, as the impact resistance of composite materials is greatly dependent on the order in which the laminas are stacked (Cantwell & Morton, 1991; J. Morton, 1989). Because of these advantages, FRP laminates were chosen as the external reinforcement in this research.

1.1 Objective

The main objective of this study was to increase the impact resistance of UHPC using externally-bonded thermoplastic composite laminate reinforcement. Literature showed that the weakest component of concrete-FRP systems is the bond between the two materials. Therefore, a main goal of this research was to perform a sensitivity study on the bond between UHPC and thermoplastic composite laminates. Two important factors that affect the concrete-FRP bond were of interest including adhesive type and consolidation pressure. The adhesives and consolidation pressures were explored to determine how they affect the impact behavior of the UHPC-thermoplastic system.

1.2 Organization

This thesis is organized in order of the research, design, manufacturing, and mechanical testing processes of the thermoplastic-composite reinforced UHPC panels. An extensive literature review was first conducted on four main topics: impact resistance of UHPC, impact resistance of composite laminates, impact resistance of sandwich composites, and the background of the concrete-FRP bond. The details of this literature review are in Chapter 2. The next step in the development process was the design and manufacturing of the thermoplastic-reinforced UHPC sandwich panels, discussed in Chapter

3. This chapter includes material selection and specimen fabrication. Mechanical testing begins in Chapter 4, in which the thermoplastic-UHPC sandwich panels were tested in low-velocity impact. The next step in the development process was characterizing the bond between thermoplastic laminates and UHPC, as discussed in Chapter 5. This section discusses both three-point bending tests and direct single-lap shear tests to assess the bond. Recommendations for future work is found in Chapter 6.

CHAPTER 2

LITERATURE REVIEW

To improve the impact behavior of the thermoplastic laminate-UHPC sandwich panels, an in depth literature review was necessary to understand how the materials respond to impact loadings. It was also important to understand the behavior of the bond between concrete and FRP. This chapter presents the findings of the literature review for four major subjects: impact resistance of UHPC, impact resistance of thermoplastic laminates, impact resistance of sandwich composites, and the background of the concrete-FRP bond.

2.1 Impact Resistance of UHPC

Since UHPC is an attractive material for protective structures, many studies exist involving impact tests on the material. Two types of impact loadings are investigated in the literature when it comes to UHPC: low-velocity impact and high-velocity impact. Low-velocity impact consists of a low projectile velocity and a high projectile mass. Low-velocity impact occurs at velocities below 10 m/s (Safri, et al., 2014). An example of low velocity impact is flying waterborne or windborne debris. Under low-velocity impact, the time of contact between the target and projectile is relatively long, resulting in a response of the entire structure. Kinetic energy is transferred to points far from the point of impact, causing a large area of delamination and reduction of residual strength (Cantwell & Morton, 1989). Contrarily, high-velocity impact consists of a high projectile velocity and a low projectile mass. High velocity impact occurs at velocities ranging from 50 m/s to 1000 m/s (Safri, et al., 2014). The most common example of high velocity impact is ballistics. High-velocity impact creates a more localized damage, resulting in energy dissipation over a smaller region and a smaller area of delamination (Cantwell, 1988).

A prevalent theme found in the literature was UHPC's superiority over normal strength concrete under impact. Due to its high strength and high fiber content, UHPC is capable of dissipating large amounts of energy at very large stress rates (Bindiganavile, et al., 2002). UHPC has been shown to reduce projectile depth, spallation, and cracking under impact when compared to normal strength concrete (Resnyansky & Weckert, 2009). Nevertheless, like normal-strength concrete, unreinforced UHPC is a brittle material and can experience brittle failure under impact loadings. UHPC's brittleness can be minimized by the addition of fibers, which enhance its tensile strength, ductility, and cracking resistance (Verma, et al., 2016; Jamnam, et al., 2020; Carey, et al., 2020). Literature showed that the proportion of fibers within the UHPC matrix has a direct effect on the compressive behavior of the material. Most studies have found that the addition of fibers had significant effects on compressive strength and resistance to failure, in which fibers were shown to provide a 50% or greater increase in compressive strength (Ibrahim, et al., 2017; Wang & Gao, 2016). Other studies have found that the addition of fibers had little effect on compressive strength, only increasing it by 10% or less (Alsalman, et al., 2017; Hoang & Fehling, 2017). It is important to note that increasing fiber content past a certain point could have an unfavorable effect on UHPC compressive strength. Meng and Khayt reported a decrease in UHPC compressive strength when the fiber content exceeded 3% volume (Meng & Khayat, 2018). The cause of this was assumed to be the clustering of fibers and entrapped air. Dingquiang et al. showed that fiber volume fractions greater than 2% decreased packing density of UHPC (Dingqiang, et al., 2021), which in turn decreases compressive strength. Literature also showed that the proportion of fibers has a substantial effect on the low-velocity impact behavior of UHPC. Increasing fiber content reduces concrete crack width due to the fibers' ability to bridge and arrest these cracks. It also increases the amount of cracks the UHPC can withstand before failure (Othman & Marzouk, 2016). This was shown through a series of flexural tests performed on ultra-high performance fiber-reinforced concrete (UHPFRC) beams with varying fiber contents. The UHPFRC beams experienced a 14% and 30% increase in peak flexural load for fiber volume fractions of 1% and 2%, respectively, compared to that of UHPFRC with a 0% fiber volume fraction (Cao, et al., 2019).

The literature grouped the local damage of UHPC under impact into five major categories: penetration, spalling, scabbing, radial cracking, and perforation. Penetration occurs when a projectile enters the front face of a target without exiting through the back face. Scabbing and spalling occur when fragments of the specimen fall off the front and back face of a target, respectively. Radial cracking is described by cracks that propagate from the point of impact towards the edges of the specimen. The most catastrophic local damage is perforation, which occurs when a projectile exits the specimen with residual velocity (Sukontasukkul, et al., 2002).

Failure patterns of UHPC have been shown to vary depending on the impact energy of a projectile. A recent study performed impact tests on UHPC beams at varying impact energies of 6.7, 33.5, and 67 J (Yao, et al., 2021). A “rebound” phenomenon was shown for impact energies of 6.7 and 33.5 J, which is caused by the release of elastic energy stored during impact. The rebound phenomenon was determined by a large decrease in specimen deflection at the end of the impact. No visible cracks were seen for the 6.7 J impact and only subtle cracks were seen for the 33.5 J impact. Partial crack closing was observed for the 33.5 J impact which can be attributed to fiber bridging and elastic deformation of the fibers. The largest impact energy of 67 J was shown to propagate a crack significantly faster, indicating energy release. The specimens tested at 67 J experienced complete fiber pullout and did not experience the rebound phenomena like the specimens tested at the lower impact energies. As shown in this study, the type of local damage experienced by a UHPC specimen is heavily influenced by the impact energy, which is directly correlated to the impact velocity.

Under low velocity impact, UHPC has shown to exhibit flexural failure (Jia, et al., 2021; Verma, et al., 2016; Yao, et al., 2021). When a striker impacts a UHPC specimen, the impact region experiences compression while the distal region experiences tension, known as the wave phenomenon. Compressive waves generated by the projectile propagate from the top face of the specimen to the bottom face, and when these waves are reflected, tensile waves are induced at the bottom of the specimen. These tensile waves catalyze cracking in concrete specimens that ultimately lead to failure. The flexural damage distribution of UHPC has been shown in the literature through low-velocity impact testing on both beams and thin panels. Low-velocity impact tests were conducted on simply supported UHPC beam specimens under multiple impacts to observe the failure in steps. After the first impact, concrete scabbing occurred on the top surface, and a flexural crack propagated from the bottom of the beam directly under the load head. After the second and third impacts, the scabbing area increased significantly, and the flexural crack enlarged and propagated closer to the top face of the beam. Fibers played an important role in bridging the cracks to resist global failure of the specimen during these impacts. The fourth impact resulted in complete failure of the beam, as it separated into two pieces with fiber pullout at the crack surface (Cao, et al., 2020). This study showed a ductile performance of UHPC, as the internal fibers were able to arrest the cracks due to impact and prolong global failure of the specimen. Similar ductile failure modes were seen in another impact study that tested UHPC beams under various impact energies. The smallest impact energies induced fine flexural cracks within the beam which were arrested by the fiber bridging phenomena. At the highest energy, the UHPC beam experienced localized failure, collapse, and complete fiber pullout (Yao, et al., 2021). The ductile performance of UHPC has also been seen in the low-velocity impact testing of thin UHPC panels. Under repeated low-velocity impacts, UHPC panels showed no significant spalling or scabbing and all panels reached the target cumulative residual displacement limit (Othman & Marzouk, 2016).

An interesting study by Ranade et al. did not demonstrate a ductile performance of UHPC. Drop weight impact tests were performed on Cor-Tuf, a type of UHPC developed by the U.S. Army Corps of Engineers. Thin Cor-Tuf slabs failed well before 20 impacts and exhibited quasi-brittle flexural and shear failures compared to high-strength, high-ductility concrete (HSHDC) slabs that survived 20 impacts. Large localized cracking and substantial spalling was seen within the Cor-Tuf panels, and premature punching shear failure was observed as the loading head of the impactor was reduced (Ranade, et al., 2017). This study suggests that in addition to internal fibers, other forms of reinforcement may be needed to increase the flexural strength and ensure a ductile failure of UHPC under impact. This conclusion was crucial in the development of the UHPC thermoplastic laminate sandwich panels and signified the importance of adding external FRP skins to the UHPC to avoid brittle failure.

It is important to acknowledge the difference of damage patterns in UHPC between low-velocity impact tests and high-velocity impact tests. As mentioned previously, low-velocity impact induces a more globalized damage pattern while high-velocity impact induces a more localized damage pattern. High-velocity impact tests have been performed on UHPC concrete slabs to analyze damage distribution. The overall damage pattern is characterized by a penetration borehole on the front face of the specimen, including a frontal crater and a following tunnel. In most cases, craters and/or spalling is seen on the rear face. Resnyansky and Weckert performed high-velocity impact tests on UHPC to observe its impact resistance. A shaped charge jet was fired against the concrete targets. Failure patterns of the UHPC panels included a borehole on the front face, cracking, and very minimal back spalling. No radial cracking occurred from the impact point, and the damage area was relatively small (Resnyansky & Weckert, 2009). This damage pattern differs greatly from those seen in the low-velocity impact tests where radial cracking and large damage areas have been observed.

Like low-velocity impact, several studies showed that high-velocity impact behavior was affected by the proportion of steel fibers in the UHPC. The addition of steel fibers was shown to decrease the damage area under high-velocity impact by increasing energy absorption of UHPC (Dancygier, et al., 2007; Jamnam, et al., 2020). Yu et al. found that hooked fibers were the most effective in improving UHPC capacity under high-velocity impact, as they increase the force needed to achieve fiber pullout (Yu, et al., 2016). Literature noted that optimization of the proportion of steel fibers can lead to improved high-velocity impact behavior.

Because UHPC is used for military purposes, this material is often subject to blast and other explosive loadings in addition to low-velocity and high-velocity impact loadings. A main concern for materials under blast loadings is the shrapnel effect, defined by fragments of a bomb, shell, or other objects in flight due to an explosion. Shrapnel can cause severe injury to people behind a concrete barrier, for example. Normal strength concrete does a poor job at reducing the shrapnel effect, as it does not absorb enough energy to prevent creation of shrapnel. UHPC however greatly reduces the shrapnel effect due to its high energy absorption and therefore is an attractive material for structures needing resistance to blast loadings. Researchers have found that UHPC resists blast explosions without or with very minimal fragmentation from the back specimen face and greatly reduces the shrapnel effect (University of Liverpool, 2009; Barnett, et al., 2010).

The information obtained in this literature review greatly influenced the development process of the thermoplastic-reinforced UHPC sandwich panels. Because low-velocity impact tests induce a global damage distribution, these tests are most commonly used to study and characterize the fundamental failure mechanisms of UHPC. Low-velocity impact tests are also much simpler to carry out in a laboratory setting due to the availability of equipment and a higher level of safety. For these reasons, low-velocity impact tests were chosen over high-velocity impact tests or blast tests for this study. The literature review also revealed that fiber-reinforced UHPC can exhibit quasi-brittle failure, as shown in the study by Ranade et al. To combat this issue, external thermoplastic skins were chosen to further reinforce UHPC under impact in this study.

2.2 Impact Resistance of Composite Laminates

To improve the impact resistance of the thermoplastic-reinforced UHPC system, it was important to understand how the composite laminates alone behave under impact. Literature showed that composite materials offer many advantages over conventional materials including great formability, light weight, high mechanical strength, high resistance to corrosion, and recyclability. Conventional fiber-reinforced composite laminates can however be highly susceptible to impact damage, and this damage can significantly decrease the strength and stiffness of a composite structure. A variety of factors have been shown to affect the impact behavior of composite laminates, including fiber type, resin type, layup thickness, loading velocity, and projectile type (Abrte, 2005).

A composite laminate's resistance to impact damage is highly dependent on the material makeup of the composite, including its fiber and matrix. Many studies have been performed to investigate the role of the fiber, matrix, and fiber-matrix interface in the impact resistance of a composite. High-strain fibers have been found to absorb a larger amount of strain energy, which is beneficial for residual properties of the laminate (Cantwell, et al., 1986). The impact energy required to initiate damage in composites with high-strain fibers was found to be twice that in composites with high-strength fibers (Cantwell, et al., 1986). Tough matrices have also shown to have a higher resistance to impact. Morton demonstrated that a tougher thermoplastic carbon fiber composite exhibited a higher compressive strength and less damage post-impact than other epoxy-based composites (Morton, 1989). This is consistent with a study by Vieille, who found that a carbon thermoplastic laminate experienced less delamination than a softer carbon epoxy-based laminate. Carbon thermoplastic laminates were shown to reduce the amount of damage, confirming that a tougher matrix can lead to better impact performance (Vieille, et al., 2013).

Literature showed that one of the most important factors affecting the impact behavior of composite laminates is fiber stacking sequence. It has been proven that impact resistance of composite materials is directly affected by how the plies are stacked (Cantwell & Morton, 1991). Unidirectional laminates with fibers orientated in one direction are extremely weak in the transverse direction and typically fail at low energies through matrix cracking, fiber breaking, and fiber-matrix debonding (Sya, et al., 2018). The brittle failure mode of unidirectional laminates makes them unsuitable for impact loadings. By orientating fibers in various directions, stiffness and strength of the composite laminate are enhanced. Multidirectional composites have also been found to be more flexible than unidirectional composites, allowing them to dissipate more energy elastically. Cantwell and Morton conducted a review on the impact response of composite laminates in which they analyzed the effect of fiber orientation on composite impact behavior (Cantwell & Morton, 1991). In their review, it was shown that plies orientated at [+/- 45°] offered superior impact resistance and improved residual strengths. Plies at [+/- 45°] were seen to protect load bearing plies orientated at 0° from a projectile. The review discussed work by Stevanovic et al. who conducted a series of impact tests on multidirectional carbon fiber composites and demonstrated that plies orientated at [+/-45°] absorbed significantly more energy than plies orientated at [0/90°], [0°, +/-45°], and [0°, 90°, +/-45°] (Stevanović, et al., 1987). The review by Cantwell and Morton also discussed work performed by Liu, in which the level of delamination was predicted based on fiber orientation. It was found that a greater level of delamination occurred between plies with a greater change in fiber orientation. For example, it was predicted that greater delamination would occur between [0°, 90°] plies than between [0°, 45°] plies (Liu, 1988). This was confirmed by a study that tested the impact resistance of composites with various stacking sequences. The study showed that laminates with an orientation of [0, 90, +/- 45]s had a greater delaminated area than those with an orientation of [0, 45, 90, -45]s (Hongkarnjanakul, et al., 2013). A greater delamination area indicates a greater amount of energy dissipated (Jalalvand, et al., 2016), so it can be inferred that the [0, 90, +/-45] laminate dissipated more energy. Another study further confirmed this claim, showing that quasi-isotropic laminates had a greater energy dissipation than cross-pry laminates (Strait, et al., 1992). These studies influenced the design decision to orientate the reinforcing laminate at [0, 90, -/+ 45]s.

Another important factor affecting the impact response of FRP laminates is the loading velocity. Cantwell and Morton performed a study on the comparison of low- and high-velocity impact response of composite laminates. Low-velocity impact tests were conducted using a conventional drop tower, and high-velocity impact tests were conducted using a nitrogen gas gun. An eight-layer [$0°_2$, +/-45°]s laminate was used for both tests. In low-velocity impact, the laminate failed in flexure, as the tensile stresses on the dismal face of the composite exceeded the ultimate failure stress of the fibers. As impact energy increased, the laminate failed in matrix cracking, delamination, and fiber fracture throughout the thickness of the laminate. Cracking and delamination propagated to points well away from the area of impact. At the highest impact energy, the laminate was penetrated by the impactor, resulting in perforation fracture of the composite. In high-velocity impact loading, initial matrix cracking occurred at a lower impact energy than low-velocity impact. As impact energy increased, the composite experienced spalling on the dismal surface of the laminate. Complete penetration by the target occurred at a higher energy than low-velocity impact and similarly resulted in a conically-shaped shear zone around the area of impact. Similar amounts of fiber damage were seen to that of low-velocity impact, however, the level of delamination was much greater for high-velocity impact. A significant conclusion from this study was that high-velocity impact loading creates a more localized target response, where energy is dissipated over a small zone. Oppositely, low-velocity impact induces an overall target response, where energy is dissipated at points well away from the target zone (Cantwell & Morton, 1989). For both types of loading velocities, high energy absorption is an important and necessary quality of a composite laminate under impact. Therefore, the laminate used to protect the UHPC core in this research was designed to have a high energy absorption capacity.

2.3 Impact Resistance of Sandwich Panels

Composite sandwich construction consists of a light core material sandwiched between two stiff skins and offers a favorable solution to types of applications where high strength, stiffness, and energy absorption capacity is needed, such as in military structures. Because of these favorable qualities, a sandwich configuration was ideal for increasing the impact resistance of UHPC in this study. Types of sandwich composites most investigated in the literature include thin face sheets on foam or aluminum honeycomb cores, as these configurations are widely popular in the aerospace industry. The two most common sandwich composites for use in protective structures are concrete cores reinforced with thin steel plates or FRP skins. For this study, it was important to understand how these hybrid systems respond to impact loads.

The literature provided a plethora of information on steel and concrete sandwich configurations. The effect of steel face sheets on the response of concrete panels under impact was investigated in a study by Abdel-Kader and Fouda (Abdel-Kader & Fouda, 2014). The following panel setups were tested: concrete panels with no external steel reinforcement, concrete panels with a steel skin only on the front face, concrete panels with a steel skin only on the rear face, and concrete panels with steel skins on both the front and rear faces. Major observations for concrete panels with reinforcement only on the front face included perforation on the front face and scabbing on the rear face. There was a 17% improvement of specimen perforation with the addition of the front steel skin. Panels with steel skins on the rear face showed perforation on the front face but no scabbing on the rear face. The presence of the rear steel skin improved perforation resistance by more than 36%. The panels with steel skins on both faces showed minimal perforation with no scabbing on the rear face. This study revealed that adding a reinforcing skin only on the back face increases impact resistance of UHPC more so than adding a reinforcing skin only on the front face, but the impact resistance of UHPC can be most improved by adding reinforcing skins to both faces.

Limited studies have been conducted on FRP and concrete sandwich systems. However, many have been performed on foam cores sandwiched between FRP skins. Similar failure modes in these FRP sandwich composites were seen compared to those in steel-concrete sandwich composites. In a study by Aryal et al., Nomex cores were sandwiched by FRP composite laminates and tested under low-velocity impact. The local damage included perforation and rupture of the FRP skin and crushing of the core. The front skin was found to slow down the projectile and resist considerably less load than the rear skin. The load resisted by the rear skin was greater than that of the front skin for all tested specimens. It was inferred from load-displacement plots that the impactor is slowed down by resistance of the front skin, resulting in an increase in force. This increase in force must then be dissipated by the rear face sheet (Aryal., et al., 2019). Similar damage patterns were shown in a study by Villanueva and Cantwell, where aluminum foam cores sandwiched between plastic composite laminates were tested under impact. The top skin was seen to exhibit fiber breakage, perforation of the impactor, and fiber-matrix delamination. The aluminum foam core experienced crushing, and the rear composite skin experienced fiber fracture and delamination. These sandwich systems exhibited numerous energy absorption mechanisms such as fiber-matrix delamination, longitudinal splitting, and fiber fracture in the composite skins. Impact testing revealed that these sandwich systems are capable of withstanding perforation energies of about 23% higher than their individual composite constituents (Villanueva & Cantwell, 2004).

An interesting study was conducted to explore the effect of external E-glass/epoxy FRP skins on the impact resistance of ceramic tiles. Four tile configurations were tested including a bare ceramic tile, a ceramic tile reinforced only on the front face, a ceramic tile reinforced only on the rear face, and a ceramic tile reinforced on both the front and rear faces. The bare ceramic tiles experienced brittle failure and fragmentation under impact, similar to UHPC. The addition of FRP reinforcement to the front face improved the ballistic efficiency by 23%, and the addition of FRP reinforcement to the back face delayed rear laminate displacement by about 25 microseconds (Sarva, et al., 2007). This study showed that a thin membrane restraint can help confine pulverized debris of brittle materials and increase their impact resistance. This information was helpful to determine how externally bonded face sheets can increase the flexural strength of brittle materials, such as UHPC.

Various production methods exist to bond FRP skins to the core material. The three methods that are most common in the literature include adhesive bonding, wet layup, and vacuum infusion (Manalo, et al., 2017). Adhesive bonding is the most conventional bonding method, where the FRP skin is bonded to the concrete using an adhesive layer. Pressure is applied to the sandwich system using weights or a hydraulic press to adhere the materials (Manalo, et al., 2017; Kulpa & Siwowski, 2019). Wet layup is also a common bonding method in which dry fibers are infused with resin and laid out on the core. The wet layup is performed by hand or using the spray-up method (Manalo, et al., 2017; Mosallam, 2016). Vacuum infusion is another common bonding process, where the dry laminates and core are placed in a vacuum bag and infused with resin. This method has shown to only introduce the minimum amount of resin, and is not well suited for small composite specimens (Manalo, et al., 2017).

Vacuum infusion and adhesive bonding through stamp thermoforming have been used in previous work on this project in an attempt to bond thermoplastic laminates to UHPC cores. Vacuum infusion was shown to be extremely labor intensive and created some manufacturing issues. Problems arose due to vacuum leaks in the bag and difficult removal of the concrete specimens after infusion. Vacuum infusion did not provide significant advantages in specimen impact strength compared to stamp thermoforming (Gillis, 2018), and therefore, this manufacturing method was not used in this study. Adhesive bonding through a stamp thermoforming process was selected as the bonding mechanism for this work.

There were two main goals for this study. The first goal was to prevent quasi-brittle failure of UHPC under impact, as seen in the experiments by Ranade et al. The second goal was to prevent the shrapnel effect of UHPC under impact loadings, as discussed in Section 2.1. This literature review showed that both steel and FRP thin plates improve impact behavior of brittle materials by increasing their flexural strength and energy absorption capacity, making them ideal external reinforcement for UHPC. The literature review also showed the importance of an external rear skin in preventing the shrapnel effect by decreasing the amount of scabbing on the rear face of the UHPC core.

2.4 Concrete-FRP Bond Background

The concrete to FRP bond is known as the weak link in a concrete-FRP system. A poorly bonded FRP-reinforced element will likely result in premature debonding, causing failure at load capacities lesser than for which it was designed (Karbhari & Ghosh, 2009). In order to improve the impact behavior of the thermoplastic-UHPC sandwich system, it was extremely important to know how the bond behaves, what affects the bond, and how the bond can be enhanced. Many studies exist in the literature on externally bonding FRP to concrete, as this has become a widely used method of strengthening and retrofitting concrete structures in the last few decades. The addition of FRP reinforcement greatly increases concrete strength. Stresses in the concrete are transferred to the different layers of the FRP skin, allowing the hybrid composite to take on a high load capacity.

The bond behavior depends on a variety of factors including type of loading, thickness and stiffness of the composite laminate, adhesive type and thickness, surface preparation of the concrete, environmental conditions, etc. (Lorenzis, et al., 2001). This research will focus on two variables that directly affect the concrete-FRP bond, including adhesive type and consolidation/bonding pressure.

Literature review showed that surface preparation of the concrete specimen has been proven to directly affect the average bond strength of FRP and concrete (Lorenzis, et al., 2001) and may be one of the most important factors affecting the performance of the bond. Surface preparation removes laitance and residue, opens voids, and roughens the concrete surface (American Concrete Institute, 2012). Common surface preparation methods include sandblasting, grinding, and using high pressure water. Almost all surface preparation techniques have been proven to increase bond strength between FRP and concrete (Toutanji & Ortiz, 2001). Chajes et al. conducted a study to compare the effectiveness of different surface preparation procedures on the bond strength of concrete and FRP. It was found that from the following procedures: no surface preparation, grinding with a stone wheel, and mechanically abrading with a wire wheel, mechanically abrading was most effective (Chajes, et al., 1996). For this research, the concrete surfaces were mechanically grinded using a 4-inch wire diamond wheel.

The type of adhesive used to bond the FRP to the concrete has also been seen to have a direct effect on the bond strength. Adhesives are categorized by their elastic moduli as soft, normal, or stiff. Shi et al. explored how properties of the adhesive affect the bond strength between concrete and FRP. In the study, an adhesive with an elastic modulus below 2.0 GPa was considered soft, an adhesive with an elastic modulus between 2.0-4.0 GPa was considered normal, and an adhesive with an elastic modulus greater than 4.0 GPa was considered stiff (Shi, et al., 2019). Stiff adhesives have been thought to be superior since they transfer interfacial stresses more efficiently (Saadatmanesh & Ehsani, 1990). However, stiff adhesives have actually been seen to cause FRP debonding at lower stress levels and lower bond capacities. Contrarily, adhesives with a lower elastic moduli, categorized as soft and normal adhesives, have been shown to delay FRP debonding (Harries, et al., 2007). Harmon et al. performed an FRP-to-concrete bond characterization study in which a stiff and a flexible adhesive were used. The study showed that the more flexible adhesive created a larger bond transfer zone in the beam specimen and resulted in a load at failure twice as high as the stiff adhesive (Harmon, et al., 2003). These conclusions were considered when developing the thermoplastic-reinforced UHPC sandwich panels. Two adhesives with varying elastic moduli were used in this research to further explore the effect of adhesive type on concrete-FRP bond strength.

The major failure mode of FRP-strengthened concrete is debonding of the FRP from the concrete. Debonding in concrete-FRP systems occurs in areas with high stress concentrations and is usually associated with discontinuities in the material and cracking along the interfaces. Debonding can occur at the concrete-adhesive interface or the adhesive-FRP interface and can cause a substantial decrease in the member capacity, leading to premature failure. Only about 30% of the FRP strength can be utilized once FRP debonding occurs (Zhou, et al., 2013; Mukhtar & Faysal, 2018).

UHPC exhibits a flexural behavior when loaded in impact (Yao, et al., 2021; Ranade, et al., 2017). Therefore, further review was performed to explore debonding of FRP from concrete when tested in bending. The fundamental debonding mechanisms under flexural loading can be categorized as: FRP debonding from a flexural-shear crack, FRP debonding from a flexural crack, FRP debonding from the plate end, and plate end shear failure (Büyüköztürk & Yu, 2006). These debonding mechanisms will be considered when observing the failure modes of the thermoplastic-reinforced UHPC sandwich specimens.

2.4.1 Bond Tests

A main objective of this study was to improve the bond between composite laminates and UHPC. Therefore, it was important know the types of concrete-FRP bond tests that currently exist. A literature review was conducted on concrete-FRP bond tests. The literature categorized these tests into five major groups: single-lap shear, double-lap shear, bending, direct tension, and mixed-mode loading (Mukhtar & Faysal, 2018). The following sections describe the various test types. The information obtained from this literature review was used to select the most appropriate concrete-FRP bond test method for this study.

2.4.1.1 Single-Lap Shear

Single-lap shear tests are the most popular method to test the concrete-FRP bond and have been utilized to test the bond in pure shear. In typical single-lap shear tests, an FRP strip is bonded to a concrete block so that it overhangs the concrete. The specimen is anchored in a material testing system and an axial tensile load is applied to the FRP, producing direct shear between the concrete and FRP. A measurement of shear stress along the bond line is then easily acquirable. Many researchers have performed direct single-lap shear tests to characterize the concrete-FRP bond. (Zhang, et al., 2020; Santandrea, et al., 2020; Hadigheh, et al., 2012). Specimen failure is most commonly caused by various debonding modes including debonding at the adhesive-concrete interface and debonding at the adhesive-FRP interface. As a result, the condition of the concrete bonding surface and preparation of the concrete surface is extremely important in single-lap shear tests.

2.4.1.2 Double-Lap Shear

Double-lap shear tests have been conducted by many researchers to test the concrete-FRP bond (Zheng, et al., 2015; Yang & Li, 2019). Double-lap shear tests are similar to single-lap shear tests in which the concrete-FRP bond is tested in pure shear. Double-lap shear tests however consist of two bonded areas of concrete and FRP. Typical double-lap shear specimens are fabricated by casting two identical concrete blocks in a mold with a threaded rod in the center. A strip of FRP is bonded to two opposite sides of the specimen. The specimen is gripped by the rod in a material testing machine and loaded in uniaxial tension. Like single-lap shear tests, the shear stress along the bond line can easily be calculated.

2.4.1.3 Bending Test

Another popular approach is to test the concrete-FRP bond in either three or four-point bending (Jia, et al., 2021; Gartner, 2007). Literature showed that these tests are utilized to examine the bond of FRP and concrete due to their simplicity and because they provide a more realistic behavior of the bond when subjected to flexural loads. The tests consist of concrete beams with an externally-bonded FRP sheet on the tension face. A notch or a hinge is usually used to initiate debonding between the FRP and concrete. As the flexural load puts the bottom of the specimen in tension, shear stresses develop and the forces are transferred between the concrete and FRP. Fracture energy or shear stress along the bond line is typically calculated using this method.

2.4.1.4 Direct Tension Pull-off Test

The direct tension pull-off test is a popular test method to assess the quality of the FRP-to-bond. It is the only standardized concrete-to-FRP bond test, known as American Society for Testing and Materials (ASTM) D7522 (ASTM 2009). The test method involves bonding a steel plate to FRP-reinforced concrete. A groove is made around the plate and direct tension is applied to the plate (Mukhtar & Faysal, 2018).

2.4.1.5 Mixed-Mode Loading

Mixed-mode loading tests are the least common concrete-FRP bond tests. The bond interface is considered to be in mixed-mode loading if it is subjected to both shear and peeling effects. There is no standard test method for mixed mode loading. Ghorbani et al. investigated the FRP-to-concrete bond under mixed-mode I/II loading conditions by conducting a test similar to a single-lap shear test. To experience mode I/II conditions, the FRP sheet was loaded at an angle. Due to the misalignment of the vertical force and the concrete substrate, there became a vertical component P_{II} and a horizontal component P_I of the applied force. P_{II} created the mode II shear force in the specimen and P_I created the mode I tensile opening force in the specimen (Ghorbani, et al., 2017). Other approaches use a standard beam type test method with slight variations such as a hinge or pin to induce peeling effects.

The most appropriate concrete-FRP test methods for this study were three-point bending tests and single-lap shear tests. Chapter 5 will discuss these tests further.

CHAPTER 3

DESIGN OF THERMOPLASTIC-REINFORCED UHPC PANELS

Literature review showed that externally bonded plates significantly enhance impact performance of UHPC. For this reason, a thermoplastic composite and UHPC sandwich hybrid system was developed to improve the impact behavior of UHPC. The materials were bonded using a stamp thermoforming process. This chapter will discuss the material selection and the manufacturing process of the thermoplastic-UHPC sandwich panels.

3.1 Materials

This section discusses the materials used in the thermoplastic-UHPC sandwich panels. These include the UHPC cores, thermoplastic composite tapes, and adhesives.

3.1.1 Ultra-High Performance Concrete Core

The UHPC mix used for this research was developed at the U.S. Army Engineer Research and Development Center (ERDC) in Vicksburg, MS. The constituents of the mix include: Portland Lime Cement (PLC), silica fume, silica sand, superplasticizer, and 19 mm long, 0.009 mm diameter Nycon-RC nylon fibers. Despite the literature's praise of steel fiber reinforcement in UHPC, ERDC selected nylon fibers over steel fibers because of nylon's lighter weight and easier handling. A future goal of this project is to use the thermoplastic-reinforced sandwich panels as the building material for military protective structures, and nylon fibers would be much more practical to work with on site. The nylon fibers are shown in Figure 1.

Figure 1: 19 mm long, 0.009 mm diameter Nycon RC nylon fibers

The proportion of fibers was determined by attempting to maximize the amount of fibers while preserving workability of the mix. Table 1 summarizes the proportions of the mix constituents.

Table 1: UHPC Mix Proportions

Mix Constituent	**Proportion by Weight**
Portland Lime Cement	0.374
Silica Fume	0.066
Silica Sand	0.461
Superplasticizer	0.012
Water	0.087
Nylon Fibers	0.003

The silica fume and silica sand were first combined in a mixer. Separately, the superplasticizer and water were mixed. The superplasticizer/water mixture was slowly added to the fume and sand until a desired workability of the mix was achieved. Only about 84-88% of the superplasticizer/water mixture was added to the mix. Once the volume of the mix significantly decreased, the PLC was added. The nylon fibers were then evenly dispersed into the mix.

12” x 12” x ½” UHPC panels were fabricated both at ERDC and at the University of Maine. Panels were first made at ERDC. Each batch of UHPC produced (15) panels and (3) 3” x 6” cylinders. To ensure consistency throughout the panels, the density of the nylon fiber-reinforced UHPC mix was calculated to find the weight needed to fill each mold. Each mold was filled with approximately 6.25 pounds (± 0.01 pound) of UHPC mix. The molds were transferred to a vibration table to consolidate and level the panels. The molds were then placed in a fog room for 24 hours. After 24 hours, the molds were taken apart and the UHPC panels were placed in an insulated Japanese soaking tub outfitted with a steam generator, as shown in Figure 2. The tub was covered with visqueen and burlap for top insulation, and the panels were steamed at 90°C for 48 hours. The panels were shipped to the University of Maine after curing.

Figure 2: Insulated Japanese soaking tub with steam generator used to cure UHPC panels (left) and tub covered in visqueen and burlap insulation (right).

The UHPC panels manufactured at ERDC were not a constant thickness, causing cracking issues during initial consolidation trials (see Section 3.2). This required the fabrication of more UHPC panels at the University of Maine. Each batch of UHPC mixed at the University of Maine produced (1) 12” x 12” x ½” panel and (3) 2 in^3 cubes. With the intent of casting UHPC panels at a uniform thickness, a six-sided mold setup was used. Small channels were cut out of a five-sided mold, as shown in Figure 3. After mixing, the UHPC was placed in the mold so the concrete slightly overflowed the mold. The mold was transferred to a vibration table to level the panels. An acrylic sheet was then applied on top of the mold. The setup was clamped together using C-clamps. As the clamps were tightened, the excess UHPC squeezed out of the mold through the small channels. The six-sided mold setup is shown in Figure 4.

The UHPC specimens were then placed in a wet room at a temperature of 24°C and a humidity of 95% for 24 hours. After 24 hours, the panels were removed from the molds and returned to the wet room to cure for 28 days.

Figure 3: Small channels cut out of 5-sided UHPC panel mold.

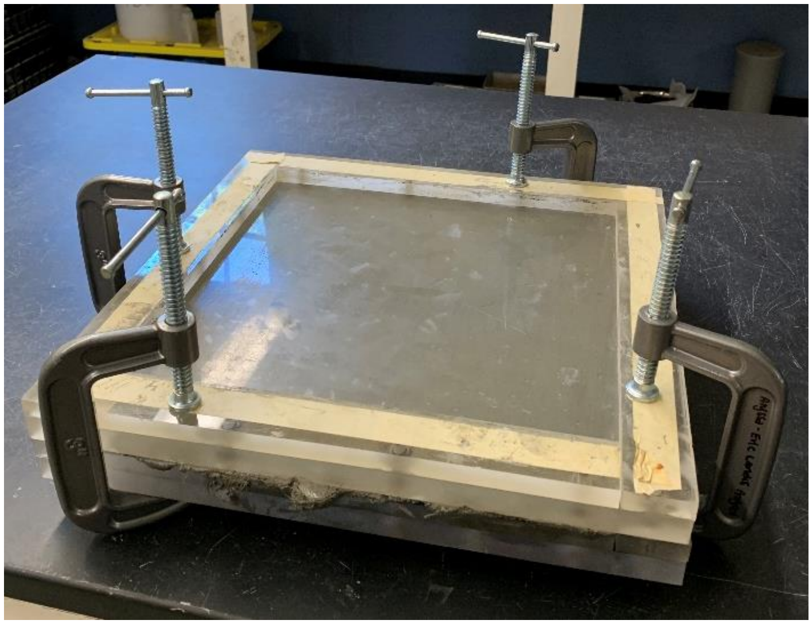

Figure 4: UHPC panel cast in the six-sided mold setup.

For the 4 batches of UHPC fabricated at ERDC, two UHPC cylinders from each batch were tested per ASTM C39. The tests were run by technicians at ERDC. At the University of Maine, (3) 2 inch cubes were tested in compression per ASTM C109. The measured compressive strengths recorded at the University of Maine were highly variable from panel to panel and also highly variable within the same panel batch. This variance stems from the variability of the different UHPC batches. Additional variability is most likely due to an uneven dispersion of the nylon fibers throughout the batch as well as the small size of the cube specimens. Table 2 presents a summary table of the compressive strength data including average compression strength, standard deviation, and coefficient of variation (COV) of the data.

Table 2: Comparison of UHPC Compressive Strengths Batched at ERDC and the University of Maine

Location of Batching	Average Batch Compressive Strength (MPa)	Standard Deviation (MPa)	COV (%)	Specimen Size and Type	Curing Method
ERDC	164	10.9	6.6	3” dia x 6” cylinders	Steamed at 90°C for 48 hours
University of Maine	108	15.7	14.5	2 in^3 cubes	Steamed at 24°C for 28 days

The difference in curing methods is assumed to have caused the significant difference in compressive strength between the UHPC batched at ERDC and the UHPC batched at the University of Maine. An increase in curing temperature has been shown to increase compressive strength (Ibrahim, et al., 2017). The UHPC batched at ERDC was cured at a higher temperature than the UHPC batched at the University of Maine. Additionally, the varying compressive specimen size and type could have played a role. Size variations in test specimens have been reported to influence compressive strength results (Fladr & Bily, 2018).

3.1.2 E-glass/PETG Pre-Impregnated Tapes

The second material in this study is a pre-impregnated (prepeg) unidirectional thermoplastic tape for external reinforcing of the concrete core. Polyethylene terephthalate glycol (PETG) was chosen as the polymer in the thermoplastic tapes due to its high toughness, high impact resistance, and high durability. PETG is an amorphous thermoplastic material, allowing it to easily be thermoformed and bonded to adhesives. PETG softens at a glass transition temperature (Tg) of about 80°C and hardens among cooling. Polystrand IE 5842 tapes manufactured by Avient were selected for this study, consisting of continuous E-glass reinforcement and PETG polymer with a fiber volume fraction of 58%. The IE 5842 tapes were manufactured at a width of 2” and laid up using an automatic Dieffenbacher tape layup machine at the Advanced Structures and Composites Center (ASCC). Mechanical properties of the IE 5842 tapes are presented in Table 3, as published by Avient (Avient Corporation, 2020).

Table 3: Mechanical Properties of Unidirectional E-glass/PETG Pre-Impregnated Tapes

Mechanical Property	**Typical Value**	**Test Method**
Longitudinal Tensile Strength	945 MPa	ASTM D3039
Transverse Tensile Strength	23.4 MPa	
Longitudinal Compressive Strength	594 MPa	ASTM D6641
Transverse Compressive Strength	57.9 MPa	
Poisson's Ratio	0.28	ASTM D3039

3.1.3 Adhesives

The third and fourth materials used in this study were PETG neat resin and ethaline acrylic acid (EAA), which is sold under the trade name Surlyn by DuPont. These materials were used as adhesives to bond the thermoplastic laminates to the concrete. PETG neat resin has been used in previous work on this project and has been successful in bonding the thermoplastic tapes to UHPC (Gillis, 2018). PETG is a copolymer of polyethylene terephthalate (PET) and is a material that is widely used for thermoforming due to its amorphous structure. EAA is a new material of interest and was recommended by Christian Carloni, Ph.D, an Associate Professor of Structural Mechanics at Case Western Reserve University. Carloni found that EAA was successful in bonding FRP to concrete. EAA is an ionomer resin known for its high toughness, durability, and high chemical resistance. It is also known to exhibit self-healing properties. The first significant study to explore the self-healing properties of EAA was carried out by Fall, in which bullet penetration tests were performed on sheets of EAA (Fall, 2001). This study showed that EAA self-healed after being struck by a 9-mm standard bullet. The self-healing properties following the projectile impact were caused by the ionic content and the order-disorder transition. The order-disorder transition refers to the transitions between different phases of a copolymer (Shi, 2013). It was hypothesized that if sufficient energy is transferred to EAA during the impact, the material is heated above the order-disorder transition and disorders the ionic aggregates. When this heat energy is dissipated, the ionic aggregates reorder themselves, resulting in self-healing of the material (Reynolds, 2011; Fall, 2001). Other studies have shown EAA's respectable impact performance. One study discovered that EAA nearly recovered to its initial shape within seconds after being dynamically compressed by a split-Hopkinson pressure bar (Sierakowski & Hughes, 2006). Because of its high impact resistance and self-healing properties, EAA is an important material of interest in this research.

The mechanical properties of PETG neat resin and EAA, acquired from McMaster Carr and Entec Polymers, respectively, are presented in Table 4 (McMaster-Carr, n.d.; Entec, 2020). Each property presented in Table 4 differs greatly between the PETG neat resin and EAA adhesives. Categorizing the stiffnesses of the adhesives according to the study by Shi et al., PETG neat resin is considered a normal adhesive and EAA is considered a soft adhesive (Shi, et al., 2019). The impact strength of EAA is about 11 times greater than that of PETG neat resin. This information alone indicates that EAA most likely has better impact behavior than PETG neat resin. In addition, the melting point of the PETG neat resin is about five times that of EAA, and the Tg of PETG is almost twice that of EAA (Lu & Li, 2016; Miwa, et al., 2018). It should also be noted that the EAA resin sheet is twice the thickness of the PETG neat resin sheet. EAA resin sheets are only commercially available at a minimum thickness of 0.125 inches.

Table 4: Mechanical Properties of PETG Neat Resin and EAA

Adhesive Type	Flexural Modulus (GPa)	Ultimate Tensile strength (MPa)	Impact Strength (ft-lbs/in)	Melting Point (°C)	Tg (°C)	Thickness (in)
PETG neat resin	2.07	53.1	1.7	500	80	0.0625
EAA	0.350	33.0	19	94	47	0.125

3.2 Stamp Thermoforming of the Sandwich Panels

This section discusses the manufacturing process of the sandwich composite panels used for impact testing and three-point bending. The first step in the manufacturing process was surface roughening of the UHPC. Concrete surface roughening has been proven to improve the bond between FRP and concrete (Lorenzis, et al., 2001). The UHPC surfaces were mechanically grinded using a 4-inch diamond wire wheel and sprayed with pressurized air to remove dust. Figure 5 shows a panel before and after surface preparation.

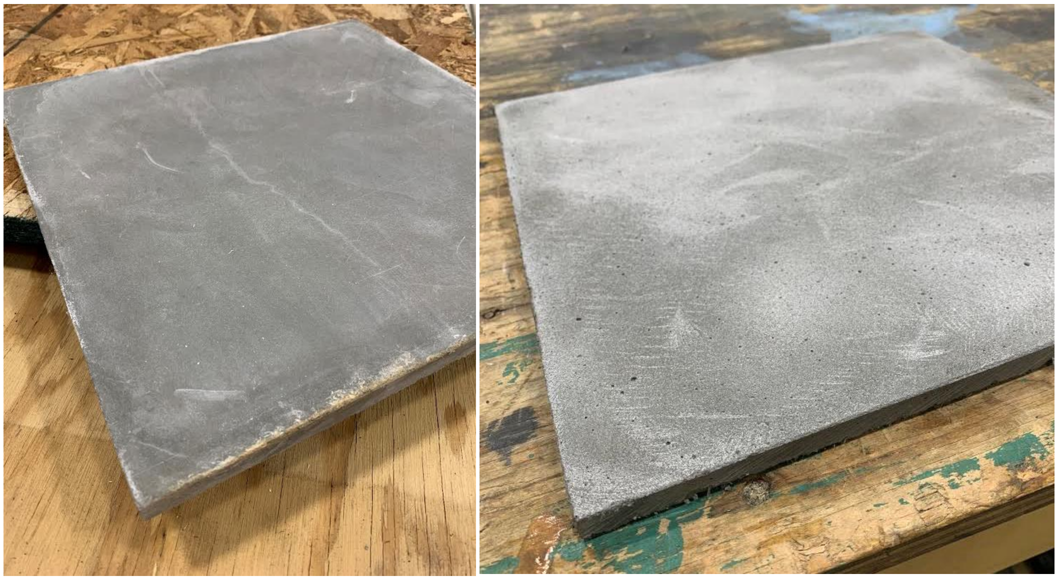

Figure 5: UHPC panel surface prior to surface preparation (left) and after surface preparation (right).

The next step in the sandwich panel manufacturing process was laying up the E-glass/PETG prepeg tapes. Literature review showed that the impact resistance of composite laminates is directly affected by the order in which the laminas are stacked. Stevanovic et al. found that laminas stacked at [+/- 45] were capable of absorbing more energy than unidirectional laminates and laminates stacked at [0,90], [0,+/-45], and [0,90,+/-45] (Stevanović, et al., 1987). The laminate stacking sequence was adopted from previous work on this project by Gillis Smith. An 8-layer laminate was used with a stacking sequence of [0, 90, -/+ 45]s (Gillis, 2018). The orientation of the fibers is illustrated in Figure 6, and the mechanical properties of the laminate are presented in Table 5. These values were tabulated using the Computer Aided Design Environment for Composites (CADEC) software. 12” x 12” laminates were laid up and consolidated at a temperature of about 165°C and an effective pressure of 100 psi prior to bonding them to the concrete.

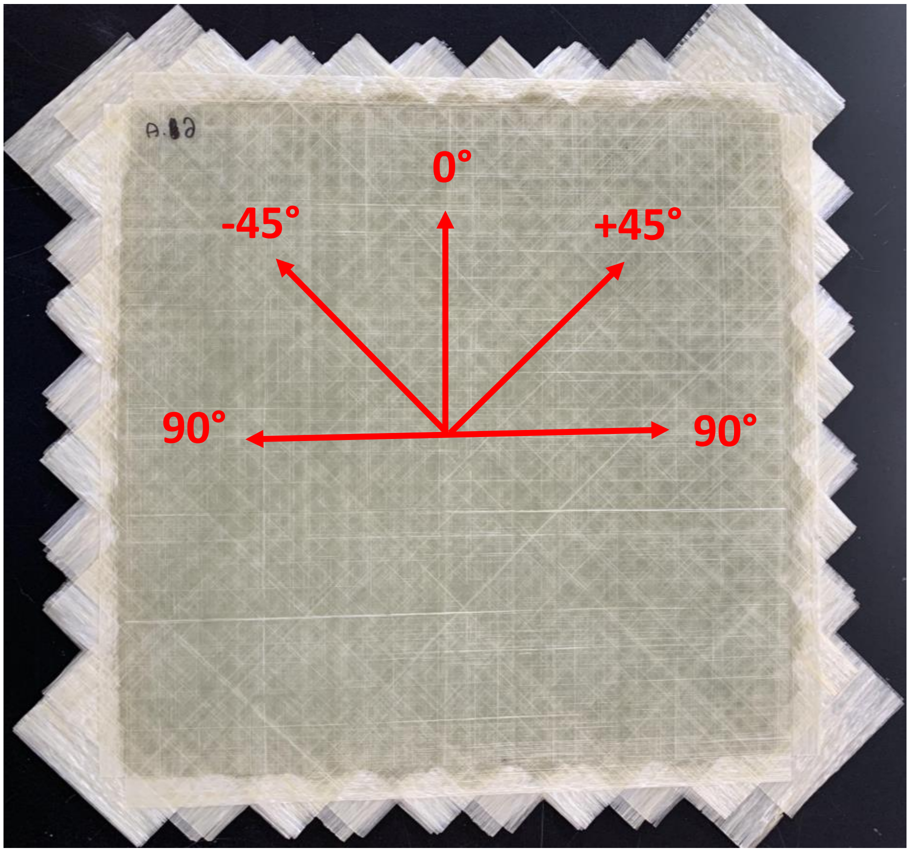

Figure 6: Fiber orientation of the thermoplastic laminates.

Table 5: Mechanical Properties of [0, 90, -/+ 45]s E-glass/PETG Laminate

Property	Tabulated Value
Laminate modulus of elasticity, E_x (GPa)	21.2
Laminate modulus of elasticity, E_y (GPa)	21.2
Laminate shear modulus, G_{xy} (GPa)	8.11
Poisson's ratio, ν_{xy}	0.305

The next step of the manufacturing process was bonding the thermoplastic laminates to the UHPC cores. One goal of this study was to improve the manufacturing process of the sandwich panels used in previous work on this project. To accomplish this, an 800-metric ton heated press was used for consolidation, and four sandwich panels were consolidated at once. The first consolidation trials used the UHPC panels fabricated at ERDC. The materials were stacked in the following order from bottom to top: thermoplastic laminate, adhesive sheet, UHPC core, adhesive sheet, and thermoplastic laminate. Figure 7 shows a sandwich panel setup in the press. Note that the thermoplastic laminates are a different color than that shown in Figure 6. The black color is caused by a dye added to the tapes to increase resistance to ultraviolet light. The color does not affect the material properties of the laminate.

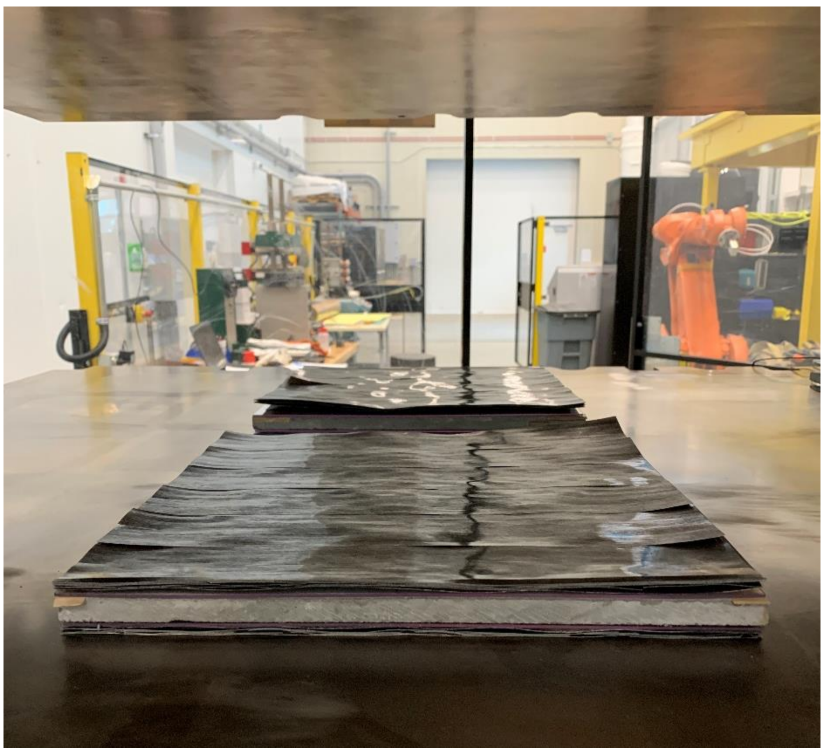

Figure 7: UHPC-thermoplastic sandwich panel in 800-ton heated press.

The panels were consolidated at 180°C and at an effective pressure of 100 psi. The press was turned off once the panels reached the desired temperature. The panels remained in the press for 24 hours to cool.

Significant issues arose following this consolidation trial. The first issue was that two out of the four concrete cores shattered. It was assumed that this was due to a non-uniform thickness throughout the panels. A high point in the concrete panel could have caused an uneven stress distribution once pressure was applied, catalyzing cracking throughout the panel. The second issue was displacement of the concrete cores from the thermoplastic laminates. The displacement of the concrete cores was most likely due to overheating of the adhesive sheets. The resin became very viscous and most likely caused the concrete cores to slide. A sandwich panel following the first trial of consolidation is shown in Figure 8.

Figure 8: Issues with the sandwich panels following the first consolidation trial.

To avoid cracking and sliding of the concrete cores, preventive measures were taken in the second thermoforming trial. Silicone mats with a thickness of ¼” were placed on the top and bottom of the sandwich panels within the press to comply with the unevenness of the UHPC panel and serve as protection for the concrete when pressure was applied. In addition, to prevent sliding of the concrete cores, a steel retainer for the sandwich panels was manufactured. Four 12” x 12” squares were cut out of a ¼”-thick steel sheet. The retainer was laid on the press, and the sandwich panels were placed in the square cutouts. Figure 9 shows the sandwich panels held by the steel retainer in the press. The panels were heated to 168°C and an effective pressure of 100 psi was applied.

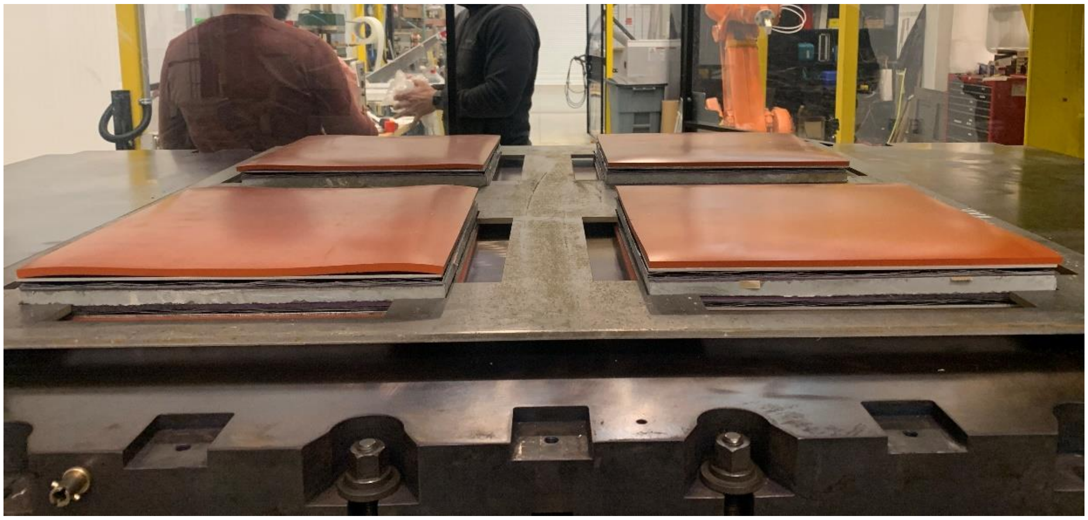

Figure 9: UHPC-thermoplastic panels held by the steel retainer in the 800-ton press.

Issues still arose from this manufacturing technique. Cracking occurred in one of the four UHPC panels. In addition, the panels were almost impossible to remove from the steel frame without damaging them. Due to the difficulties from using the 800-ton press, this manufacturing process was no longer used.

As a result, the manufacturing process used in previous work was utilized which entailed a two-step consolidation process. The first step was to heat the sandwich panels in an oven to an appropriate bonding temperature. The second step was to transfer the panels to a non-heated press and consolidate the panels. A total of 12 thermoplastic-bonded UHPC panels were manufactured using this technique, following the consolidation test matrix shown in Table 6. There were three key variables in this test matrix: adhesive type, consolidation pressure, and concrete type. PETG neat resin and EAA were the adhesives explored, as well as two consolidation pressures of 80 and 100 psi. Two UHPC panels cast at ERDC were used in the test matrix along with the UHPC panels cast at the University of Maine to determine if the concrete behaved similarly.

Table 6: Consolidation Test Matrix for UHPC-Thermoplastic Sandwich Panels

Adhesive	**Consolidation Pressure (psi)**	**Concrete Type**	**Quantity**
PETG neat resin	100	University of Maine	2
	80	University of Maine	2
EAA	100	University of Maine	3
		ERDC	1
	80	University of Maine	3
		ERDC	1

The composite sandwich panels were stacked in the same order as the previous manufacturing process. For heating, 12” x 12” aluminum caul sheets were placed on the top and bottom of the specimen to encourage uniform heating throughout the thermoplastic layups. Chemlease 41-90 was applied to the caul sheets to prevent the laminate and adhesive from adhering to it. A thermocouple wire was inserted between the top thermoplastic laminate and adhesive sheet, as shown in Figure 10. The thermocouple wire was connected to a data logger which reported the temperature of the bond throughout the heating process. The thermocouple wire setup is shown in Figure 11.

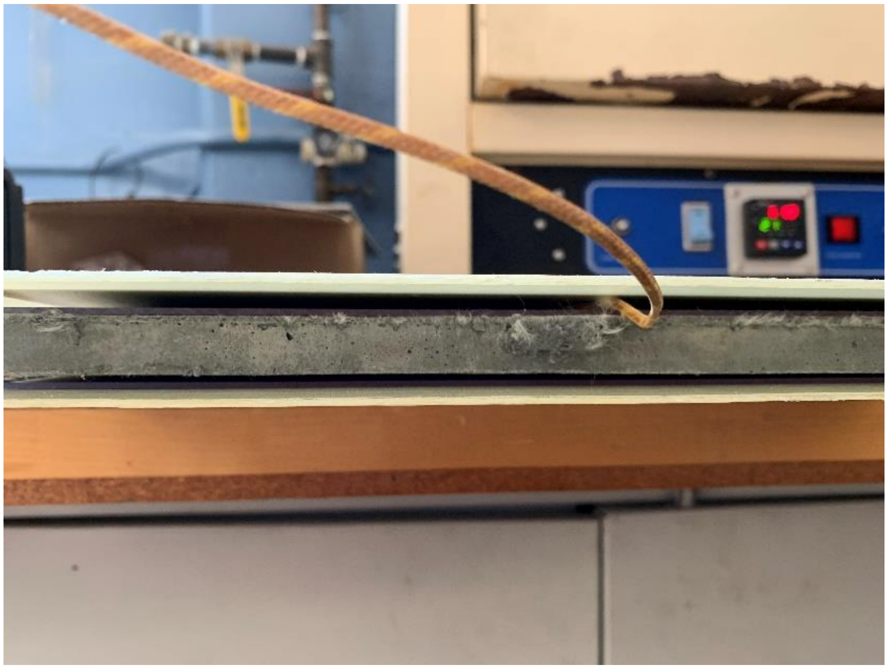

Figure 10: Thermocouple wire inserted between layup and adhesive layers.

Figure 11: Thermocouple wire set up to panel prior to heating.

The specimens manufactured with PETG neat resin adhesive were heated in an oven until the thermocouple logger read 165°C. This oven temperature was chosen using previous knowledge of E-glass/PETG prepeg tapes at the ASCC. As shown in Table 4, the melting temperatures of PETG neat resin and EAA differ greatly. The melting temperature of PETG neat resin is about five times greater than the melting temperature of EAA. As a result, an attempt was made to bond the thermoplastic laminates to the concrete using a lower oven temperature of 100°C for EAA specimens. This attempt was unsuccessful however, as the PETG tape laminates were not heated high enough to melt and successfully bond to the concrete. The bond area between the laminate and EAA was poor, causing the thermoplastic layups to easily rip off of the adhesive. As a result, the remaining EAA specimens were heated to the same temperature as the PETG neat resin specimens of 165°C.

After heating, the panels were transferred to a 400-kip Baldwin testing frame, shown in Figure 12. ¼” silicone mats were placed on the top and bottom of the panel setup. A 12” x 12” x ¼” steel sheet was then placed on top of the entire setup to act as a top platen for the press. The part undergoing consolidation is shown in Figure 13.

Figure 12: 400-kip Baldwin testing frame used for consolidation.

Figure 13: UHPC-thermoplastic sandwich panel undergoing consolidation.

The panels were pressed at their corresponding consolidation pressures for 10 minutes. The thermocouple wire was left in the specimen to record heat loss when in the press. From the time the part was taken out of the oven to the start of consolidation, the temperature of the bond dropped by roughly 20°C. After being pressed for 10 minutes, the temperature of the bond dropped an average of 80°C from the initial temperature. Following consolidation, the panels were left to cool for at least three days before cutting and testing.

Because the EAA resin was heated at a temperature much higher than its melting point, issues arose with displacement of the concrete cores for specimens manufactured with this adhesive. In addition to overheating, the EAA resin sheets were 0.0625 inches thicker than the PETG neat resin sheets. The combination of the thick resin sheet and the high consolidation temperature caused the EAA to become extremely viscous, leading to displacement of some of the concrete cores. This was not an issue with the specimens manufactured with PETG neat resin.

CHAPTER 4

LOW-VELOCITY IMPACT TESTING

Low-velocity impact tests are typically used to gain a fundamental understanding of composite sandwich impact behavior, as low-velocity impact induces global damage to the specimen. In this study, a combination of low-velocity impact tests and quasi-static tests were used to investigate the impact behavior of the thermoplastic-reinforced UHPC panels. The following sections will discuss the experimental procedures, results and discussion, and summary and conclusions of these tests.

4.1 Introduction

An estimate of energy absorption was desired for the thermoplastic laminate-reinforced UHPC sandwich panels using both quasi-static testing and low-velocity impact testing. The quasi-static testing performed before and after impact provided the change in compliance and residual deflection that the specimen underwent as a result of impact. The low-velocity impact testing provided the maximum impact force.

Drop weight testing is the most typical low-velocity impact testing method. Many researchers have used this method to assess the failure mechanisms of UHPC (Ranade, et al., 2017; Verma, et al., 2016; Sukontasukkul, et al., 2002). Since a future goal of this project is to test the thermoplastic-UHPC sandwich panels under high-velocity impact, a drop tower setup that mimicked a high-velocity projectile was selected. A striker with a small diameter and low mass was used in the drop weight testing. The impact energy of the drop weight system was calculated as a function of mass and drop height. The low mass required a high drop height and a high velocity. Although the high velocities of ballistics are not achievable using a drop tower setup, a fundamental understanding of the UHPC failure mechanisms under impact was gained through these tests.

It is important to consider inertial effects when discussing low-velocity impact testing. It has been established that due to inertial effects, the observed impact load is not the true bending load of the specimen, and the true load may only be a fraction of the reported impact load. The inertial load can be defined by the force caused by the acceleration of a specimen from rest to a velocity near that of the impactor (American Society for Testing and Materials, 1973). Ong et al. accounted for inertial effects by using two accelerometers during impact testing. One accelerometer was instrumented inside the tup, and the other was attached to the tested concrete slabs. The accelerometer inside the tup measured the observed acceleration of the drop weight system, and the accelerometer attached to the slabs measured acceleration of the specimens due to impact. The inertial impact load was then calculated through equations of virtual work, and the inertial impact load was subtracted from the reported drop-tower impact load to get the true impact load (Ong, et al., 1999).

Two studies have shown that there are certain situations in which inertial effects can be neglected (Leissa, 1969; Verma, et al., 2016). Leissa reported that if the mass of the impactor is greater than 2 times the mass of the panel, inertial effects of the panel can be neglected (Leissa, 1969). This conclusion was used in the work of Verma et al., as inertial effects were ignored in drop-weight tests since the mass of the impactor was 3.5 times the mass of the panels (Verma, et al., 2016). For this research, the mass of each thermoplastic-UHPC sandwich panel was less than 1 kilogram, and the total mass of the impactor was 3.50 kilograms. The mass of the impactor therefore was at least 3.5 times greater than that of the panel. Considering the technical report by Leissa and the study by Verma et al., inertial effects were not considered in this study.

4.2 Experimental Procedure

Following the stamp thermoforming process, each 12” x 12” composite panel was cut into (3) 5.75” x 5.75” impact plates and (5) 5.75” x 1” beams using a waterjet. The beams were used in three-point bending and will be discussed in Chapter 5. Figure 14 presents the cutting layout of the 12” x 12” panels. Impact plates were cut from quadrants 1, 2, and 4, and beams were cut from quadrant 3. A top and side view of an impact plate is shown in Figure 15.

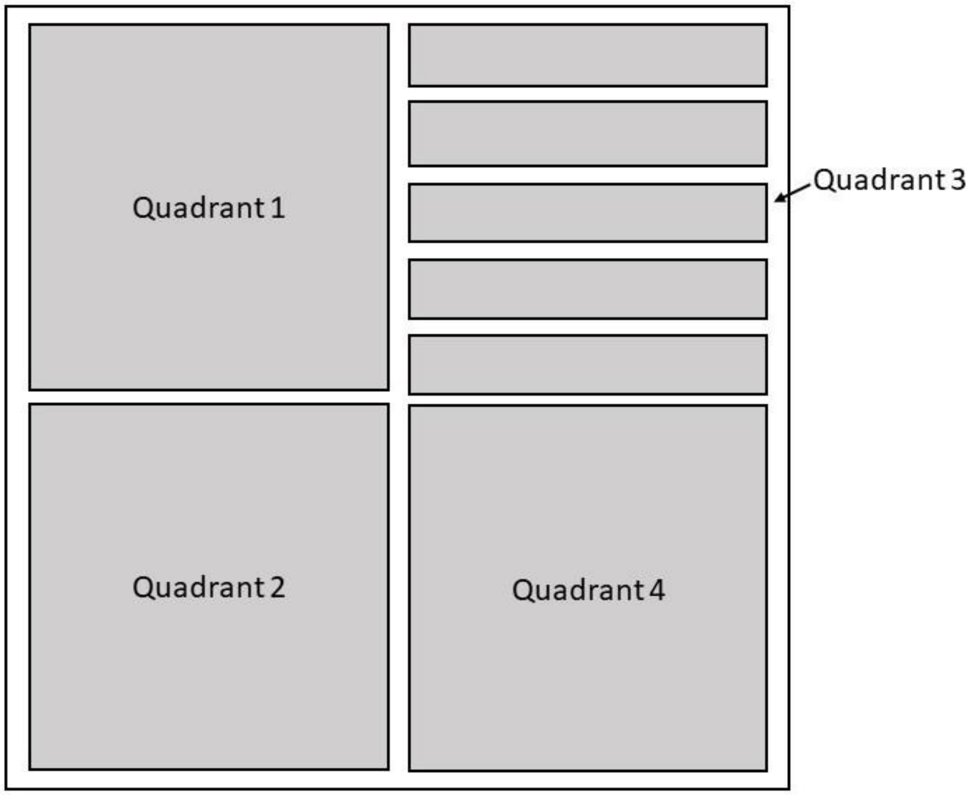

Figure 14: Cutting layout of the 12” x 12” thermoplastic-UHPC sandwich panels.

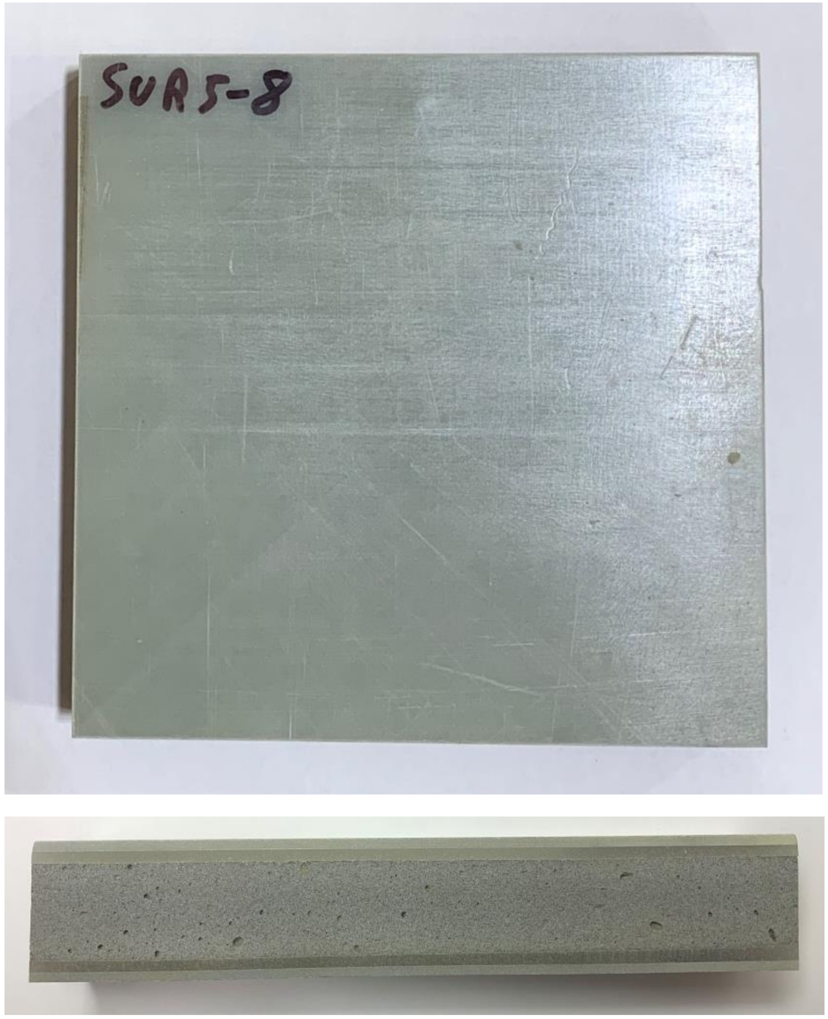

Figure 15: Top and side view of thermoplastic-UHPC sandwich impact plate.

Due to the concrete sliding that occurred during consolidation of the EAA specimens, some of the 12” x 12” sandwich panels were extremely misaligned. As a result, not all impact plates cut from each panel were salvageable and testable. Table 7 presents the test matrix for low-velocity impact and presents each panel name with its corresponding adhesive type, consolidation pressure, type of concrete used, and the number of testable impact plates cut from the 12” x 12” panel. The acronym UM under concrete type represents the concrete manufactured at the University of Maine.

Table 7: Number of Impact Plates Tested from Each Consolidated Sandwich Panel

Panel Name	Adhesive Type	Consolidation Pressure (psi)	Concrete Type	No. of Testable Impact Plates
P1	PETG	100	UM	3
P2	PETG	100	UM	2
P3	PETG	80	UM	3
P4	PETG	80	UM	3
SUR1	EAA	100	ERDC	2
SUR2	EAA	80	ERDC	0
SUR3	EAA	80	UM	2
SUR4	EAA	80	UM	3
SUR5	EAA	80	UM	2
SUR6	EAA	100	UM	0
SUR7	EAA	100	UM	3
SUR8	EAA	100	UM	2

Prior to testing, each impact plate was measured using a dial caliper. A measurement of total depth, UHPC depth, and length was taken on each side of the panel for a total of four measurements per panel. These measurements were then averaged for each panel. The panels were also massed. All units of length were recorded in millimeters and units of mass were recorded in grams.

4.2.1 Quasi-Static Testing

A total of (25) 5.75” x 5.75” sandwich panels were tested statically prior to low-velocity impact and after low-velocity impact. Quasi-static testing was performed to gain an understanding of stiffness, compliance, residual deflection, and overall damage experienced from impact testing. The static portion of the test was performed using a 100 kN servo-hydraulic Instron. The test fixture and load head were designed with the same geometry as the test fixture and load head used for impact testing. A 16-mm ball bearing acted as the load head and was centered in the middle of the panel. The test fixture consisted of a two-piece 6” x 6” square steel frame. The top piece of the fixture held the panel in place and the bottom piece of the fixture was gripped by the hydraulic grips on the Instron. A linear variable differential transformer (LVDT) was mounted to the bottom piece of the steel frame and contacted the bottom-center of the panel to measure residual displacement. Figure 16 shows the quasi-static testing setup.

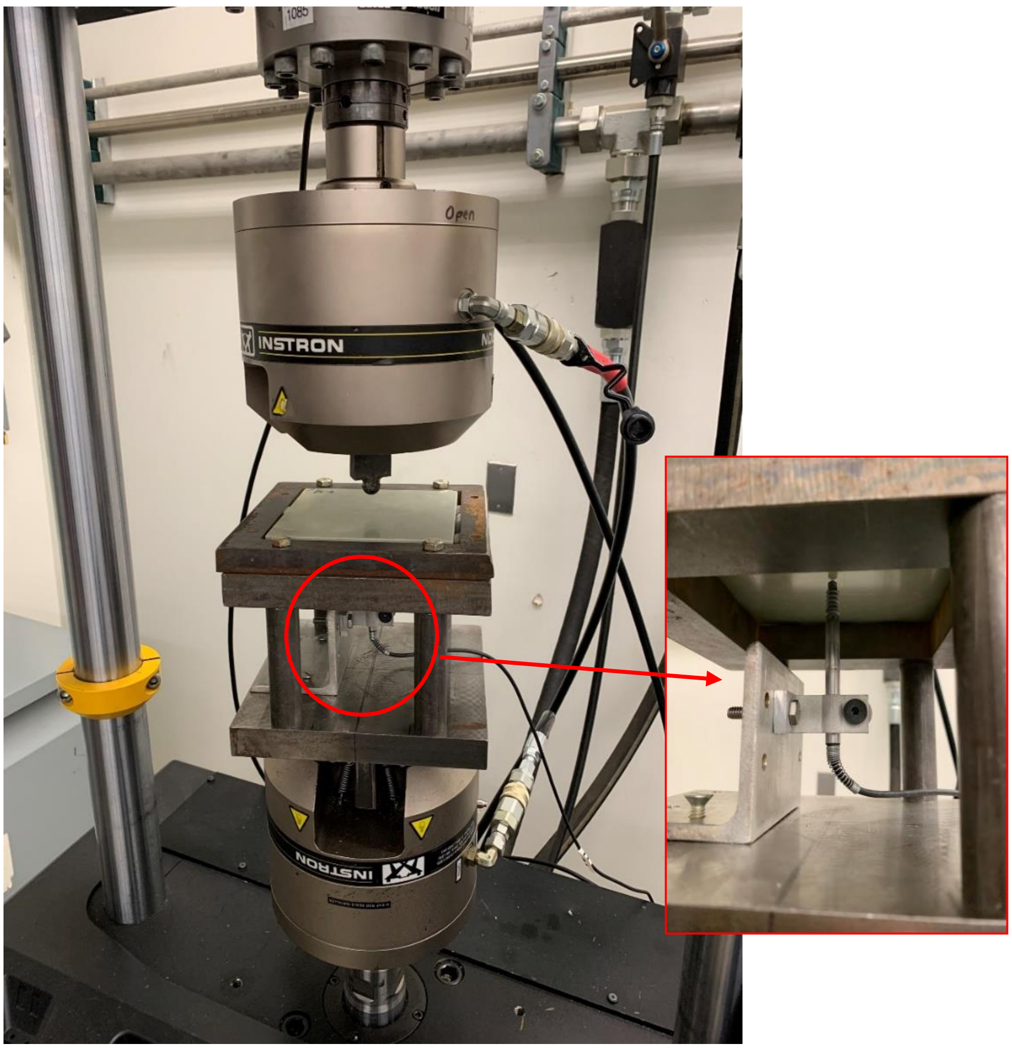

Figure 16: Quasi-static testing setup on a 100-kN Instron.

The LVDT was balanced before contacting the specimen. The specimen was then preloaded to 300 N. The LVDT was adjusted to have a reading between 0.2 mm and 0.5 mm to ensure that the LVDT was engaged. The specimens were tested under a load control rate of 5000 N/min until the load reached 2500 N. The specimens were then unloaded at the same rate. This provided a measure of stiffness prior to impact. The test was paused and the specimen was removed from the Instron and tested under low-velocity impact, as discussed in the next section. Once finished low-velocity impact testing, the specimen was returned to the 100-kN Instron and again tested statically under a load control rate of 5000 N/min until the load reached 2500 N. The specimen was then unloaded at the same rate. The second round of static-testing provided a measurement of stiffness after impact. Data from the quasi-static tests were analyzed using MATLAB by plotting the load-displacement curves. Residual deflection and change in compliance from pre to post impact were acquired from the data.

4.2.2 Low-Velocity Impact Testing

A total of (25) 5.75” x 5.75” sandwich panels were tested in low-velocity impact. The low-velocity impact testing was performed using an Instron CEAST 9350 drop tower impact system. The test fixture had the same geometry as the fixture used for quasi-static testing and consisted of a 6” x 6” square steel retention frame. To prevent the panel from residual shock movement, tape was placed around the edges of the panel and bolts and washers were used to secure the panel. A 16-mm hemispherical tup acted as the striker. This was identical to the loading head used in the quasi-static testing portion. An additional mass of 1 kg was added to the loading frame. Figure 17 presents the labeled Instron CEAST 9350 impact machine, and Figure 18 shows a test specimen in the test fixture prepared for impact.

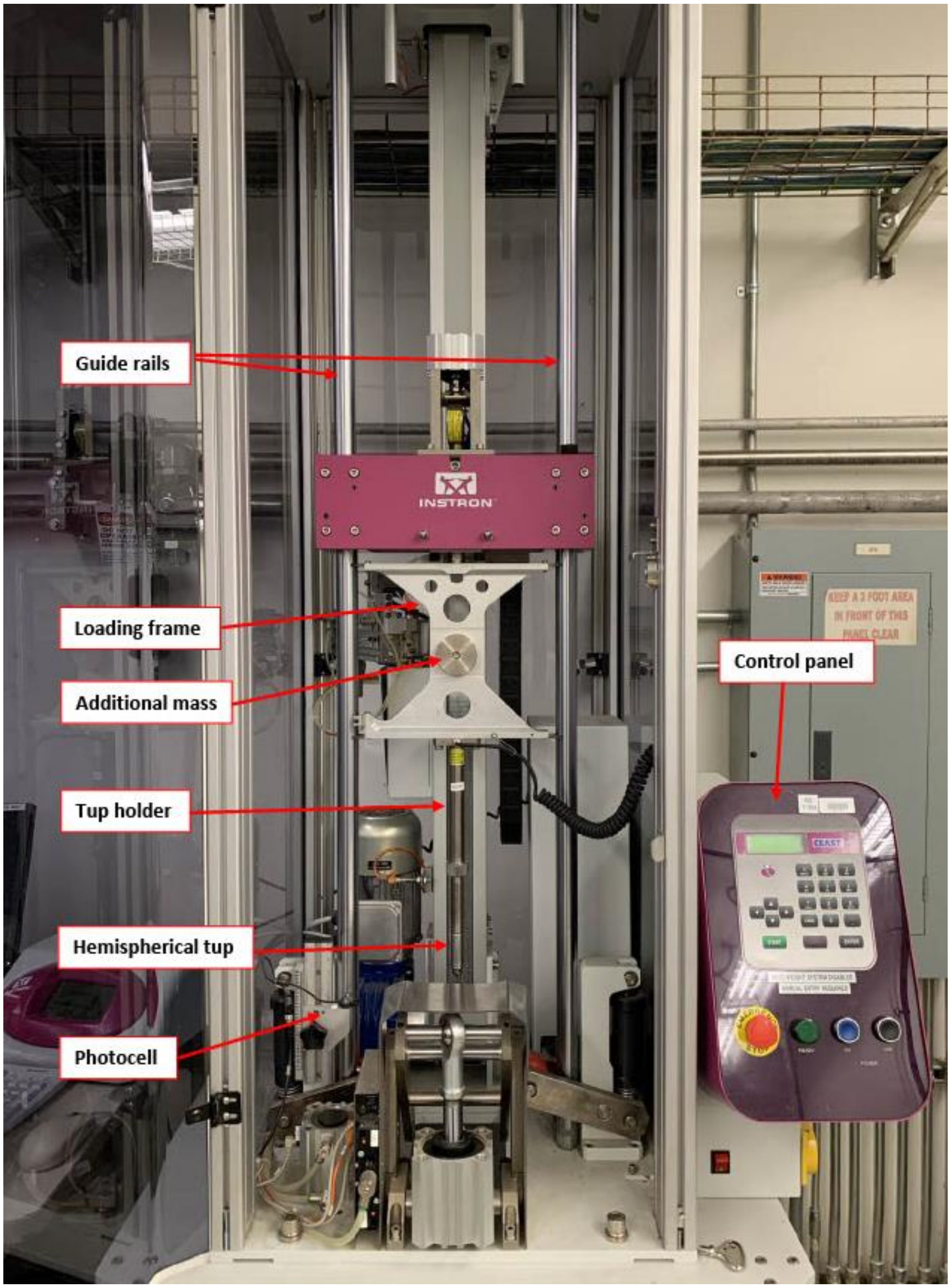

Figure 17: Labeled components of the Instron CEAST 9350 drop tower.

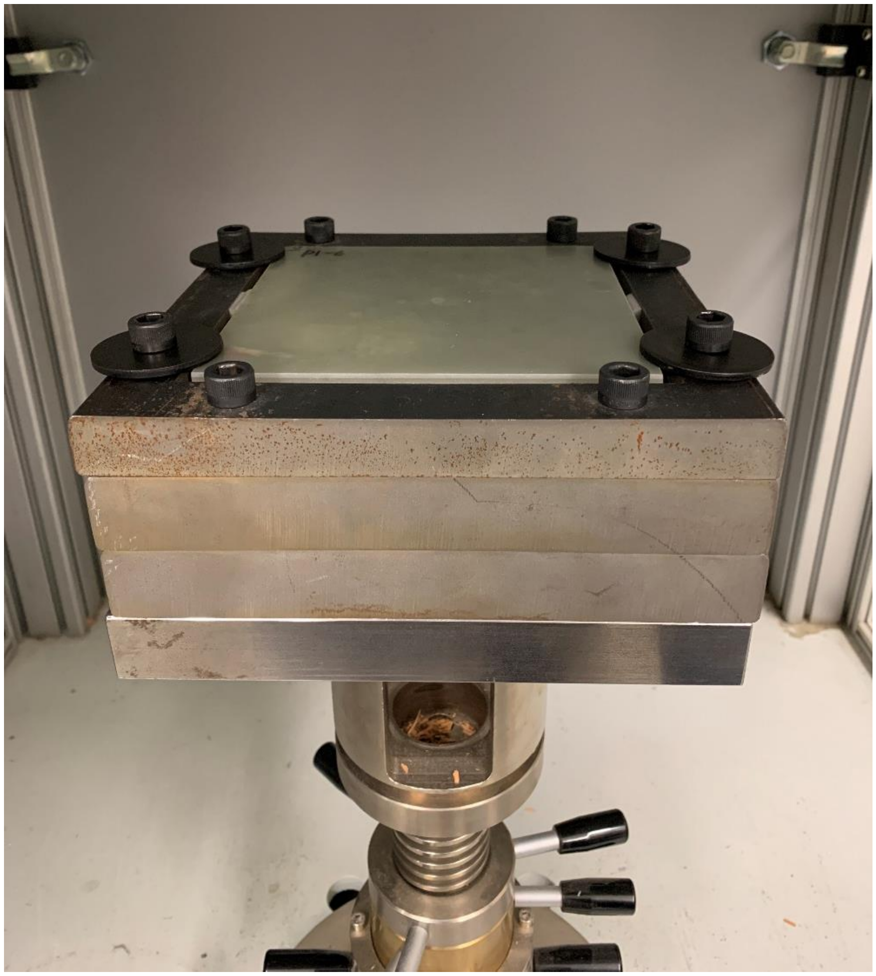

Figure 18: UHPC-PETG panel ready for impact.

The Instron CEAST drop tower was controlled by a computer system with the Instron Visual IMPACT software. The software took an input of either impact energy, desired drop height, or desired mass. The remaining parameters were automatically set by the software using formulas of kinetic energy. As shown in Figure 17, there is an adjustable photocell on the Instron CEAST setup. This measures the velocity of the impactor. A load cell was present within the tup which recorded the impact load and calculated acceleration using Newton's Second Law of Motion, $F = ma$. The tup displacement was then found by integrating the acceleration data. This data was transferred to the Visual IMPACT software.

The software was programmed to impact the panels with 50 J of energy. The falling weight parameters are listed in Table 8. Following impact, delamination area and qualitative impact damage were recorded for both faces of the specimen. The specimen was then returned to the 100-kN Instron to be tested statically for post-impact damage.

Table 8: Instron CEAST 9350 Falling Weight Parameters

Impact energy (J)	50
Mass (kg)	3.50
Impact Velocity (m/s)	5.35
Drop Height (m)	1.46

4.3 Results and Discussion

The results from the impact tests can be separated into two categories depending on the testing type: quasi-static testing and impact testing. The data collected from the quasi-static tests provided a measure of impact damage by calculating the change in the specimen's compliance and residual deflection from the impact. The data acquired from the CEAST impact machine and its data acquisition system was impact force. The following sections discuss the results of the quasi-static and impact testing.

4.3.1 Qualitative Impact Damage

The low-velocity impact tests revealed that the specimens manufactured with PETG neat resin and the specimens manufactured with EAA resin performed quite differently under impact. Figures 19 and 20 show the typical delamination pattern of the PETG neat resin specimens and the EAA specimens, respectively. The EAA specimens typically underwent a smaller, more contained damage area on the front face of the panel. They experienced radial delamination on the front face with a diameter ranging from 3-9 centimeters and experienced larger radial delamination on the back face with a diameter ranging from 7-14 centimeters. 14% of the EAA specimens experienced no delamination on the back face, and about 80% of the EAA specimens experienced no debonding of the laminates from the UHPC core. The PETG neat resin specimens experienced larger radial delamination on the front face with a diameter ranging from 8-11 centimeters. Multiple “sprays” of delamination propagating from the center of the panel to the edges of the panel were also observed, as shown in Figure 19. These sprays were common in about 70% of the PETG neat resin panels. Radial and overall delamination occurred on the back face of the panels with a diameter ranging from 12-14.5 centimeters. 90% of the PETG neat resin specimens experienced debonding of the laminate from the UHPC core on the back face. The failure typically occurred at the concrete-adhesive interface.

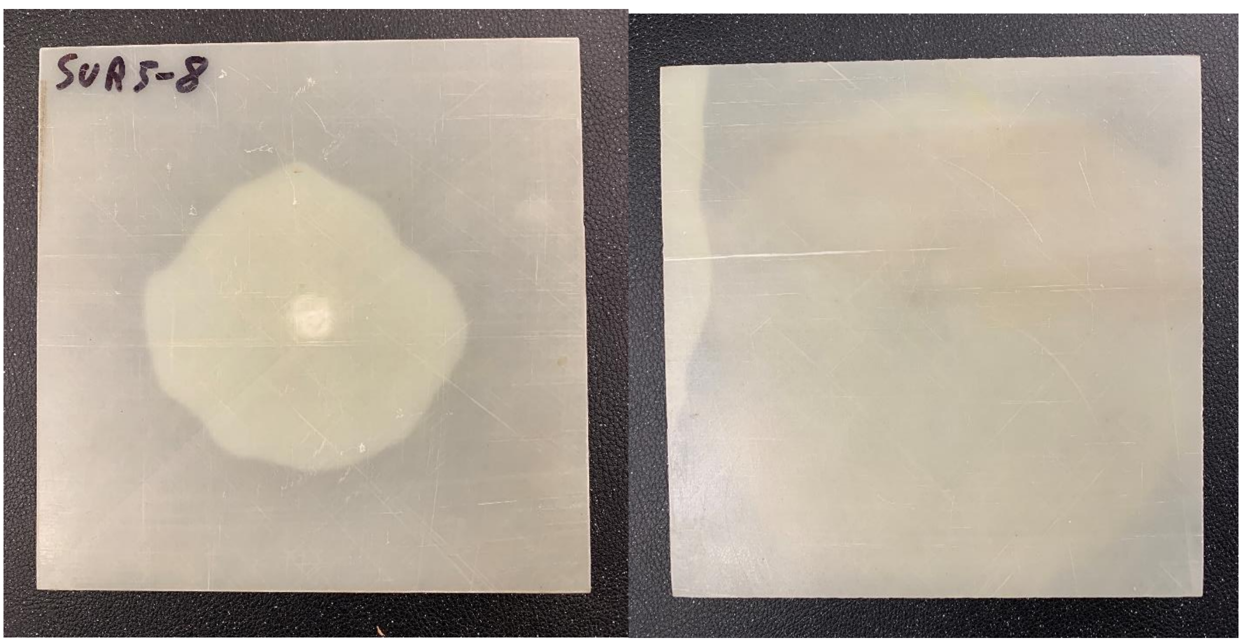

Figure 19: Typical delamination of specimens manufactured with EAA resin on the front face (left) and the back face (right).

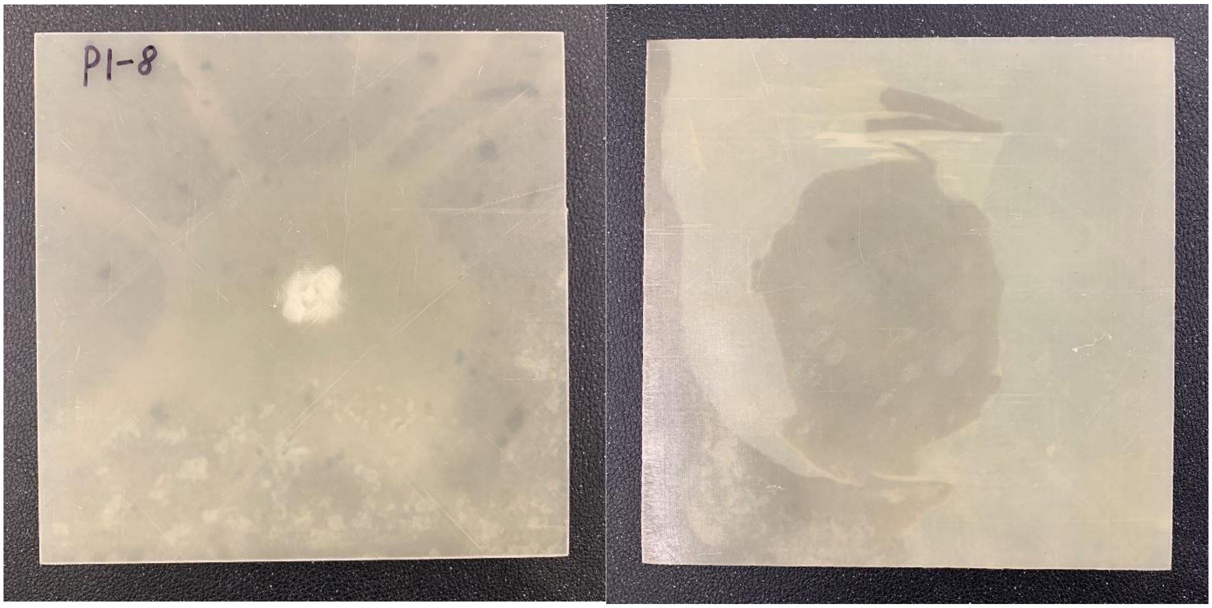

Figure 20: Typical delamination of specimens manufactured with PETG neat resin on the front face (left) and the back face (right).

Shear failure of the concrete was observed in multiple PETG neat resin specimens. Figure 21 shows a typical shear crack in the concrete core following impact of the specimen. The shear crack propagated along the adhesive-concrete interface, resulting in debonding of the laminate and adhesive from the concrete core.

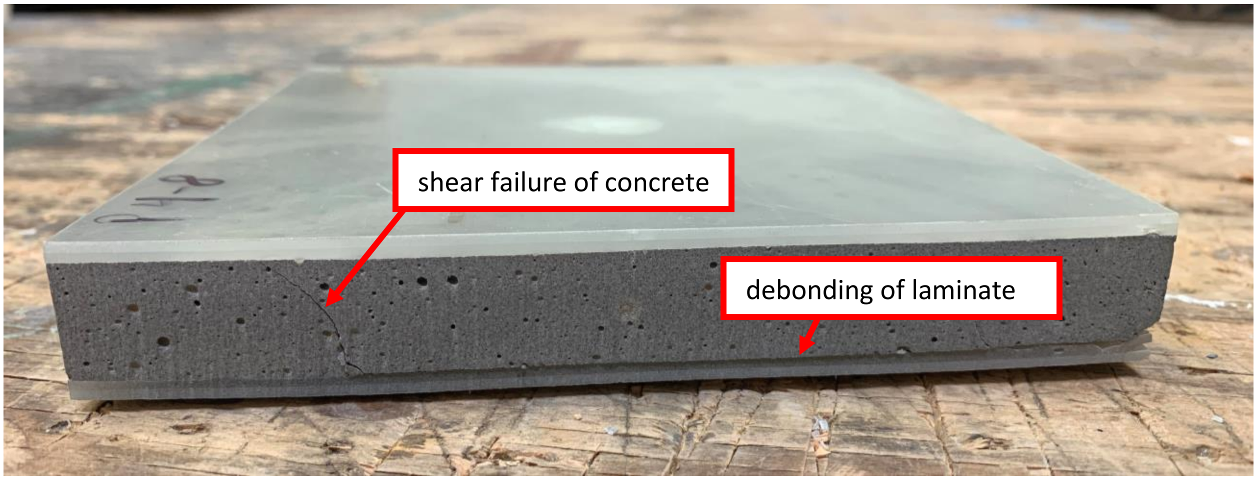

Figure 21: Shear failure of the UHPC core following low-velocity impact test.

The laminates on the rear face were removed from the concrete cores to inspect cracking patterns. The cracking patterns differed greatly between the PETG neat resin specimens and the EAA specimens. Figures 22 and 23 show the cracking patterns on the rear face of the PETG neat resin specimens and EAA specimens, respectively. The UHPC cores of the PETG neat resin specimens exhibited a more brittle failure than those of the EAA specimens. Radial cracking and back spalling of the UHPC was seen in the PETG neat resin specimens. The UHPC cores in the EAA specimens experienced less radial cracking and nearly no back spalling. It can be inferred from the qualitative data that the EAA adhesive has a greater level of ductility than the PETG neat resin adhesive, allowing it to dissipate a greater amount of energy under impact.

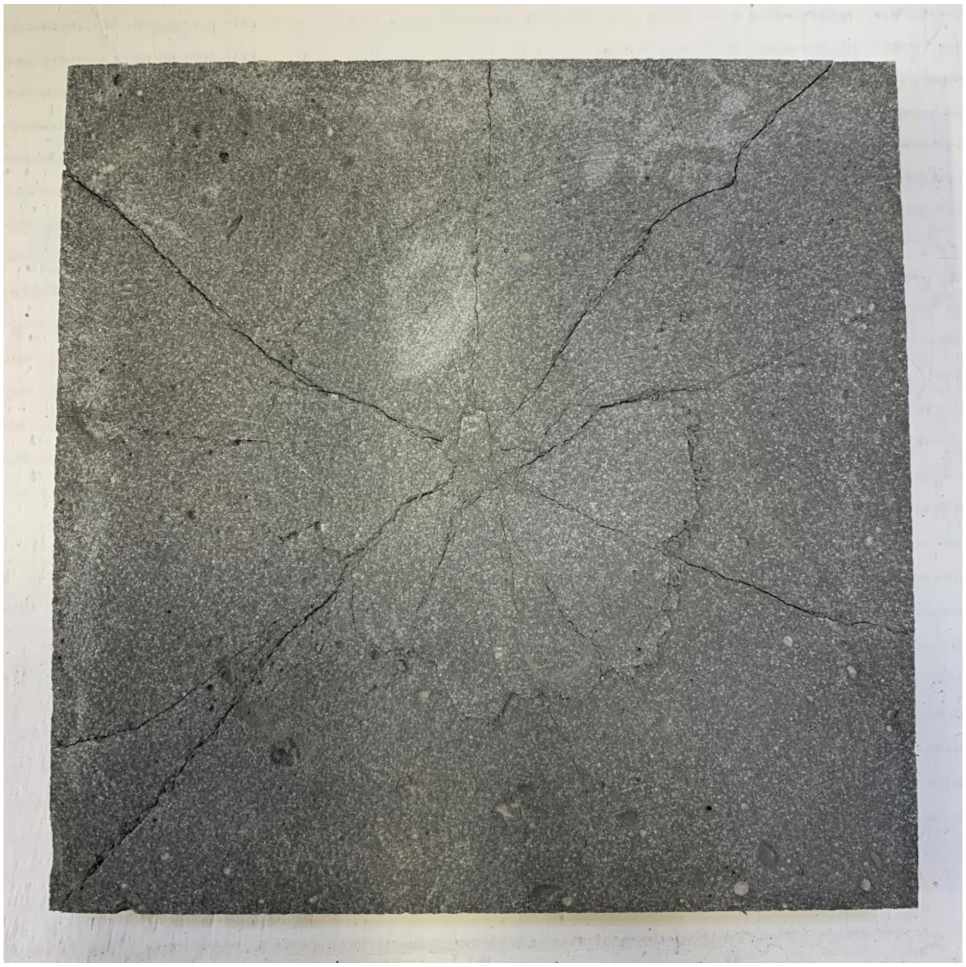

Figure 22: Typical cracking pattern on the rear face of UHPC core for a specimen manufactured with PETG neat resin.

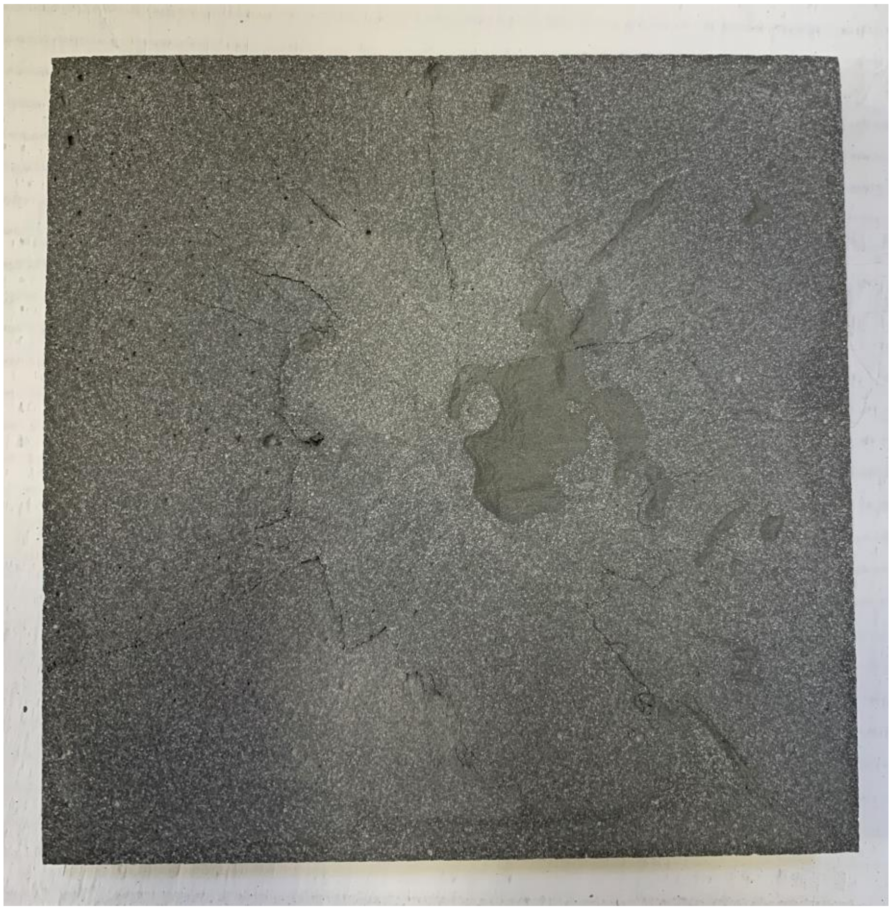

Figure 23: Typical cracking pattern on the rear face of UHPC core for a specimen manufactured with EAA resin.

4.3.2 Quasi-Static Testing

Change in compliance and residual deflection were the results of interest from the quasi-static testing. Change in compliance will be discussed first and residual deflection second.

4.3.2.1 Change in Compliance

It is important to consider stiffness and compliance in structural engineering applications. The stiffness of a structure is defined by its ability to resist deformation when loads are applied. Compliance is the inverse of stiffness. A material that is more compliant will have a greater displacement when loads are applied. Compliance was found in this study from the load-deflection plots of each specimen. The pre-impact and post-impact stiffnesses were calculated by finding the slopes of the loading curves before and after impact. The change in compliance was calculated by taking the inverse and difference of these values. Figure 24 illustrates the undamaged specimen stiffness pre impact and damaged specimen stiffness post impact on a load-deflection plot. The slopes of the red lines in Figure 24 were calculated to approximate the stiffnesses of each specimen before and after impact.

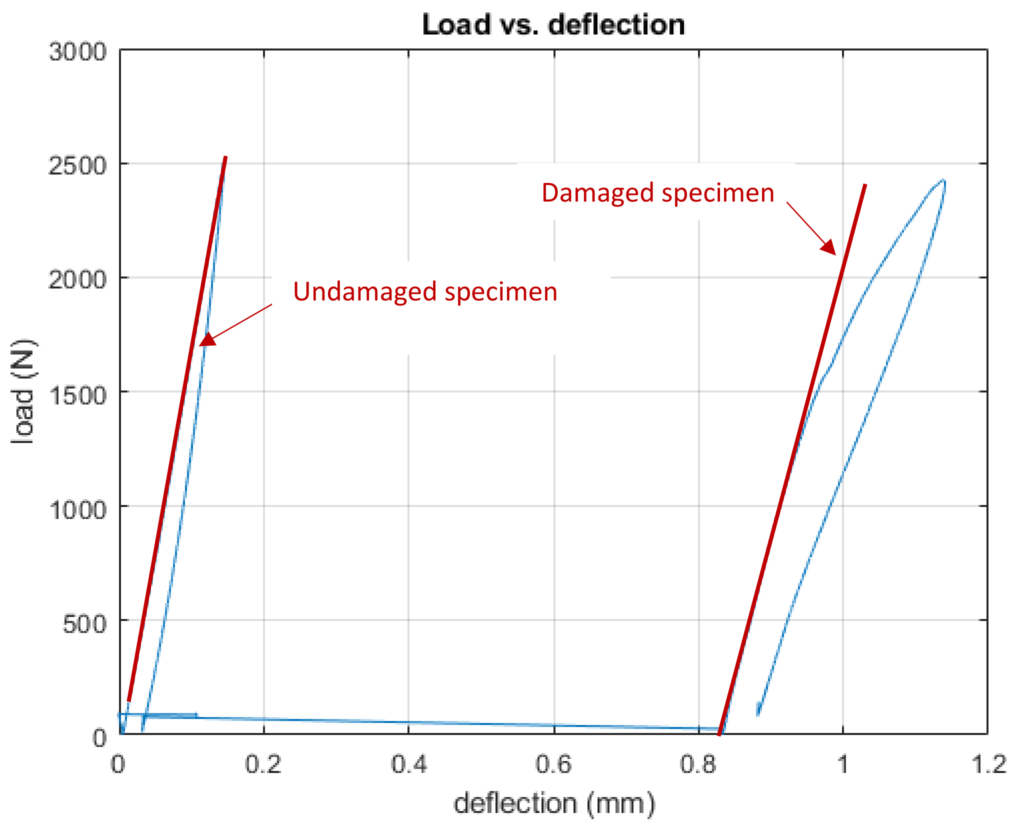

Figure 24: Load-deflection plot showing undamaged specimen stiffness and damaged specimen stiffness of impact plates.

Figure 25 shows a typical load-deflection plot for a specimen manufactured with PETG neat resin and for a specimen manufactured with EAA. As shown in Figure 25, the change in slope from pre to post impact for the PETG neat resin specimen is much greater than that of the EAA specimen, implying that the change in compliance was greater for PETG neat resin specimens than EAA specimens.

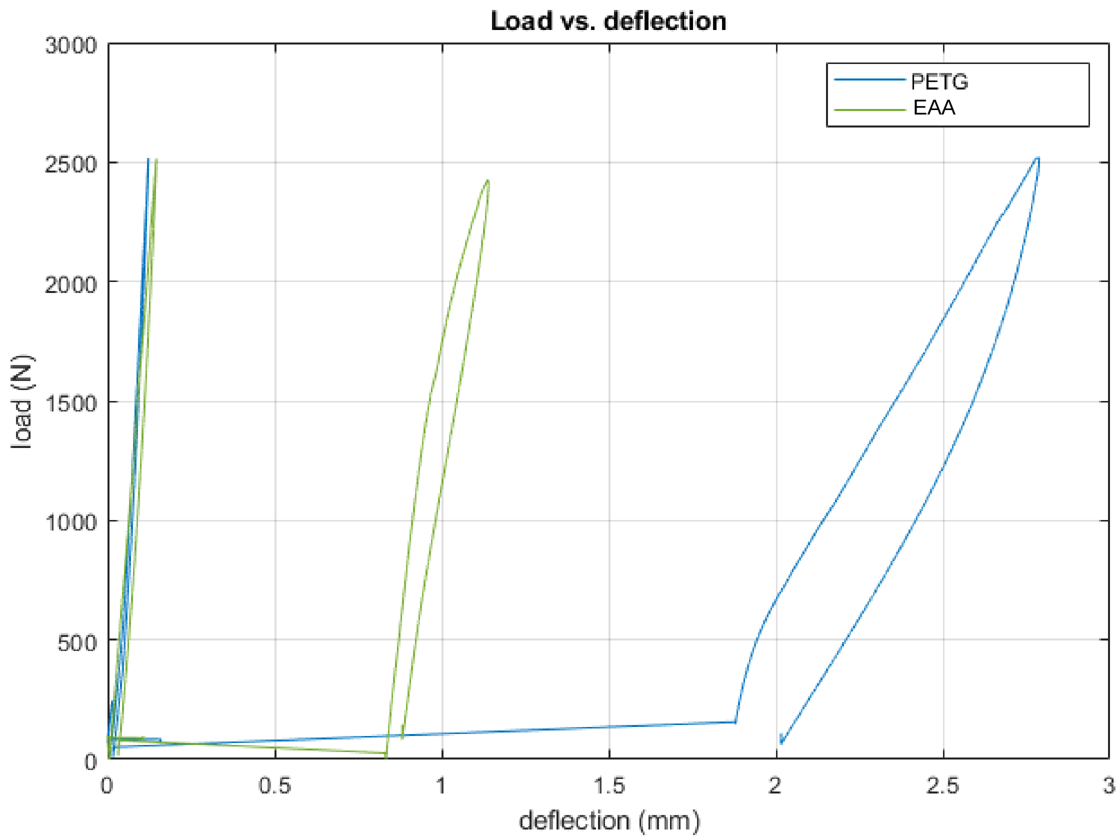

Figure 25: Load-displacement plot comparing the change in compliance of the EAA and PETG neat resin specimens.

A summary of the change in compliance data is presented in Table 9 including the average, standard deviation, and COV for each adhesive type and consolidation pressure. Figures 26 presents the average change in compliance based on adhesive type and consolidation pressure, and Figure 27 presents the percent change in compliance for each individual panel. It should be noted that panels SUR2 and SUR6 are not shown in Figures 26 and 27. Due to a manufacturing error, these panels were delaminated prior to testing and were not used. The quasi-static data including change in compliance and residual deflection for each specimen can be found in Appendix A.

Table 9: Summary of Change in Compliance Data

Adhesive Type	Consolidation Pressure (psi)	Average (mm/kN)	Standard Deviation (mm/kN)	COV (%)
PETG neat resin	80	1.03	0.350	34
	100	0.92	0.313	34
EAA	80	0.18	0.136	74
	100	0.13	0.154	114

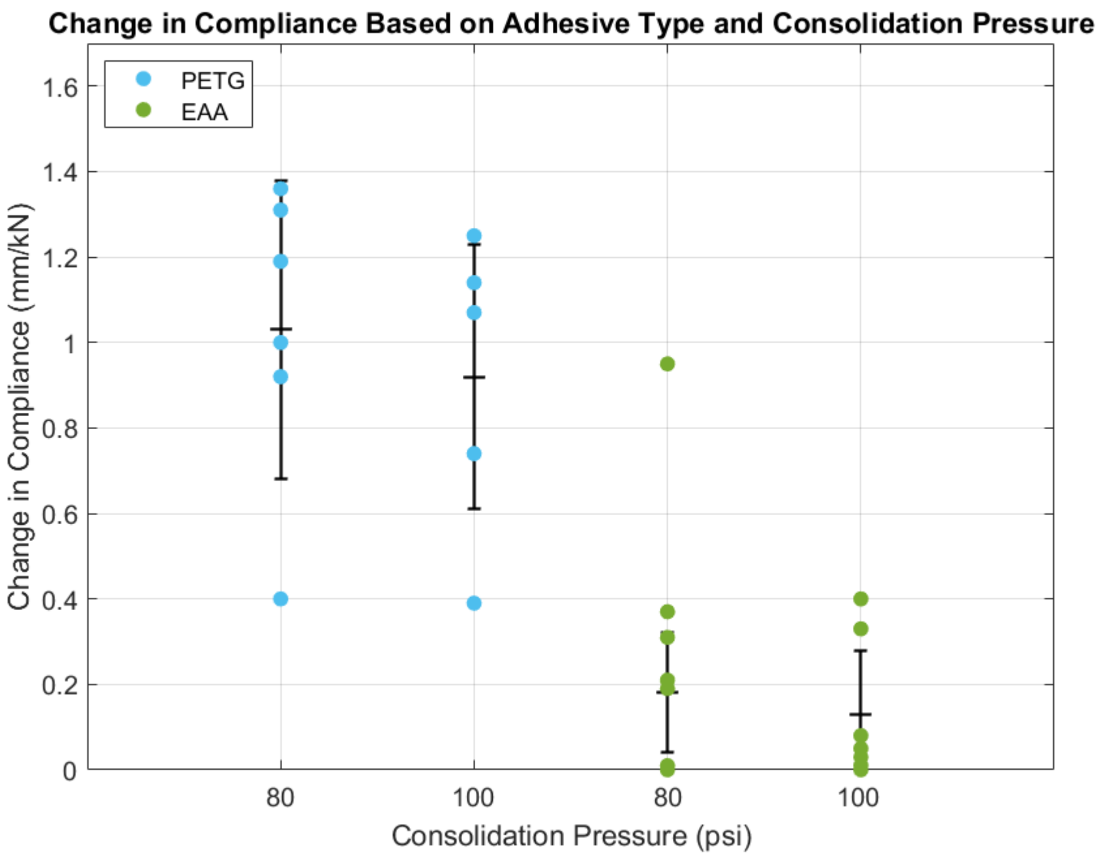

Figure 26: Change in compliance of each panel based on adhesive type and consolidation pressure.

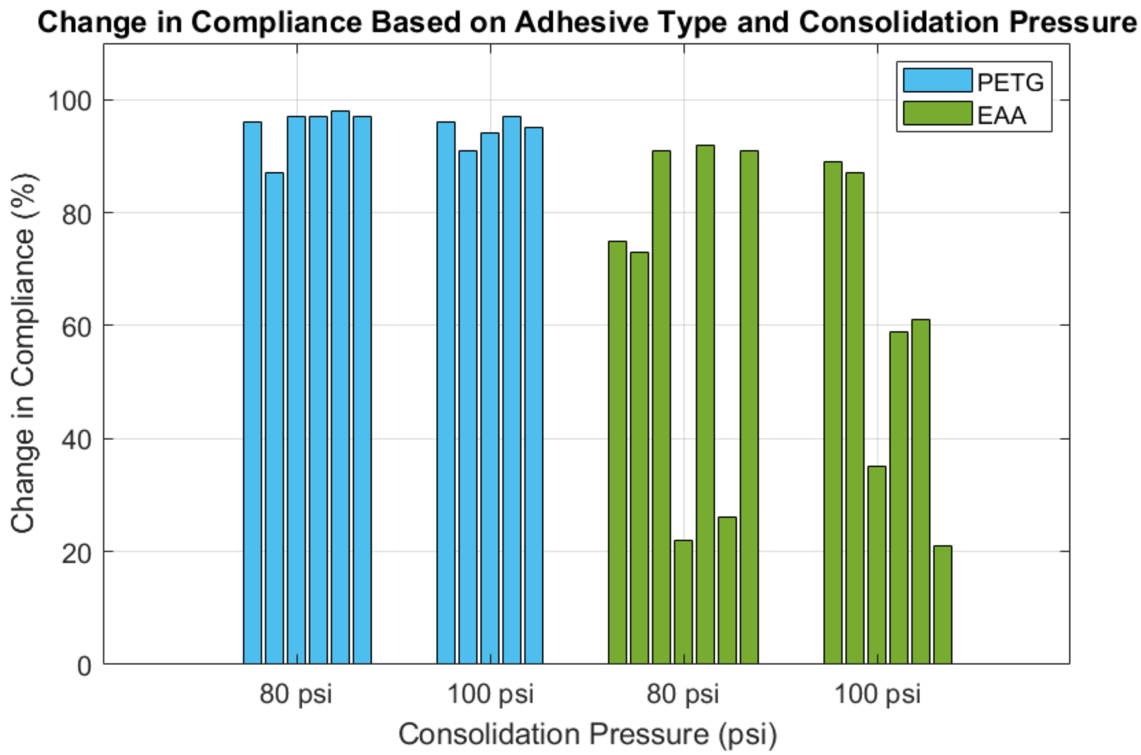

Figure 27: Percent change in compliance based on adhesive type and consolidation pressure.

Looking at Table 9 and Figure 26, it is highly evident that the specimens manufactured with EAA had a smaller change in compliance than the specimens manufactured with PETG neat resin. The average change in compliance increased by 472% from the EAA specimens to the PETG neat resin specimens for a consolidation pressure of 80 psi. The average change in compliance increased by 608% from the EAA specimens to the PETG neat resin specimens for a consolidation pressure of 100 psi. This trend can further be seen in Figure 27, as majority of the percent changes in compliance were far less for the EAA panels than for the PETG neat resin panels. All PETG neat resin specimens had a change in compliance close to 100%, meaning that the compliance nearly doubled from pre to post impact. Some EAA specimens had a high change in compliance of around 90%, but many of the specimens had changes in compliance significantly less. One EAA specimen manufactured at 100 psi even had a 0% change in compliance, which cannot be shown in Figure 27 but should be noted. Since compliance is a measure of impact damage, it can be concluded from this data that the EAA specimens experienced less damage during impact, resulting in a small change in stiffness and compliance. It can also be inferred that the EAA resin has a greater level of ductility than the PETG neat resin, as it dissipated a greater amount of energy than the PETG neat resin. It should be noted however that the EAA resin sheets were double the thickness of the PETG neat resin sheets, as reported in Table 4. Thicker adhesive sheets have been shown to decrease shear stress on the adhesive layer, allowing it to avoid failure and decrease fragmentation of the brittle core under impact, increase energy absorption of the back face sheet, and transfer stresses from the core to the reinforcement under impact (Lo´pez-Puente, et al., 2005). While these results show that EAA performed better under impact than PETG neat resin, the difference in adhesive thickness should be taken into consideration.

The effect of consolidation pressure on change in compliance was not significant. Looking at Table 9 and Figure 26, the panels manufactured with PETG neat resin had a relatively greater change in compliance for panels consolidated at 80 psi than those consolidated at 100 psi. The average change in compliance for PETG neat resin panels consolidated with pressures of 80 and 100 psi was 1.03 and 0.92 mm/kN, respectively. Similarly, for the panels manufactured with EAA, those consolidated at 80 psi had a greater change in compliance than those consolidated at 100 psi. The average change in compliance for EAA panels consolidated with pressures of 80 and 100 psi was 0.18 and 0.13 mm/kN, respectively. It seems as though the panels consolidated with 100 psi performed slightly better than those consolidated with 80 psi, but the difference is small.

The data for change in compliance was relatively variable, specifically for the EAA specimens. Looking at Table 9, the standard deviation of the change in compliance data was less for the EAA specimens, however, the COV was much greater for the EAA specimens. The variability of the EAA specimens is also shown in Figure 27. The EAA specimens had far more variability than the PETG neat resin specimens. The variability of the data is most likely due to the manufacturing process of the thermoplastic-reinforced UHPC sandwich panels. The panels were not continuously heated during consolidation, causing a non-uniform temperature gradient throughout the panel. This can cause non-uniform bonding of the thermoplastic laminate to the concrete. In other words, some areas of the panel may have been better bonded than others, leading to high variability of specimens within the same panel. Nevertheless, the EAA specimens had a more favorable baseline than the PETG neat resin specimens. Even though the COV was smaller for PETG specimens, Figure 27 shows that the change in compliance of the PETG panels was consistently high. The EAA specimens had a larger COV, however, these specimens showed to have a smaller change in compliance than the PETG neat resin specimens.

4.3.2.2 Residual Deflection

Residual deflection is defined by the deflection from an applied load which remains after the load is removed. Residual deflection was considered as a measurement of impact damage in this study and was determined by finding the difference in displacement from pre to post impact, as shown in Figure 28.

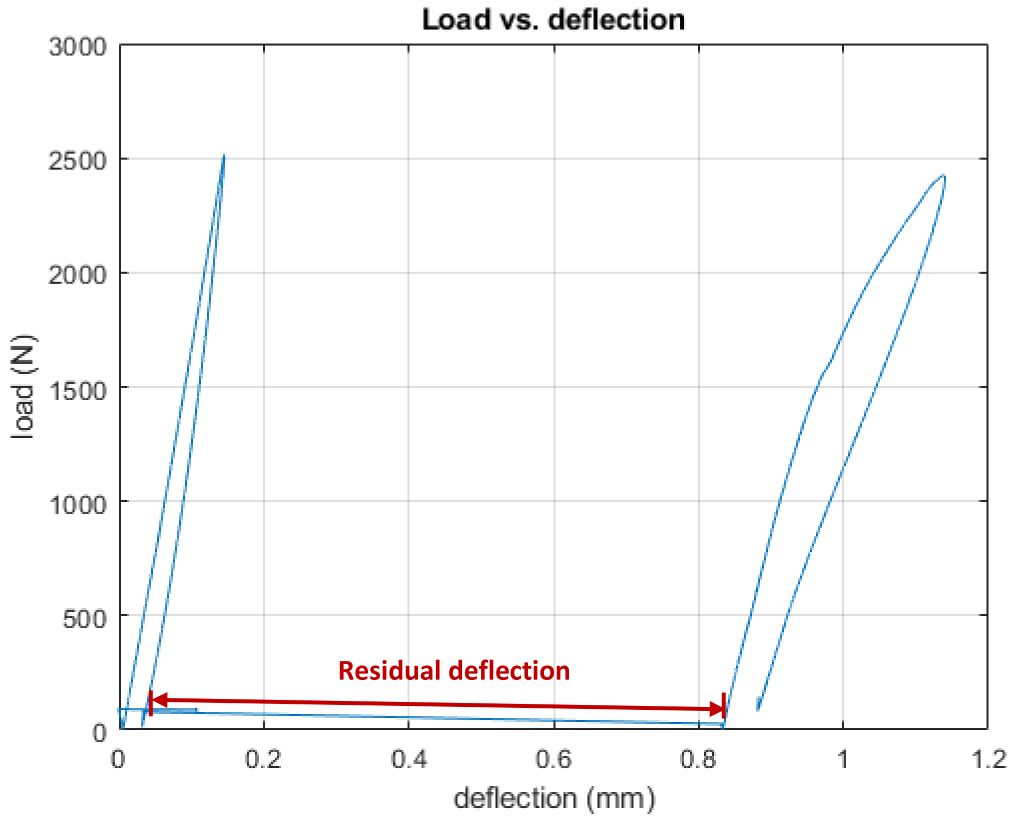

Figure 28: Load-deflection plot showing residual deflection.

Figure 29 presents the average residual deflection of each panel. Looking at Figure 29, it is highly evident that the residual deflection of the PETG neat resin specimens was greater than that of the EAA specimens. The average residual deflection for all EAA specimens was 0.81 millimeters, while that of the PETG neat resin specimens was 2.29 millimeters. This is a 183% increase in residual deflection from the EAA to the PETG neat resin specimens.

The effect of consolidation pressure on residual deflection was not entirely clear. The average residual deflection of the PETG neat resin specimens was higher for a consolidation pressure of 100 psi. However, the average residual deflection of the EAA specimens was higher for a consolidation pressure of 80 psi. No conclusion can be drawn regarding the consolidation pressure’s effect on residual deflection.

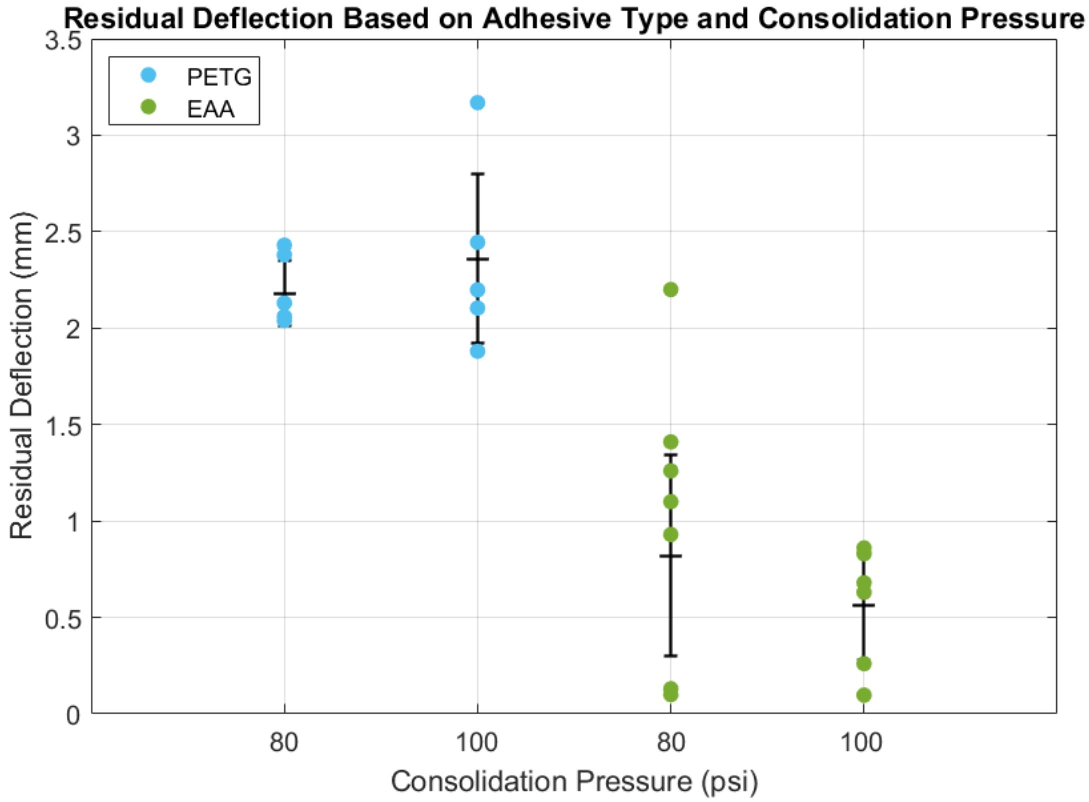

Figure 29: Average residual deflection of each panel based on adhesive type and consolidation pressure.

4.3.3 Low-Velocity Impact Testing

The Visual IMPACT software from the CEAST 9350 impact drop-tower provided measurements of force, impact energy, velocity, and displacement. Impact force was the main parameter of interest and was used as a measure of initial compliance. It should be noted that the impact force obtained from the tup does not represent the actual impact force applied to the panel due to inertial effects (Fujikake, et al., 2013), i.e. a portion of the impact load is used to accelerate the specimen from its resting position to the direction opposite the acceleration. Figure 30 presents the force-time plots of two PETG neat resin impact plates, P4-6 and P1-7, and two EAA specimens, SUR5-7, and SUR5-8 under impact. It typically took the EAA specimens a longer amount of time to reach their peak impact force. The impact force of the EAA specimens was also generally larger than the impact force of the PETG neat resin specimens.

This is most likely due to the higher impact resistance of the top EAA adhesive layer compared to the top PETG neat resin layer. The resistance of the laminate and EAA adhesive slowed down the impactor, resulting in a spike in load (Aryal., et al., 2019). The higher peak impact force for the EAA specimens indicates that this adhesive was more well-suited for impact loads than the PETG neat resin.

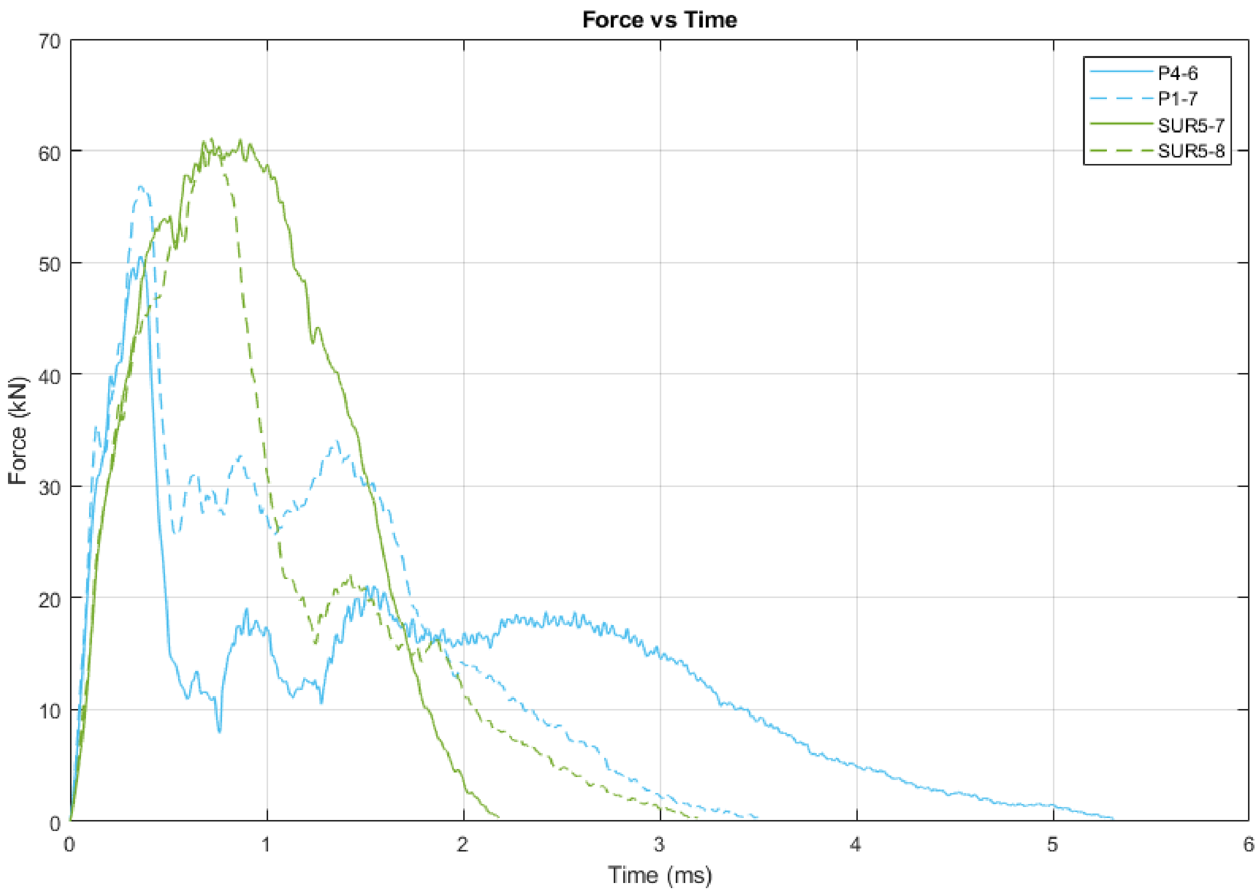

Figure 30: Typical Force-Time plots for the thermoplastic-reinforced UHPC panel impacts for both PETG neat resin and EAA adhesives.

Figure 31 presents the maximum impact force recorded for each panel under impact. The average maximum impact force for EAA panels and PETG neat resin panels was 49.4 and 56 kN, respectively. The maximum force was about 13% greater for the EAA specimens than that of the PETG neat resin specimens. Panel SUR8 had the greatest maximum impact force of 67.9 kN. This is 24% greater than the maximum impact force of PETG neat resin specimens of 54.7 kN for panel P1.

Looking at Figure 31, there is not a clear trend between consolidation pressure and maximum impact force. There was a large amount of scatter in the data. The standard deviations of the PETG neat resin specimens with consolidation pressures of 80 and 100 psi were 2.58 and 12.0 kN, respectively. The standard deviations of the EAA specimens with consolidation pressures of 80 and 100 psi were 9.27 and 8.05 kN, respectively. This high variability is most likely due to the manufacturing process of the specimens, as mentioned previously. The variability could also be due to an error in the CEAST 9350 impact machine.

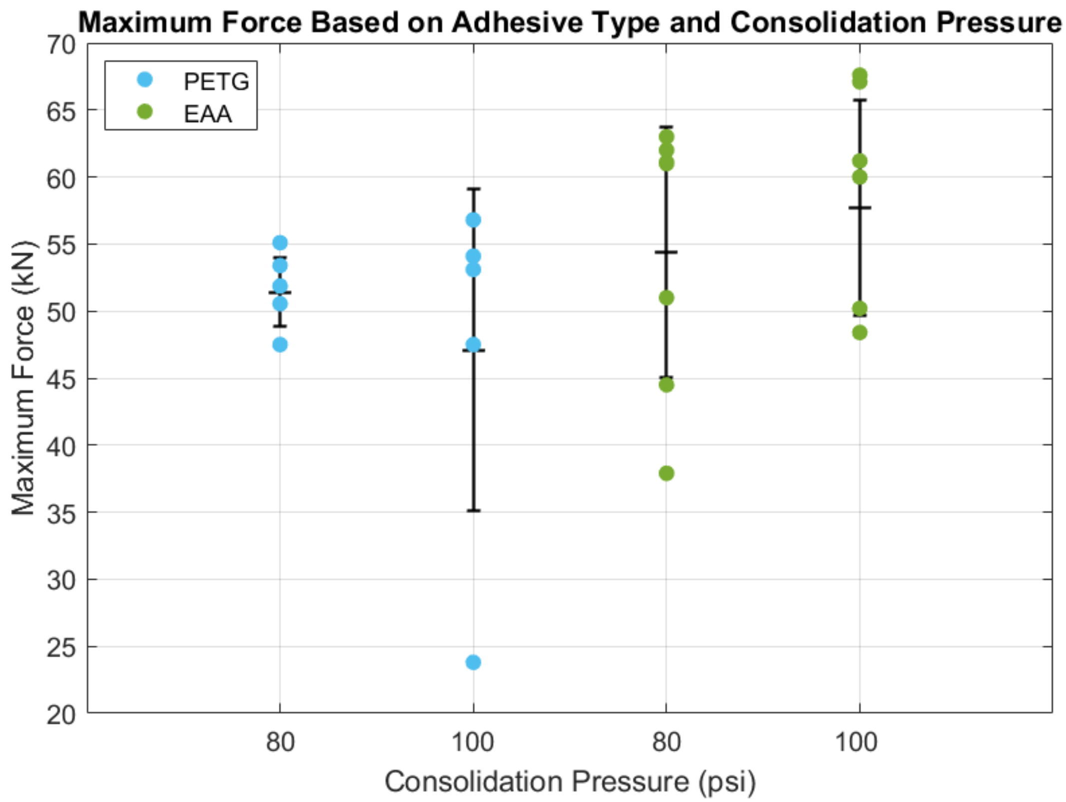

Figure 31: Maximum impact force recorded of each panel based on adhesive type and consolidation pressure.

4.4 Summary and Conclusions

The impact tests revealed that the EAA adhesive generally performs better under impact than the PETG neat resin. The EAA adhesive resulted in a smaller and more confined area of delamination, a smaller change in compliance, a smaller residual deflection, and a larger maximum impact load than the PETG neat resin. The rear thermoplastic skin rarely debonded from the back face of the UHPC panel when bonded with EAA. The rear thermoplastic skin almost always debonded from the back face of the UHPC panel when bonded with PETG neat resin. One cause of concern is the difference in thickness of the adhesives. The EAA adhesive was 0.125 inches thick while the PETG neat resin was 0.0625 inches thick. The thickness of the EAA was double that of the PETG neat resin, which could have enhanced its ability to perform under impact. Therefore, this data does not provide a direct comparison between the EAA and PETG neat resin. In future work, UHPC-thermoplastic panels should be manufactured with EAA and PETG neat resin adhesives with the same thickness. EAA resin sheets were only commercially available at a minimum thickness of 0.125 inches, but this should be further investigated in the future. If EAA adhesive sheets can't be purchased at a thickness of 0.0625 inches, two options should be considered. Option 1 would require two PETG neat resin adhesive sheets to be used per panel side to achieve an adhesive thickness equal to that of the EAA. Option 2 would require melting the EAA adhesive sheets prior to consolidation which would cause the resin sheet to expand and minimize in thickness.

CHAPTER 5

UHPC-THERMOPLASTIC BOND ANALYSIS

The most widely used tests to analyze the bond between concrete and FRP are bending tests and single-lap shear tests. The literature review presented in Chapter 2 revealed that bending tests are most representative of how the bond responds to flexural loads. The literature review also revealed that single-lap shear tests are the most common test method to acquire a quantitative bond-strength of the concrete and FRP. The following sections will discuss the experimental procedures, results, discussion, and conclusions of these tests.

5.1 Introduction

The bond between the thermoplastic laminate and UHPC core is the most crucial part of the composite system. Studies have shown that the most common failure mode of externally bonded FRP composites to concrete is premature FRP debonding from the concrete substrate (Franco & Royer-Carfagni, 2014). It is important to understand the behavior of the bond between FRP and concrete so that it can be optimized. Optimization of this bond will ultimately result in better impact performance of the entire composite system.

Results from the low-velocity impact tests revealed that EAA exhibited greater ductility and the ability to protect the UHPC core under impact more so than the PETG neat resin. A quantitative measurement was necessary to understand how the EAA and PETG neat resin affect the bond between the thermoplastic laminates and UHPC. To achieve this, concrete-thermoplastic bond tests were performed.

Initially, three-point bending tests were utilized in this study to test the bond between UHPC and thermoplastic laminates due to their simplicity and because these tests provide a more realistic behavior of the bond in flexure. As mentioned in Section 2.1, UHPC exhibits flexural behavior under impact, so it seemed most appropriate to test the sandwich composite in flexure. Testing revealed that the bond exhibited a more ductile behavior in bending than a brittle one. The typical failure mode of the beam specimens was shear cracking of the concrete that propagated to the concrete-adhesive interface and resulted in debonding of the adhesive and laminate from the concrete. The bond between the laminate and concrete did not fail before the concrete itself. To further investigate the bond between UHPC and the thermoplastic laminate, direct single-lap shear tests were performed.

The following chapter will first discuss the experimental procedure and results of the three-point bending tests. The main results acquired from these tests were energy dissipation and maximum bond strength. The manufacturing process, experimental procedure, and relevant results will then be discussed for the direct single-lap shear tests.

5.2 Three-Point Bending

Three-point bending tests were performed on thermoplastic-UHPC sandwich beams. The following subsections will discuss the experimental procedure, results, and discussion of the three-point bending tests.

5.2.1 Experimental Procedure

A total of (53) UHPC-thermoplastic sandwich beams were tested in three-point bending. 5.75” x 1” beams were cut from the 12” x 12” UHPC thermoplastic-reinforced sandwich panels, as shown in Figure 14. Figure 32 shows a typical sandwich beam specimen.

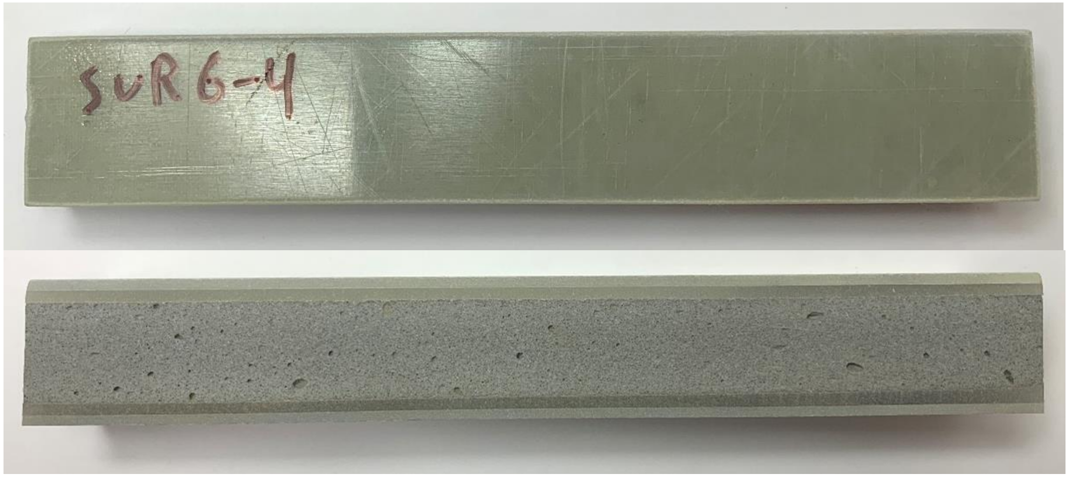

Figure 32: Top and side view of a UHPC thermoplastic-reinforced sandwich beam specimen.

On average, five beams were cut from each panel. However, due to the concrete sliding that occurred during consolidation of the EAA specimens, some of the 12” x 12” sandwich panels were extremely misaligned. As a result, not all beam specimens cut from each panel were salvageable and testable. Table 10 presents the number of beams that were testable from each 12” x 12” sandwich panel.

Table 10: Number of Beams Tested from Each Consolidated Sandwich Panel

Panel Name	**Adhesive Type**	**Consolidation Pressure (psi)**	**Concrete Type**	**No. of Testable Beams**
P1	PETG	100	UM	5
P2	PETG	100	UM	5
P3	PETG	80	UM	5
P4	PETG	80	UM	5
SUR1	EAA	100	ERDC	5
SUR2	EAA	80	ERDC	3
SUR3	EAA	80	UM	5
SUR4	EAA	80	UM	5
SUR5	EAA	80	UM	5
SUR6	EAA	100	UM	0
SUR7	EAA	100	UM	4
SUR8	EAA	100	UM	6

Prior to testing, each beam was measured for average width, average depth, average length, and mass. Beam specimens were tested using a 5-kN servo-hydraulic Instron. Two external LVDTs were used to measure the deflection of the beams at midspan. A thin aluminum plate was placed between the load head and the beam specimen to act as the contact surface for the LVDTs during testing. A preload of about 300 N was set on the specimen and the LVDTs were adjusted to read a small displacement prior to beginning the test. The beam span measured 140 mm. The specimens were loaded in displacement control at a rate of 0.5 mm per minute until failure. Figure 33 shows a beam in flexure in the three-point bending test setup.

Figure 33: Beam specimen in the three-point bending test setup.

5.2.2 Results and Discussion

Test results of the three-point bending tests including major failure modes, energy dissipation, and bond strength of the thermoplastic-UHPC sandwich beams are reported in the following subsections.

5.2.2.1 Failure Modes

Two main failure modes existed in the three-point bending tests. The dominating failure mode of the thermoplastic-reinforced UHPC beams was shear failure of the concrete, as shown in Figure 34.

Figure 34: Typical concrete shear failure of the beams.

Specimens that underwent this failure mechanism initially experienced interlaminar cracking in the thermoplastic laminate and a small shear crack in the concrete. As the load increased, this shear crack propagated towards the bottom concrete-adhesive interface and grew along this interface until it reached the edge of the beam. The laminate and adhesive debonded from the concrete beam, ending the test. Note that this is the same failure mode that was seen in the low-velocity impact tests. Figure 35 presents a typical load-deflection plot of the beam specimens that failed in concrete shear, leading to debonding of the thermoplastic laminate and adhesive from the concrete. As shown in Figure 35, there are small drops in load at the beginning of the test. These drops represent the small interlaminar cracking of the thermoplastic laminate. The load increases until a large shear crack grows in the specimen, resulting in a sudden drop in load. The laminate then debonds from the specimen and the specimen is unloaded.

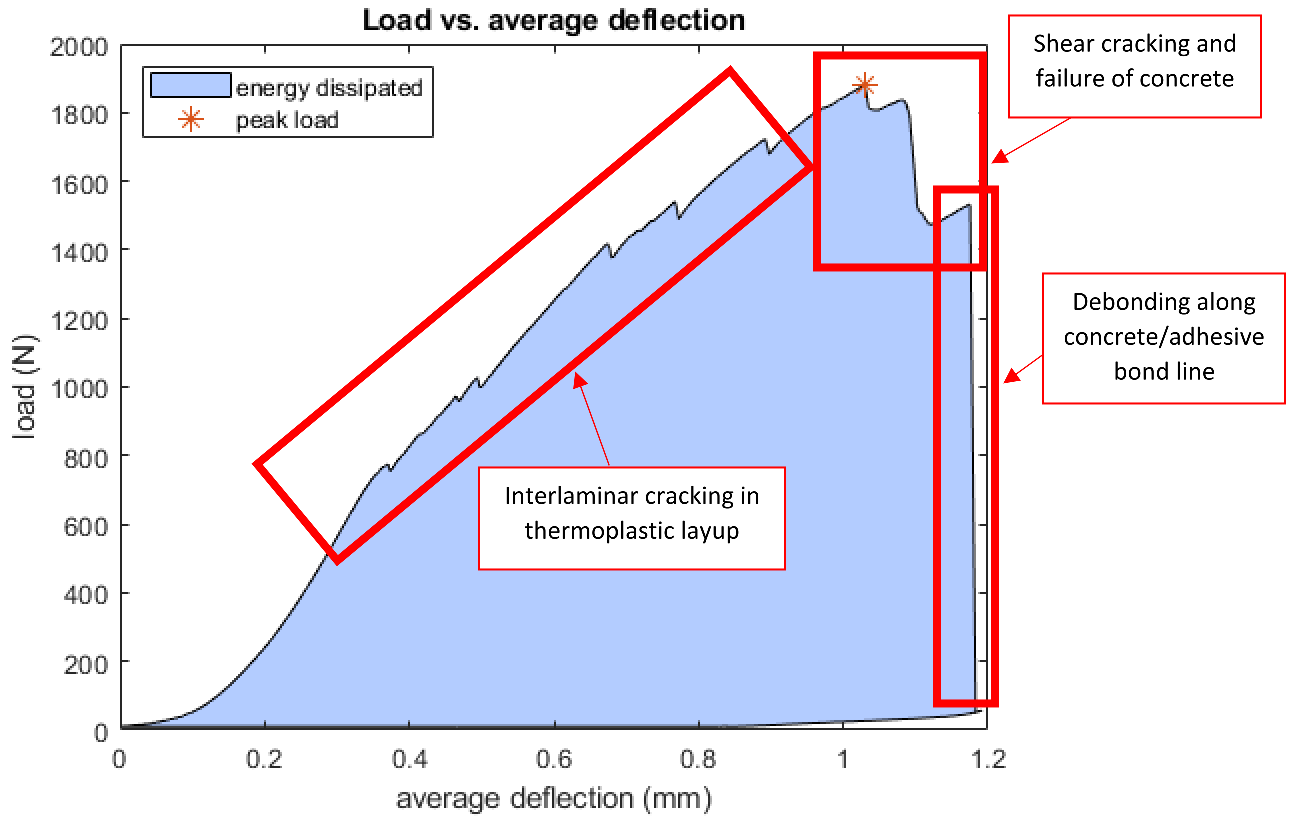

Figure 35: Typical load-displacement plot of concrete shear cracking failure mode.

The second main failure mode was debonding of the thermoplastic laminates from the adhesive and concrete. This failure mode only occurred in specimens manufactured with EAA. These particular specimens typically experienced laminate debonding before the concrete even cracked, indicating that the bond area between the layup and EAA adhesive was poor. A poor bond area can be seen in Figure 36. The light spots on the left edges of the beams were totally unbonded areas between the EAA resin and the thermoplastic laminate. These poorly bonded areas appeared in panels SUR5 and SUR6 following waterjet cutting of the panels, indicating that the debonded areas were due to a manufacturing error. Data was acquirable from panel SUR5 but not from panel SUR6. As a result, the data from panel SUR6 were not considered in this study.

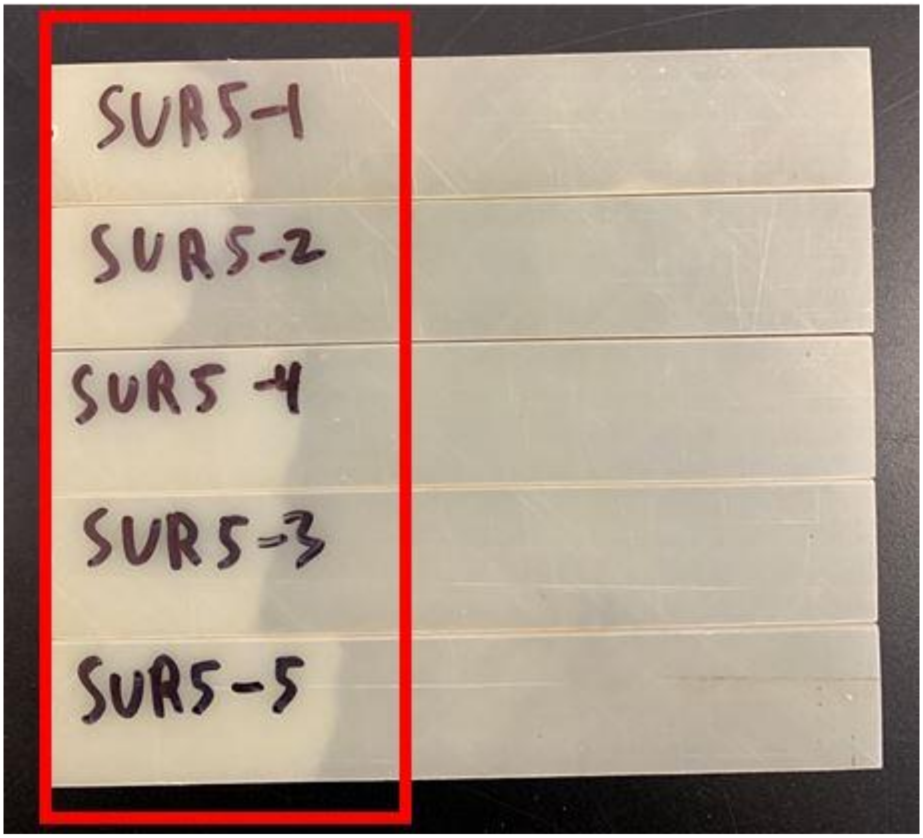

Figure 36: Poorly bonded area between thermoplastic laminate and EAA.

5.2.2.2 **Energy Dissipation**

UHPC has been shown to exhibit flexural failure when tested under impact (Verma, et al., 2016; Ranade, et al., 2017). A parameter of interest when conducting impact tests is the amount of energy dissipated by the specimen. To simulate this, the energy dissipated was calculated for the thermoplastic-reinforced UHPC beams under flexure. The energy dissipated was calculated by finding the area under the load-deflection curve, as shown in Figure 35. Figure 37 presents the average energy dissipated for each panel.

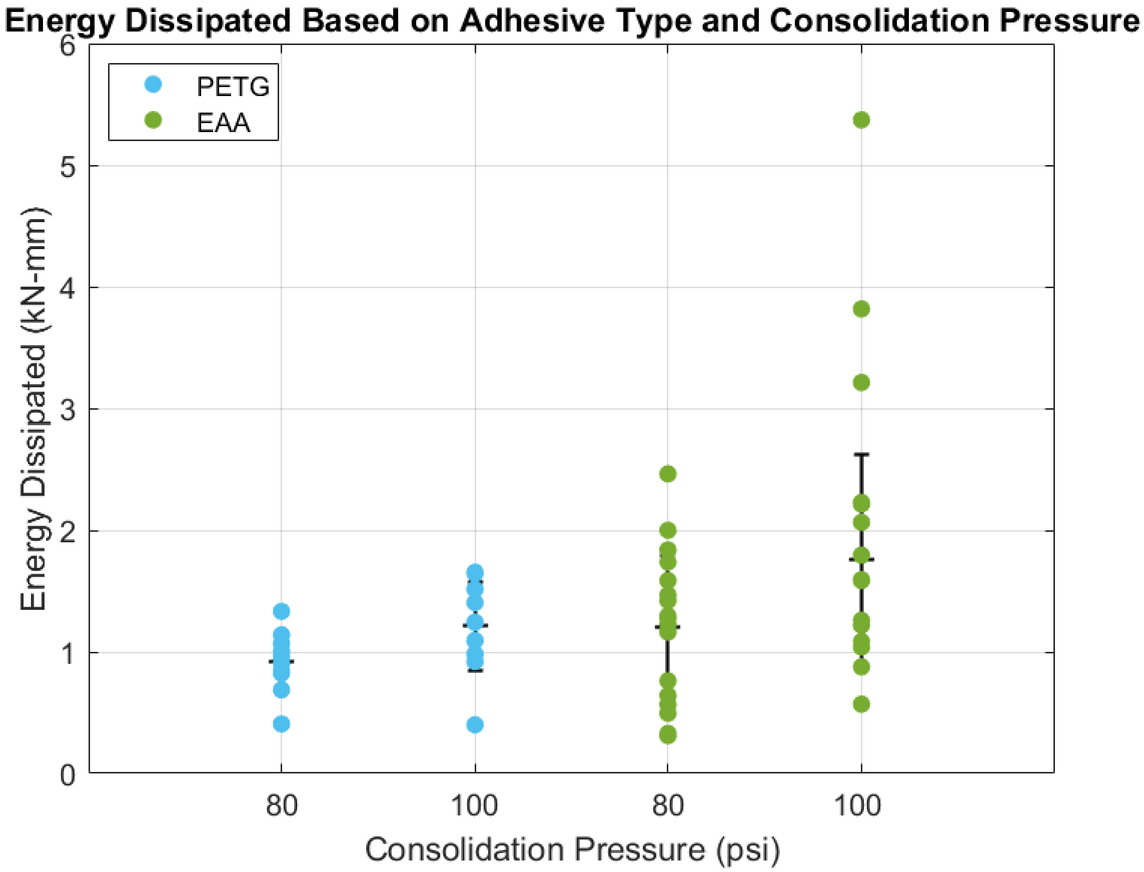

Figure 37: Energy Dissipated Based on Adhesive Type and Consolidation Pressure

The average energies dissipated by the PETG neat resin specimens at consolidation pressures of 80 and 100 psi were 0.917 and 1.21 kN-mm, respectively. Those of the EAA specimens at 80 and 100 psi were 1.21 and 1.75 kN-mm, respectively. On average, the bond strength of the EAA specimens was 32% and 44.6% greater than the PETG neat resin specimens for consolidation pressures of 80 and 100 psi, respectively. Additionally, the bond strength of specimens manufactured with a consolidation pressure of 100 psi within the same adhesive was greater than those manufactured with 80 psi. For the PETG neat resin specimens, the bond strength was 32% greater for specimens consolidated at 100 psi than those consolidated at 80 psi. For the EAA specimens, the bond strength was 45% greater for those manufactured at 100 psi than those manufactured at 80 psi. There was an upper outlier for the EAA specimens at a consolidation pressure of 100 psi, with an energy dissipation of 5.37 kN-mm. The variability in the data was greater for specimens manufactured with EAA. For EAA specimens manufactured at 80 and 100 psi, the standard deviation of the data was 0.586 and 0.872 MPa, respectively. For PETG neat resin specimens manufactured at 80 and 100 psi, the standard deviation of the data was 0.242 and 0.364 MPa, respectively. The variability in the EAA data is most likely due to the variability in the manufacturing process of the specimen, as mentioned in previous sections. Regardless of the high variability, the EAA specimens, on average, showed higher energy dissipation. Greater values of energy dissipation indicate a greater level of ductility and better impact performance.

5.2.2.3 Bond Strength

Since there was no brittle failure along the UHPC and thermoplastic bond line, a fracture mechanics approach to bond characterization was deemed inappropriate, and a strength-based approach was used. The maximum bond strength of the UHPC-thermoplastic bond was calculated along the UHPC-adhesive bond line using Equation 1.

Equation 1: Maximum bond shear strength for a composite beam.

$$\tau_{max} = \frac{VQ_{tr}}{I_{tr}t}$$

Where τ_{max} = maximum shear stress in the UHPC-thermoplastic bond (MPa); *V* = peak shear force (N); Q_{tr}= transformed first moment of area between the location of where the shear stress is being calculated and the neutral axis of specimen (mm^3); I_{tr} = transformed moment of inertia of the cross section (mm^4); t= width of the cross section (mm).

The three-material composite beam was transformed into the same material. The PETG thermoplastic laminates and adhesive sheets were transformed into UHPC based on their stiffnesses provided in Table 4. The elastic modulus of the UHPC was estimated using Equation 2 developed by Ma et al. for UHPC containing no coarse aggregates, where E_c is the elastic modulus of the concrete (psi) and f'_c is the compressive strength of the concrete (psi) (Ma, et al., 2004; Ma & Schneider, 2005). Figure 38 presents the normal cross section and the transformed cross section of the composite beam. I_{tr} and Q_{tr} were found using the transformed section, and t was taken as the width of the UHPC.

Equation 2: Elastic modulus of UHPC containing no coarse aggregate

$$E_c = 525{,}000\ (\frac{f'_c}{10})^{1/3}$$

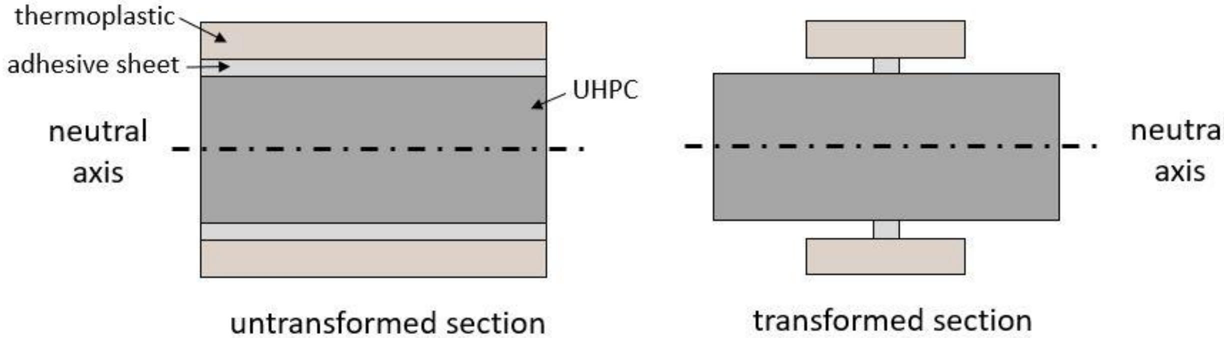

Figure 38: Untransformed and transformed section used to find bond shear stress.

The maximum shear stress in the bond line will be referred to as the maximum bond strength from hereafter. Table 11 presents a summary of the maximum bond strength data based on adhesive type and consolidation pressure. Figure 39 presents the maximum bond strength of the UHPC-thermoplastic beams based on their adhesive type and consolidation pressure.

Table 11: Summary of Maximum Bond Strength Data

Adhesive Type	Consolidation Pressure (psi)	Average (MPa)	Standard Deviation (MPa)	COV (%)
PETG	80	0.554	0.104	19
	100	0.668	0.125	19
EAA	80	0.555	0.142	26
	100	0.840	0.154	18

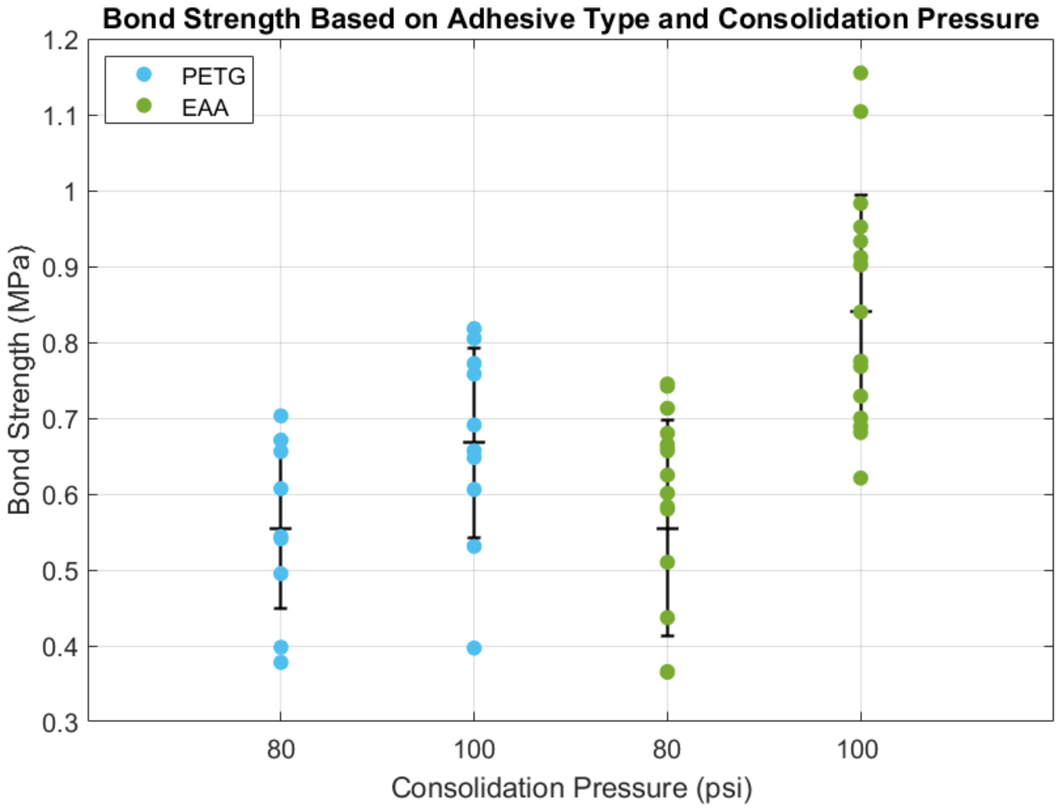

Figure 39: Maximum bond strength based on adhesive type and consolidation pressure

On average, the bond strength of the PETG and EAA specimens for a consolidation pressure of 80 psi was about the same. For a consolidation pressure of 100 psi, the EAA specimens on average had a greater bond strength than the PETG neat resin specimens by 26%.

Additionally, the bond strength of specimens manufactured with a consolidation pressure of 100 psi within the same adhesive was greater than those manufactured with 80 psi. For the PETG neat resin specimens, the bond strength was 21% greater for specimens consolidated at 100 psi than those consolidated at 80 psi. For the EAA specimens, the bond strength was 51% greater for those manufactured at 100 psi than those manufactured at 80 psi.

The variability in the data was greater for specimens manufactured with EAA, as shown in Table 11. Both the standard deviation and COV was greater for EAA. This is most likely due to the manufacturing process and the overheating of the EAA resin. It is possible that there was resin bleed out during consolidation which affected the bond strength within these panels. Nevertheless, on average, the EAA specimens showed a higher bond strength in flexure than the PETG neat resin specimens.

5.3 Direct Single-Lap Shear

To further investigate the bond between UHPC and thermoplastic laminates, a series of direct single-lap shear tests were performed. The following subsections will discuss the manufacturing process of the single-lap shear specimens, experimental procedure, results, and conclusions of the single-lap shear tests.

5.3.1 Manufacturing

Typical concrete-FRP single-lap shear tests are conducted using rectangular concrete blocks (Mazzotti, et al., 2009; Khshain, et al., 2015). Blocks could not be fabricated from the panels used in previous work, as the depth of the panels was far too thin. As a result, a new manufacturing process was developed to fabricate single-lap shear specimens. A total of (8) 6” x 10” x 3” UHPC blocks were cast at the University of Maine using the same mix proportions presented in Section 3.1.1. Each batch of UHPC produced (1) UHPC block and (3) 2 in cubes for compressive testing. The block and cubes were placed in a wet room for 24 hours at 24°C and 95% humidity and then removed from their molds. The specimens were then placed in a hot water bath at 70°C for 7 days. Studies have shown that hot water baths greatly accelerate curing time of concrete specimens. Among four curing regimes: ambient air curing, hot air curing, hot water bath curing, and boiling water curing, hot water baths have shown to produce the highest concrete compressive strength (Hiremath & Yaragal, 2017). The optimum temperature range for accelerated concrete strength development was reported as 74°C to 82°C (McGhee, 1970), and it was found that concrete cured in a hot water bath at 75°C achieved 70% of its 28-day strength in just one day (Ramakrishnan & Dietz, 1975). Therefore, 70°C was a reasonable temperature to cure the concrete blocks at. The setup of the hot water bath is shown in Figure 40.

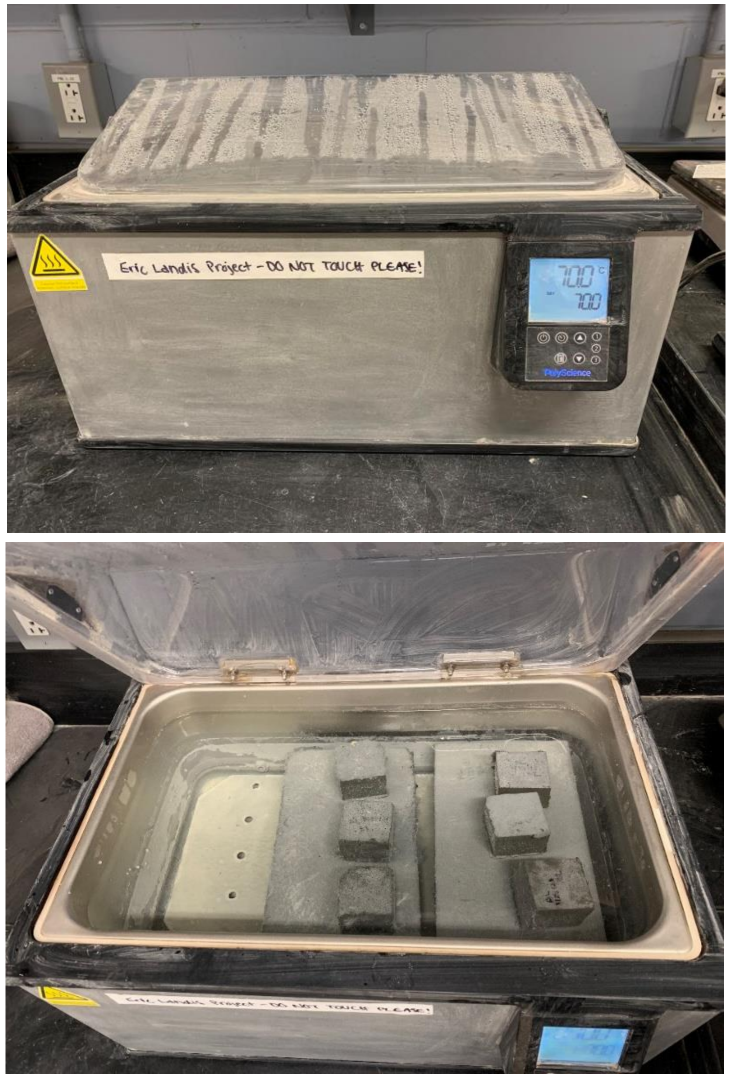

Figure 40: Hot water bath to accelerate curing process of UHPC blocks.

Once the specimens were cured, the concrete cubes were tested in compression per ASTM C109. The average compressive strength of the cubes is presented in Table 12.

Table 12: Average Compressive Strength of UHPC used for Single-Lap Shear Testing

Average Batch Compressive Strength (MPa)	Standard Deviation (MPa)	COV (%)	Specimen Size and Type
124	12.0	10	2 in cubes

The next step in the specimen development process was bonding of the thermoplastic laminates to the UHPC blocks. The surfaces of the concrete blocks were first roughened using a 4-inch wire diamond wheel, and the specimens were blown with pressurized air to remove any dust. The thermoplastic laminates used for the single-lap shear specimens consisted of the same layup as the thermoplastic-reinforced UHPC sandwich panels, mentioned in Section 3.2. The 12” x 12” laminates were pre-consolidated at a temperature of 165°C and an effective pressure of 100 psi prior to bonding them to the concrete. The laminates were then cut into the shape shown in Figure 41 using a waterjet. The intent of this shape was to create FRP strips for single-lap shear tests.

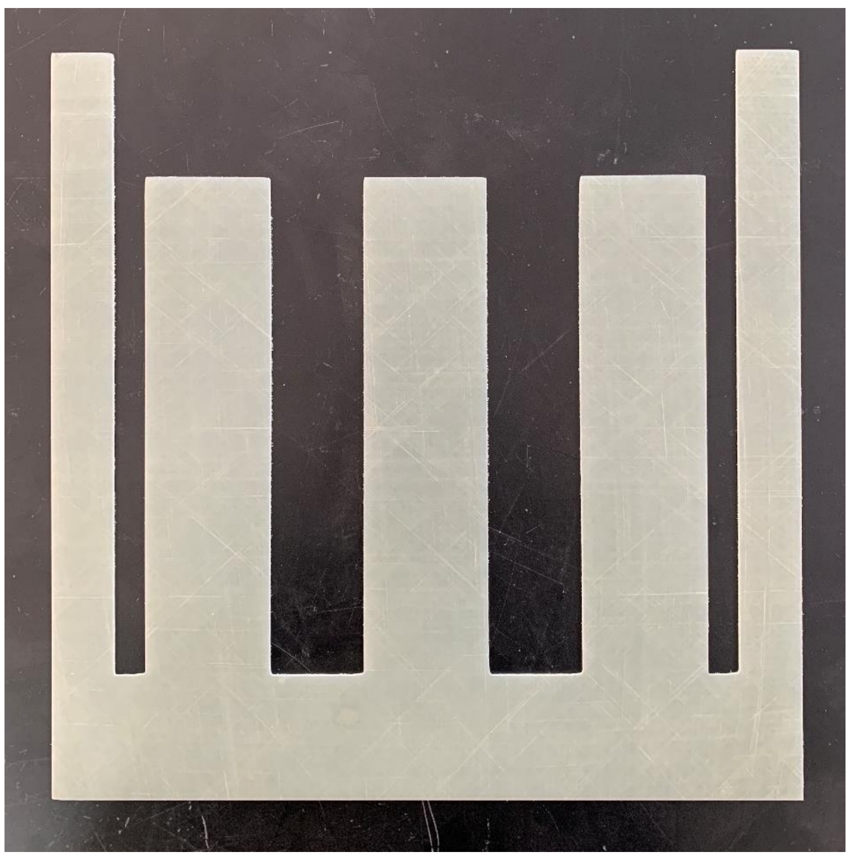

Figure 41: Waterjet-cut thermoplastic laminates for single-lap shear specimens.

A thermoplastic laminate was bonded to one side of the concrete block using the same stamp thermoforming procedure discussed in Section 3.2. The test parameters considered were adhesive type and consolidation pressure, as in the impact testing and three-point bending. The consolidation test matrix is shown in Table 13. Each consolidation was designed to produce three specimens for single-lap shear testing.

Table 13: Consolidation and Test Matrix of Single-Lap Shear Specimens

Specimen ID	**Adhesive Type**	**Consolidation Pressure (psi)**	**No. of Consolidations**	**No. of Single-Lap Shear Testing Specimens**
P1_80 and P2_80	PETG Neat Resin	80	2	6
P1_100 and P2_100		100	2	6
SUR1_80 and SUR2_80	EAA	80	2	6
SUR1_100 and SUR2_100		100	2	6

The stacking setup for heating of the single-lap shear specimen is shown in Figure 42. The concrete block was offset from the laminate so that the laminate tabs overhung the concrete. A 4-inch wide adhesive sheet was placed in between the concrete and the laminate. The entire setup was placed on a 12” x 12” aluminum caul sheet for easy transfer from the oven to the press. Chemlease 41-90 was applied to the caul sheet to prevent the laminate and adhesive sheet from adhering to it.

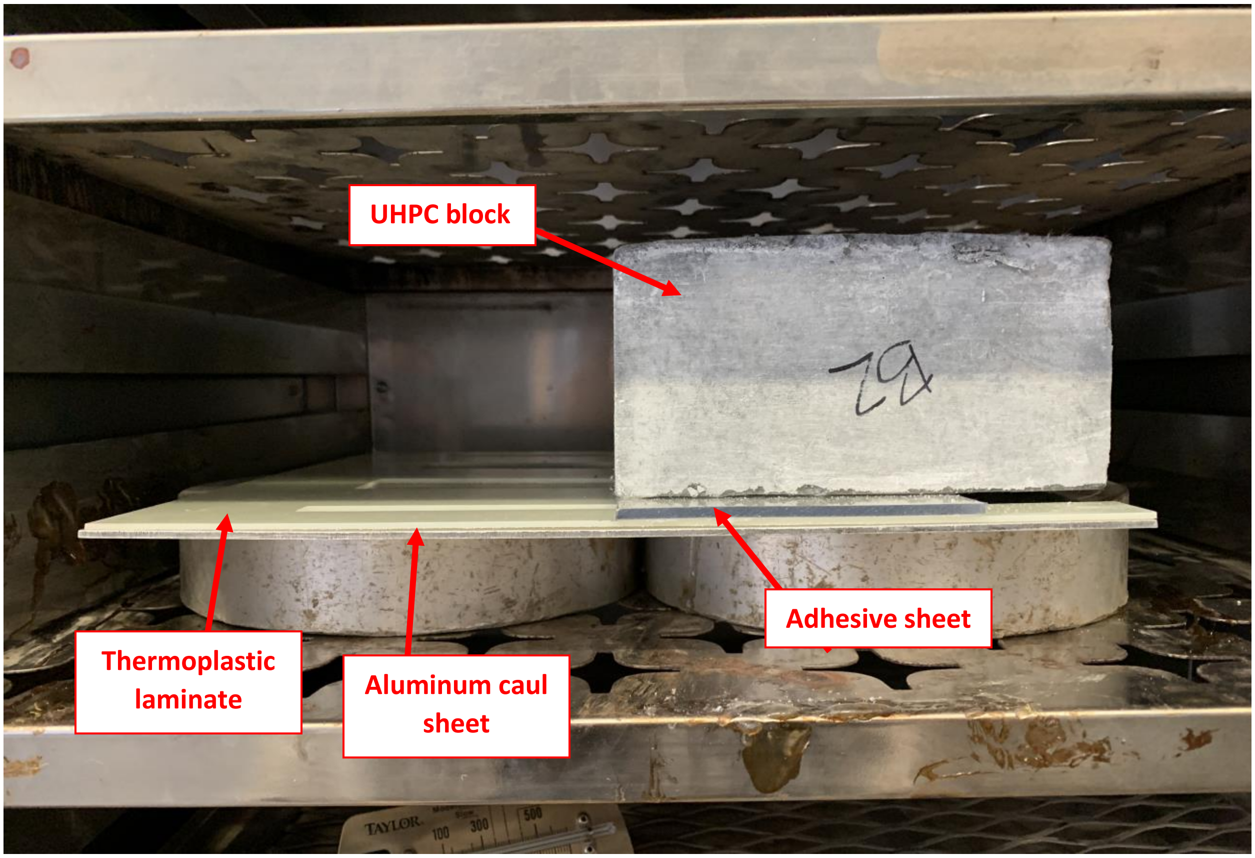

Figure 42: Stacking setup for heating of single-lap shear specimens.

A thermocouple wire was placed between the adhesive sheet and thermoplastic laminate to read the temperature of the bond throughout the heating process. This entire setup was placed in an oven until the thermocouple read 165°C. The setup was then transferred to the 400-kip Baldwin press. A ¼” silicone sheet was placed underneath the caul sheet and another ¼” silicone sheet was placed on top of the concrete block. A 12” x 12” x ¼” steel sheet was then placed on top of the entire setup, acting as a top platen for the press. Each specimen was consolidated for 10 minutes at its appropriate consolidation pressure.

Each FRP-bonded UHPC block was then cut using a waterjet. The final single-lap shear test specimen was a 3” x 3” x 6” concrete block bonded to a 2” x 8” FRP strip. The bond length of the FRP strip and UHPC was 4 inches. A single-lap shear test specimen is presented in Figure 43.

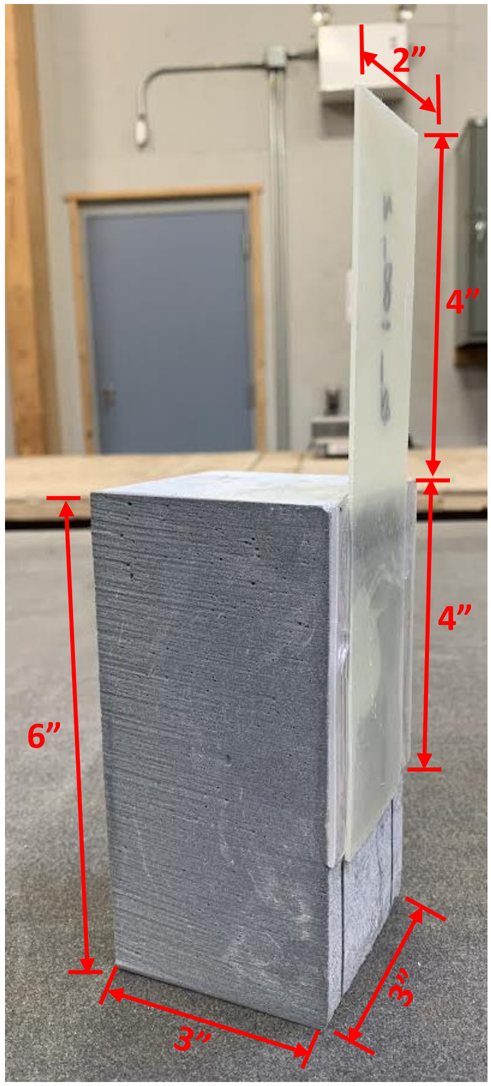

Figure 43: Single-lap shear UHPC-thermoplastic specimen.

5.3.2 Experimental Procedure

A total of (22) FRP-bonded concrete specimens were tested in single-lap shear using a 100-kN servo-hydraulic Instron. Prior to testing, 2” x 2” aluminum plates were adhered to the end of the FRP strip with an epoxy resin to grip the laminate during testing. A steel L-bracket was adhered to the start of the bonded area using an epoxy resin to act as the contact surface for the LVDT during testing. The aluminum plates and L-bracket are shown in the test setup in Figure 44.

The test fixture consisted of a bottom steel plate that was gripped into the bottom hydraulic grips on the Instron and a top steel plate that resisted vertical displacement of the concrete block when loaded in tension. These plates where attached using four threaded rods and nuts. The test fixture was spring-loaded for easy removal and transfer of the specimens. The Instron hydraulic grips gripped the FRP strip. The LVDT contacted the L-shape bracket to measure global slip. The test setup is shown in Figure 44.

Figure 44: UHPC-thermoplastic single-lap shear test setup.

The specimen was then preloaded to 300 N. The tests were conducted under displacement control at a constant rate of 1 mm/min until failure. Failure modes were recorded, and the load and displacement data were analyzed using MATLAB.

5.3.3 Results and Discussion

Maximum bond strength was the main result of interest for the single-lap shear tests. In conventional single-lap shear tests, multiple strain gages are placed along the FRP to record the bond-slip behavior of the FRP-concrete bond. The placement of the strain gages on small specimens can become difficult and highly scattered stress-slip relationships can occur. As a result, a method developed by Dai et al. (Dai, et al., 2005) to determine bond stress was intended to be used. In this method, the FRP strain vs. slip curve at the start of the bonded area must be obtained by experimental testing. The interfacial bond-slip models can be represented by the function indicated in Equation 3.

Equation 3: Strain-displacement curve fit proposed by Dai et al.

$$\varepsilon = A(1 - e^{-B\delta})$$

Where ε is the strain of the FRP strip, and δ is the displacement of the FRP strip δ (mm). Displacement is found using an LVDT during testing, strain is found using Equation 4, and A and B are parameters found by performing exponential regression of the experimental data.

Equation 4: Laminate strain calculation using pullout load and laminate properties.

$$\varepsilon = \frac{F}{E_f b_f t_f}$$

Where F is the pullout force recorded from the load cell (N) and E_f, b_f, and t_f are the elastic modulus (MPa), width (mm), and thickness of the FRP plate (mm), respectively. Parameters A and B in Equation 2 are used to find the maximum bond strength, τ_{max} (MPa), the interfacial fracture energy, G_f (N/mm) , and the maximum pullout load, P_{max} (N), as indicated in Equations 5, 6, and 7.

Equation 5: Bond fracture energy proposed by Dai et al.

$$G_f = 0.5A^2 E_f t_f$$

Equation 6: Maximum bond strength proposed by Dai et al.

$$\tau_{max} = 0.5BG_f$$

Equation 7: Maximum pullout load proposed by Dai et al.

$$P_{max} = b_f E_f t_f A$$

The two-parameter nonlinear model has been widely accepted and used by many researchers to analyze the nonlinear bond stress-slip data of FRP and concrete (Mohammadi, 2014; Bencardino, et al., 2017; Dong & Hu, 2016). As a result, the method by Dai et al. seemed like an appropriate method to calculate the bond strength of the UHPC and thermoplastic laminate in this study. However, this method assumes stable crack growth throughout testing and also assumes a relatively ductile failure. Majority of the UHPC-thermoplastic specimens tested in single-lap shear failed in a brittle manner, and the strain vs. slip data did not follow the curve fit presented in Equation 3. A typical experimental strain-slip curve is presented in Figure 45, represented by the blue line. The orange line represents the curve fit presented by Dai et al. It is clear that this curve fit does not accurately represent the strain-slip data. The strain-slip curve for the experimental data is much more linear than Dai et al.'s approximation due to the brittle failure of the specimen. Therefore, the nonlinear bond-slip method proposed by Dai et al. was deemed inappropriate for this study and was not used to calculate bond strength.

Further investigation of the literature was performed to approximate the bond strength of concrete bonded to FRP that fails in a brittle manner. The literature provided a review of bond-slip models for FRP sheets bonded to concrete in single-lap shear (Lu, et al., 2005). Most models included in the review assumed a failure at the concrete-adhesive interface and a ductile failure (Tanaka, 1996; Hiroyuki & Wu, 1997; van Gemert, 1980; Maeda, et al., 1997; Cheng & Teng, 2005). One of the proposed models assumed a linear-brittle failure, but this method was deemed to be unrealistic (Neubauer & Rostasy, 1997; Lu, et al., 2005). As a result, an appropriate way to estimate the nonlinear bond strength was not found in the literature, and a quantitative measure of bond strength was not calculated from the single-lap shear tests. The qualitative results were closely analyzed instead.

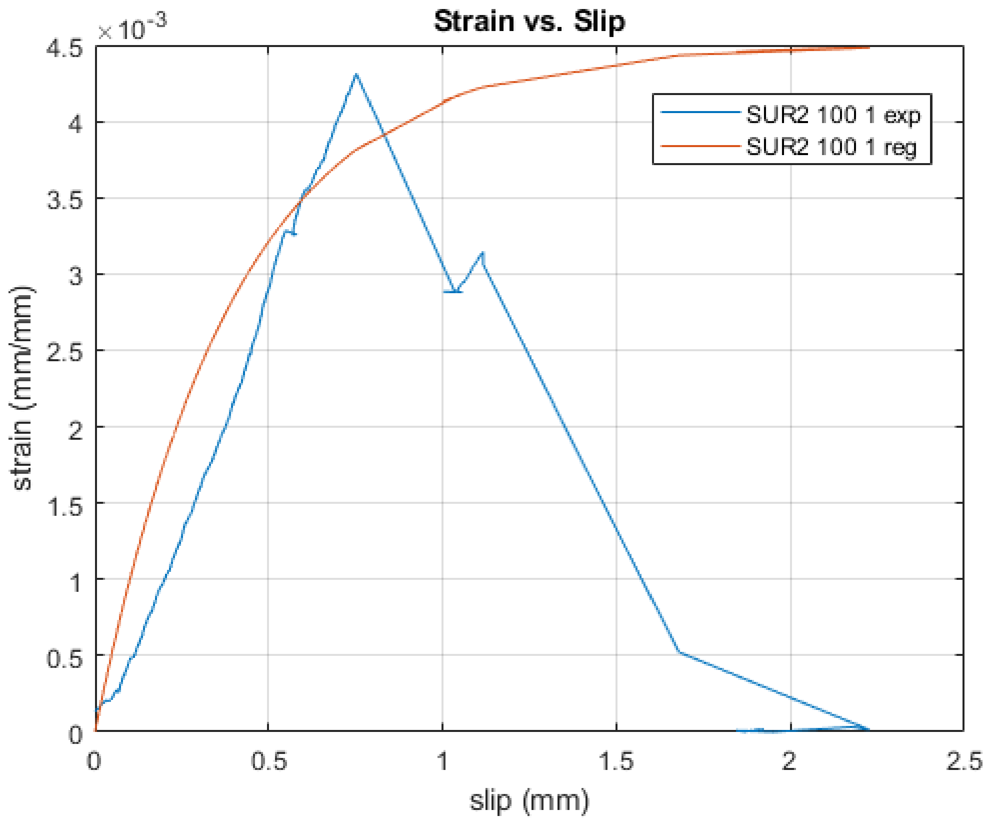

Figure 45: Experimental strain-slip data compared to curve fit proposed by Dai et al.

The main failure mode of the single-lap shear tests was debonding of the FRP strip. The interface at where the failure occurred depended on the specimen's adhesive type. Specimens manufactured with PETG neat resin experienced debonding at the concrete-adhesive interface. The laminate remained bonded to the adhesive sheet and was removed from the concrete as a single entity. A layer of the concrete substrate was left on the adhesive sheet, as shown in Figure 46. Specimens manufactured with EAA experienced debonding at the laminate-adhesive interface. The adhesive sheet remained bonded to the concrete, and the laminate debonded from the adhesive sheet. Only one EAA specimen experienced debonding at the concrete-adhesive layer. Figure 47 shows the debonding mechanism at the adhesive-laminate interface. There was not a clear relationship between adhesive type and type of failure, i.e. ductile or brittle. Both adhesive types experienced ductile and brittle failures.

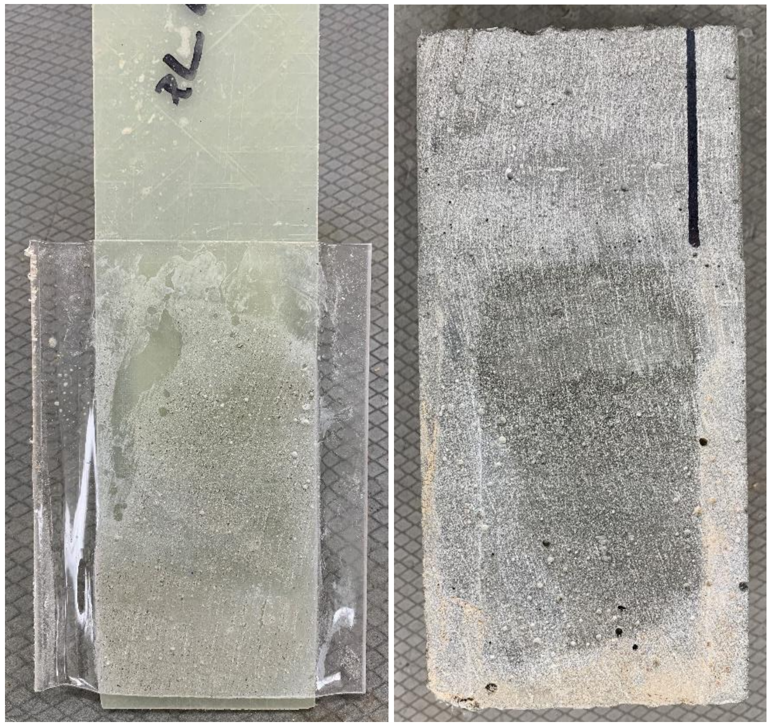

Figure 46: Debonding of PETG neat resin specimens at the concrete-adhesive interface.

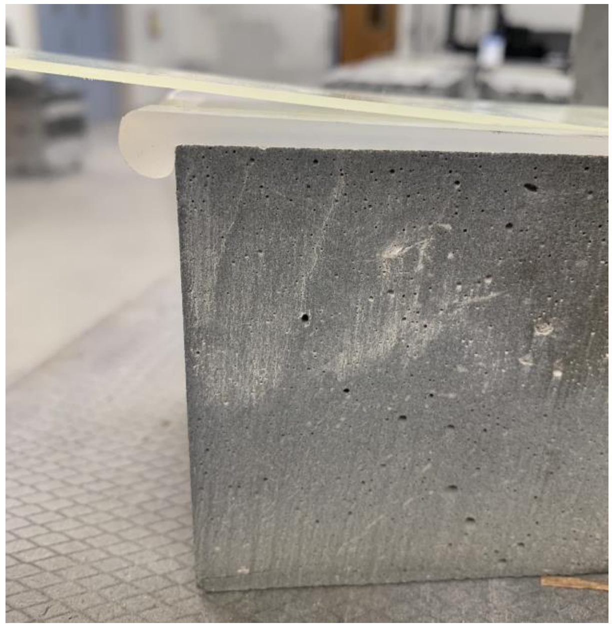

Figure 47: Debonding of EAA specimens at the adhesive-laminate interface.

The peak load was noticeably different between the PETG neat resin specimens and the EAA specimens. The EAA specimens were typically able to undergo a higher maximum load than the PETG neat resin specimens. The peak load for the single-lap shear specimens based on adhesive type and consolidation pressure is presented in Figure 48. Note that several of the UHPC-FRP specimens made with PETG neat resin are not included in Figure 48. Specimens P1_80 and P2_100 were completely unbonded prior to testing. The reason of the debonding is most likely a manufacturing issue. This issue did not occur with specimens made from EAA, indicating that the bond between EAA and the laminate may be of higher quality than that of the PETG neat resin and laminate.

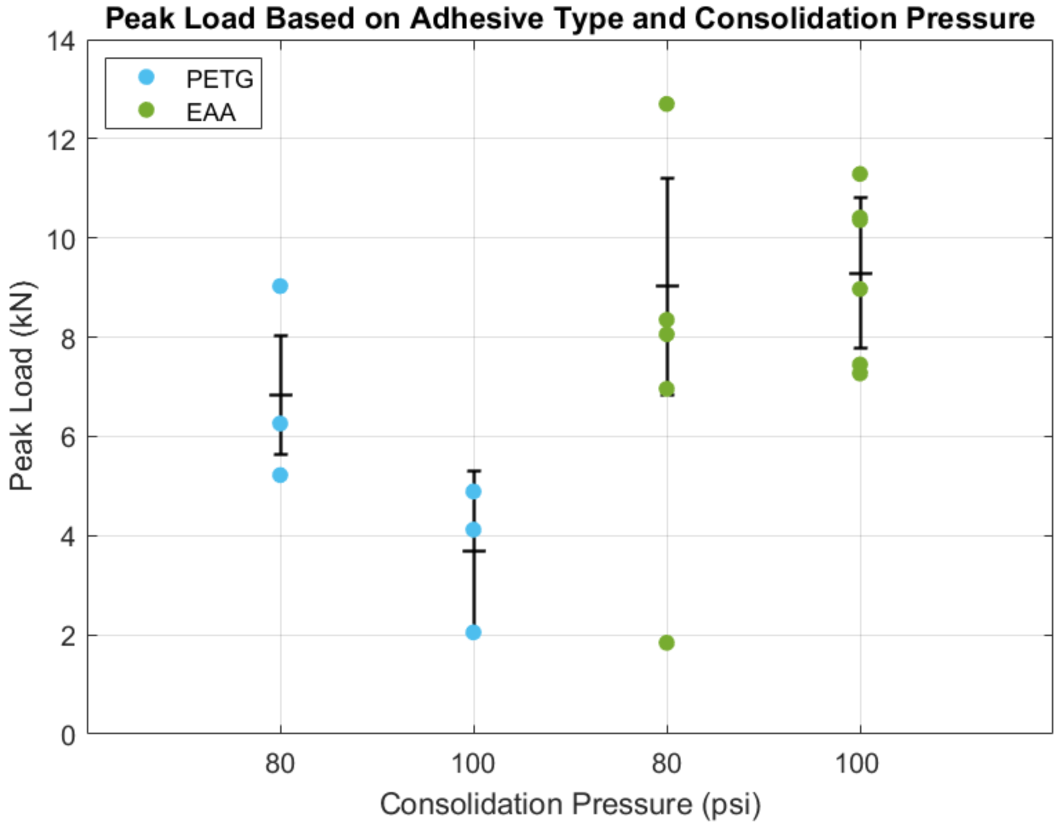

Figure 48: Peak load of single-lap shear specimens based on adhesive type and consolidation pressure.

The average maximum peak loads of the PETG neat resin specimens manufactured at 80 and 100 psi were 6.84 and 4.51 kN, respectively. Those of the EAA specimens manufactured at 80 and 100 psi were 9.02 and 9.29 kN, respectively. On average, the EAA specimens had a 31.9% and 106% increase in peak load for consolidation pressures of 80 and 100 psi, respectively. The scatter for the EAA data was greater than that for the PETG neat resin data. EAA specimens with a consolidation pressure of 80 psi had a small outlier of 1.84 kN. However, it is important to note that only three PETG neat resin specimens manufactured were tested at 80 psi and 100 psi due to a manufacturing issue. The small amount of specimens tested for PETG neat resin most likely lowered its variability. Nevertheless, the UHPC-thermoplastic specimens bonded with EAA underwent a higher peak load, on average, than those bonded with PETG neat resin.

5.4 Summary and Conclusions

This section will first discuss the summary and conclusions of the three-point bending tests and will then discuss the summary and conclusions of the direct single-lap shear tests.

5.4.1 Three-Point Bending

The three-point bending tests revealed that the EAA resin produced a stronger bond between the thermoplastic laminate and UHPC than the PETG neat resin. The beams manufactured with EAA resulted in a higher maximum bond strength in three-point bending. Again, a reason for concern is the difference in adhesive thickness. The EAA resin sheet was double the thickness of the PETG neat resin sheet, which may have contributed to its higher bond strength. However, in the calculation of the bond strength using Equation 1, adhesive thickness was considered when calculating the transformed moment of inertia, I_{tr}. Therefore, the calculated bond strengths can be considered to be a direct comparison between the EAA and PETG neat resin specimens. The three-point bending results also showed that specimens manufactured with a consolidation pressure of 100 psi generally performed better than those manufactured with a consolidation pressure of 80 psi within the same adhesive type. Therefore, the optimal bond for this study was achieved by using the EAA resin and a consolidation pressure of 100 psi.

The three-point bending tests also provided a measurement of energy dissipation of the beam specimens. On average, the EAA specimens dissipated more energy than the PETG neat resin specimens. This is a good indicator of impact performance. A specimen that dissipates more energy is more likely to withstand higher impact loads. As mentioned previously, a cause for concern is the adhesive thickness. The greater thickness of the EAA most likely contributed to its higher energy absorption, and therefore this is not a direct comparison between EAA and PETG neat resin. However, literature revealed EAA's respectable performance under impact due to its self-healing properties (Fall, 2001). These material properties allow EAA to return almost to its original shape after experiencing a force. This characteristic of EAA most likely played a large role in increasing the energy absorption capacity of the beams under bending.

The major failure mode of the beams in three-point bending was similar to the cracking patterns seen the panels manufactured with PETG neat resin in low-velocity impact testing. Both tests resulted in shear failure of the concrete which led to debonding along the adhesive-concrete layer. This conclusion solidifies the claim that these sandwich panels perform similar in flexure as they do under impact. As a result, three-point bending tests should continue to be utilized to analyze the concrete-thermoplastic bond.

5.4.2 Direct Single-Lap Shear

The single-lap shear tests were all in all unsuccessful. The specimens tested in single-lap shear did not experience stable crack growth or a ductile failure, which is what most bond-slip models assume. As a result, the experimental data did not accurately fit nonlinear bond-slip models found in the literature, and a quantitative measure of bond strength was not able to be calculated. The average bond strength could have been calculated by dividing the maximum load by the bond area, however this is not necessarily accurate for FRP bonded to concrete. Instead, maximum pullout load was compared among specimens. On average, the EAA specimens underwent a greater maximum pullout load than the PETG neat resin specimens. The consolidation pressure did not have a significant effect on the maximum pullout load. The single-lap shear tests showed some interesting qualitative information, specifically regarding the failure modes and failure interfaces. The failure interface differed depending on the type of resin. The specimens manufactured with EAA resin almost always failed at the adhesive-laminate interface. The specimens manufactured with the PETG neat resin almost always failed at the concrete-adhesive interface. These results are not consistent with the failure interfaces of the three-point bending tests. All of the PETG neat resin specimens failed at the concrete-adhesive interface in three-point bending. 70% of the EAA specimens failed at the concrete-adhesive interface as well. This reveals that the bond between the concrete and thermoplastic behaves differently when tested in three-point bending versus single-lap shear.

A few difficulties arose during the single-lap shear testing. Several of the FRP strips became completely unbonded to the UHPC block prior to testing due to a manufacturing error. Therefore, there were minimal specimens to test. Additionally, when the specimens were placed in the Instron, it was extremely difficult to directly align the FRP strip under the load head. When the FRP strips weren't directly aligned with the load head, torsion occurred in the FRP strip which induced mixed mode loading. It is possible that not all specimens were tested in complete direct shear. Due to the manufacturing and testing difficulties, as well as the inability to obtain a quantitative bond strength measurement, single lap shear tests are not recommended to be conducted in future work. Three-point bending tests should be utilized instead. These tests proved to be simpler, the test specimens were easier to manufacture, and the results were much more accurate than the single-lap shear tests.

CHAPTER 6

SUMMARY AND RECOMMENDATIONS FOR FUTURE WORK

The externally-bonded thermoplastic laminates were effective in increasing UHPC's impact resistance and decreasing brittle behavior of UHPC under impact. Two main processing parameters were of interest throughout this research: adhesive type and consolidation pressure. The adhesive type had a direct effect on the impact strength of UHPC. The consolidation pressure had a slight effect on the bond strength between the UHPC and the thermoplastic laminate. The following sections with discuss recommendations for future work regarding manufacturing, bond analysis, and impact testing.

6.1 Manufacturing of UHPC-Thermoplastic Panels

The EAA resin overall performed better under impact than the PETG neat resin. The specimens manufactured with EAA underwent less impact damage, dissipated a greater amount of energy, and produced a stronger bond with the UHPC. It is, of course, important to consider the greater adhesive thickness for the EAA resin, which may have contributed to its superior impact behavior and bond strength. Nevertheless, the literature noted the impressive impact performance of EAA, as this material possesses self-healing properties (Fall, 2001; Sierakowski & Hughes, 2006). The impact strength of EAA is also about 11 times that of the PETG neat resin, as shown in Table 4. Therefore, EAA should be considered an important material of interest in future work. Further investigation of this material should be performed to enhance the impact resistance of the UHPC-PETG laminate sandwich panels.

The consolidation pressure did not have a significant effect on the impact behavior of the UHPC-thermoplastic sandwich specimens in low-velocity impact. It did however, have a slight effect on the bond strength and energy dissipation of these specimens in three-point bending. For both EAA and PETG neat resin adhesives, the bond strength was higher, on average, for those consolidated with 100 psi than those consolidated with 80 psi. The energy dissipated by the beams was also greater on average for beams consolidated with 100 psi. In future work, panels should be consolidated at 100 psi.

In addition to consolidation pressure and adhesive type, consolidation temperature is an extremely important processing parameter for the bond between the thermoplastic laminates and UHPC. The manufacturing process used in this study was not suitable to test the effect of consolidation temperature on the bond between UHPC and the thermoplastic laminate because the temperature was not easily controlled. The press was not heated, and therefore the specimens underwent heat loss during bonding. In future work, consolidation temperature of the UHPC-thermoplastic sandwich panels should be explored using a heated press during manufacturing. Using a heated press would be more efficient and would decrease variability of bond strength in the specimens. In addition to using a heated press, a singular panel should be consolidated at a time. As mentioned in Section 3.2, the UHPC panels experienced cracking during the initial stamp thermoforming trials. These initial trials consolidated four panels at a time. The causes of the cracking are most likely due to the uneven concrete thickness within a singular panel and the uneven concrete thickness among the four different panels in one consolidation round. The UHPC cracking is expected to be minimized if one panel is consolidated a time.

Since a heated press will be utilized in future work, displacement of the concrete cores becomes a concern. Displacement of the concrete cores was seen in the initial thermoforming trials due to overheating of the resin sheets. To prevent this issue, a retention frame should be manufactured for a singular panel to hold the panel in place during consolidation. This retention frame must be fairly heavy in order to prevent movement of the concrete core. Another issue that occurred with the initial thermoforming trials was the difficulty to remove the panels from the retention frame without damaging the panels. Therefore, the retention frame used in future work should be designed for easy removal of the panels. This could include adding a hinge to the frame to easily open the frame and remove the specimens.

Heating the specimens manufactured with EAA to lower temperatures should be explored in future work. In this study, the EAA resin was heated far past its Tg and melting temperature, making the manufacturing process of these specimens difficult due to the high viscosity of the resin. Overheating the EAA resin may have also caused much of the variability in this data. The temperature used to consolidate the UHPC-thermoplastic panels in the future needs to be high enough to bond the PETG laminates to the adhesive but not too high to cause the EAA resin to flow. Testing different temperatures would be an effective way to improve the manufacturing process of the specimens fabricated with EAA.

A challenge to be tackled in future work is large-scale production of the UHPC-thermoplastic sandwich panels. A future goal of this work is to expand the panels from a square foot to a square yard (Gillis, 2018). Production of the thermoplastic laminates would remain the same and would be fabricated in the automatic Dieffenbacher tape layup machine at the ASCC. This machine is capable of laying up laminates much larger than a square yard. The more challenging aspect would be the manufacturing of a square yard UHPC panel. This will require more material, equipment, and labor. A large area of concern is cracking of the concrete panel when consolidated in a hydraulic press. Cracking of the concrete was an issue in the UHPC panels at the current scale. One defect or abnormality in the concrete surface or thickness caused an unequal stress distribution when pressure was applied which catalyzed cracking throughout the panel. This issue is even more probable at a larger scale. As a result, a six sided mold would need to be used to cast the UHPC panel to ensure a uniform thickness. Thick silicone pads would also need to be used within the press to protect the concrete from the platens.

6.2 Bond Analysis

Three-point bending and single-lap shear tests were performed in this study to characterize the bond between UHPC and the thermoplastic laminate. Three-point bending tests proved to be simpler than single-lap shear tests and also provided a quantitative measurement of bond strength. In future work, three-point bending tests should be utilized to analyze the bond behavior between UHPC and the thermoplastic laminate. In addition to the simplicity, concrete performs similarly in flexure as it does under impact, as shown in the cracking patterns of the three-point bending and impact tests. Testing the UHPC-thermoplastic bond in bending will provide a better representation of how the bond behaves under impact loading.

The bond analysis of the UHPC-thermoplastic laminates can be further improved by using a test method that was developed by Gartner et al. to specifically test the bond capacity between FRP composites bonded to small concrete beams (Gartner, et al., 2011). This is a three-point bending test method and requires the application of an FRP sheet that is two-thirds of the beam span length. The test method also requires a saw cut within the concrete at the midspan of the beam that is half of the concrete beam depth. This saw cut is to be performed prior to bonding it to the FRP sheet, hence the saw cut is only to be present within the concrete beam. The intent of the saw cut is to develop concentrated moment at the cut and weaken the section so that a flexural crack will form at the tip of the saw cut to allow the full developmental length of the composite to be reached (Gartner, et al., 2011). The depth to width and span to depth ratios are also important for this beam test. The depth to width ratio shall be equal to 1, while the span to depth ratio shall be equal to 3. Figure 49 shows the proposed beam configuration for the concrete-FRP three point bending tests.

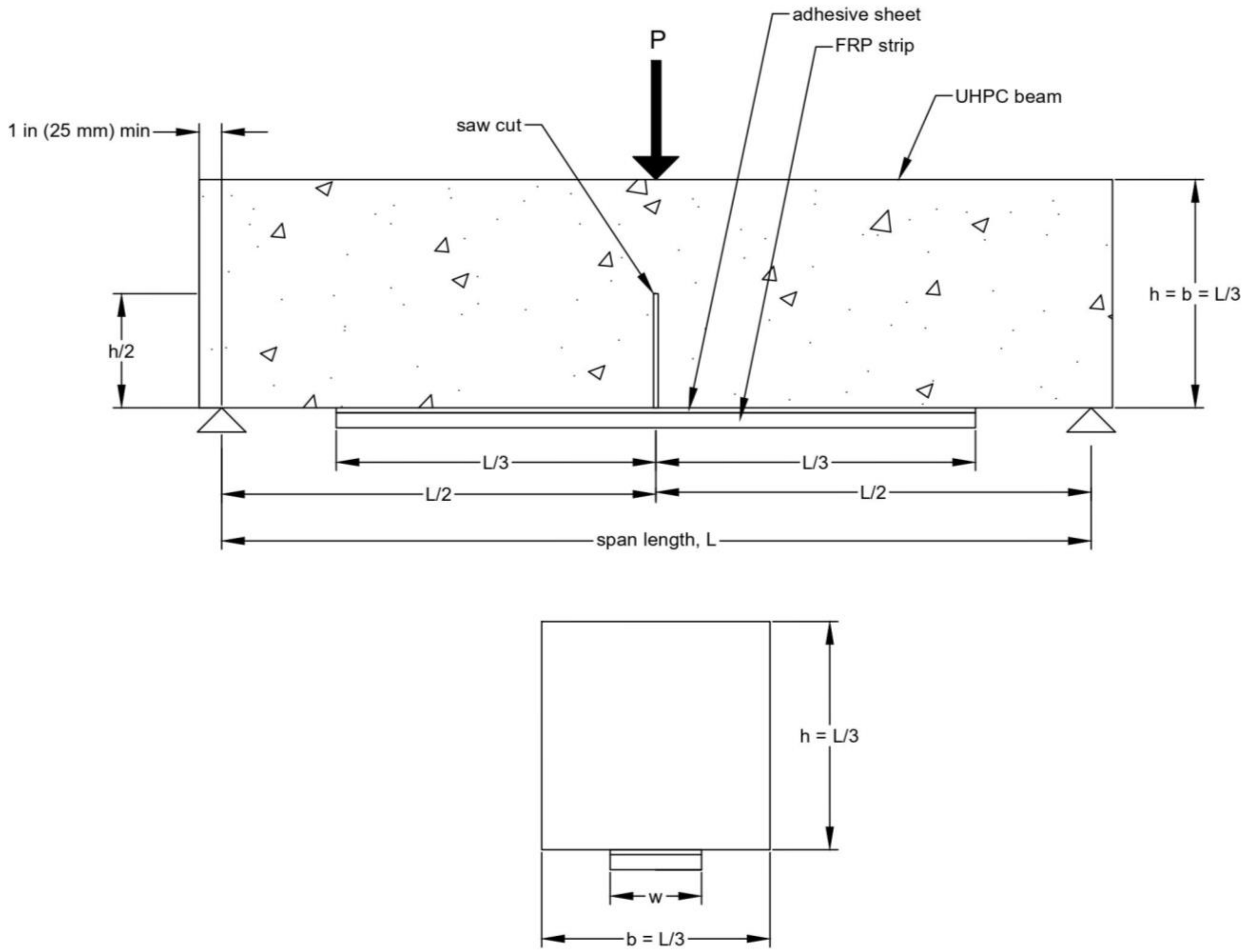

Figure 49: Proposed future three-point bending setup developed by Gartner et al.

The bond strength can then be calculated using Equation 8. This equation assumes a linear stress distribution over the concrete compressive zone.

Equation 8: Maximum bond strength of FRP sheet and concrete beam proposed by Gartner et al.

$$\tau_b = \frac{3PL}{5hwS}$$

Where τ_b= average shear stress in the UHPC-thermoplastic bond (MPa), P = peak load applied at midspan (N), L = beam span length (mm), h = beam height (mm), w = width of FRP sheet (mm), and S = length of FRP sheet (mm) (Gartner, et al., 2011).

The beam configuration shown in Figure 49 will require different fabrication and manufacturing processes than the ones used for the sandwich panels. The depth to width ratio of the beams used in this work was only 0.5 and the span to depth ratio was 11.5. The depth to width and span to depth ratios required for the proposed test method are 1 and 3, respectively. As a result, beams should be cast at a size of 2" x 2" x 6". Following casting, a 1"-deep saw cut can be cut at the midspan of the beams prior to bonding them to the laminate. A PETG laminate should then be bonded only to the tension face of the beam.

Since the laminate will not cover the full span of the beam, the laminate should be cut into the shape presented in Figure 50 prior to bonding it to a UHPC panel. Figure 50 shows a plan view of the laminate placed over the UHPC panel for consolidation. The setup requires the laminate to overhang the concrete panel by an amount equal to $Lp - Lc$, where *Lp* is the length of the FRP laminate and *Lc* is the length of the concrete panel. This will allow for easy alignment of the laminate and the concrete panel during consolidation. Two adhesive sheets with a width of the FRP sheet should be placed directly underneath the contact area between the thermoplastic laminate and the UHPC panel. Once the panel is consolidated, it can be cut in half along the centerline shown in Figure 50. It can then be cut longitudinally to acquire beam specimens. This manufacturing process will fabricate beam specimens needed for the setup shown in Figure 49.

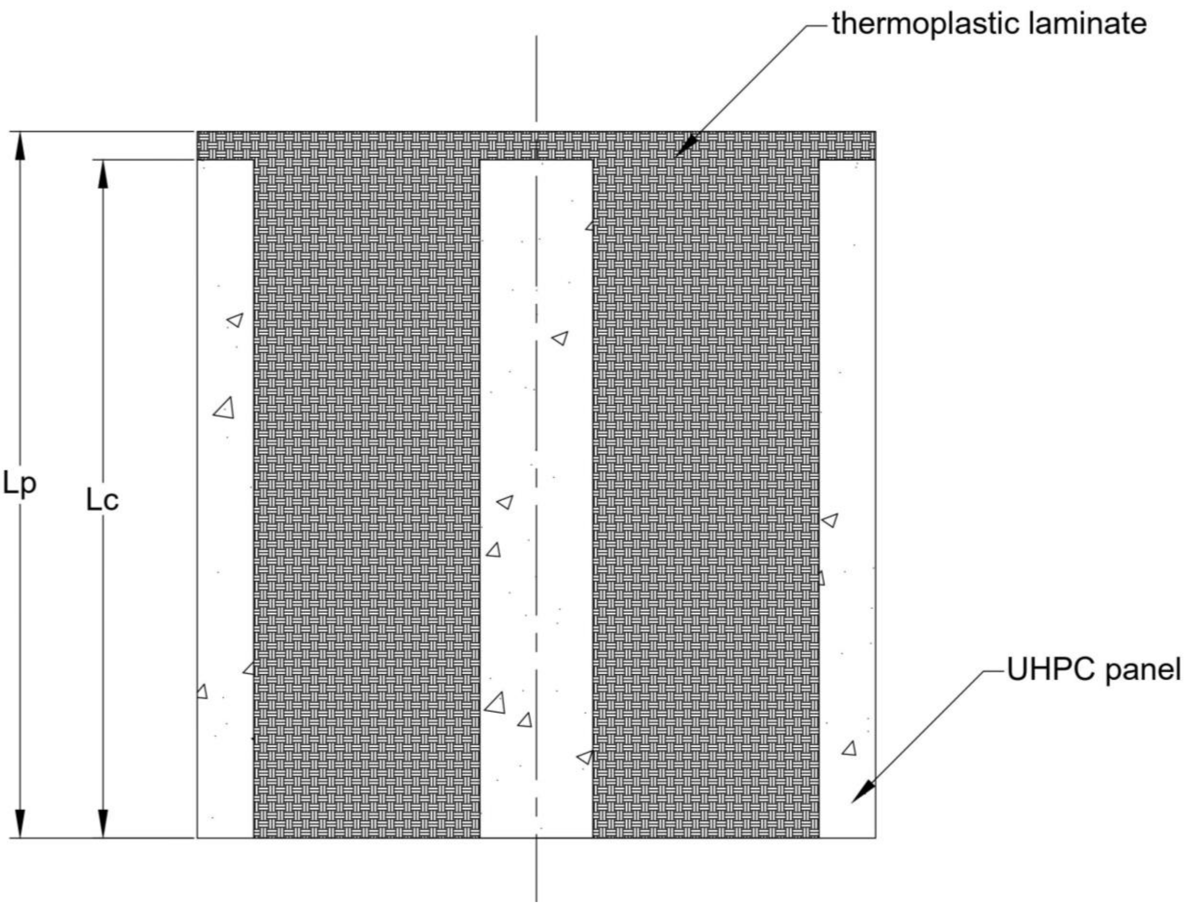

Figure 50: Plan view of proposed UHPC-thermoplastic laminate setup for new three-point bending specimens.

6.3 Impact Testing

As mentioned in section 4.1, it is important to consider inertial effects when performing impact tests. Because the mass of the panels used in this study was less than 2 times the mass of the impactor, inertial effects were not considered (Leissa, 1969; Verma, et al., 2016). However, in future work, inertial effects should be investigated. This could be accomplished by using two accelerometers like the study by Ong et al. (Ong, et al., 1999). One accelerometer could be instrumented inside or attached to the tup and the other accelerometer could be attached to the test specimen. The inertial load due to impact of the specimen can then be subtracted from the total impact load to get the true impact load.

The low-velocity impact tests revealed that the addition of thermoplastic skins significantly increased the impact resistance of UHPC and minimized its brittle failure behavior. Impact resistance could be improved even more by altering the stacking sequence and thicknesses of the thermoplastic laminates. Literature showed that the energy absorption capacity, strength, and flexibility of a composite laminate are directly affected by its stacking sequence and thickness (Cantwell & Morton, 1991). Literature also showed that the load resisted by the rear skin is greater than that of the front skin under impact (Aryal., et al., 2019). Therefore, the rear skin should be designed with higher ductility and energy absorption capacity than the front skin. This could be achieved by altering the stacking sequence of the laminate or adding additional plies to the laminate to increase the thickness. A more flexible and energy absorbing rear skin would potentially reduce scabbing, reduce delamination, and catch concrete debris from the rear face of the panel. An E-glass/PETG laminate with high ductility should be developed for the rear face of the UHPC panel to further prevent brittle failure of the UHPC.

Future work should look more carefully into high-velocity and blast loadings, as a main goal of this work is to use this sandwich composite system in military structures. High-velocity impact tests should first be carried out on the current design and scale of the UHPC-thermoplastic sandwich panels. The CEAST 9350 impact drop tower system located at the ASCC is unable to perform high velocity impact tests, as its maximum impact speed is 4.65 m/s which falls in the low-velocity impact range (Safri, et al., 2014). As a result, high-velocity impact tests should be conducted by ERDC using bullet penetration tests. Once high-velocity impact tests are performed and analyzed, blast loadings can be tackled.

REFERENCES

Abdel-Kader, M. & Fouda, A., 2014. Effect of reinforcement on the response of concrete panels to impact of hard projectiles. *International Journal of Impact Engineering,* Volume 63, pp. 1-17.

Abrte, S., 2005. *Impact on Composite Structures.* s.l.:Cambridge University Press.

Alsalman, A., Dang, C. N. & Hal, W. M., 2017. Development of ultra-high performance concrete with locally available materials. *Construction and Building Materials,* Volume 133, pp. 135-145.

American Concrete Institute, 2012. Guide Test Methods for Fiber-Reinforced Polymers (FRPs) for Reinforcing or Strengthening Concrete Structures. *ACI 440.3R-12.*

American Society for Testing and Materials, 1973. *Instrumented Impact Testing,* Philidelphia, Pennsylvania: s.n.

Aryal., B. et al., 2019. Effects of impact energy, velocity, and impactor mass on the damage induced in composite laminates and sandwich panels. *Composite Structures,* Volume 226.

Avient Corporation, 2020. *Polystrand™ IE 5843 Technical Data Sheet,* s.l.: Avient.

Barnett, S., Millard, S., Schleyer, G. & Tyas, A., 2010. Briefing: Blast tests of fibre-reinforced concrete panrls. *Construction Materials,* 163(CM3), pp. 127-129.

Bencardino, F., Condello, A. & Ashour, A. F., 2017. Single-lap shear bond tests on Steel Reinforced Geopolymeric Matrix-concrete joints. *Composites Part B,* Volume 110, pp. 62-71.

Bindiganavile, V., Banthia, N. & Aarup, a. B., 2002. Impact Response of Ultra-High-Strength Fiber-Reinforced Cement Composite. *ACI Materials Journal,* 99(6).

Büyüköztürk, O. & Yu, T.-Y., 2006. *Understanding and Assessment of Debonding Failures in FRP-Concrete Systems,* Istanbul, Turkey: Seventh International Congress on Advances in Civil Engineering.

Cantwell, W., 1988. The Influence of Target Geometry on the High Velocity Impact Response of CFRP. *Composite Structures,* Volume 10, pp. 247-265.

Cantwell, W. J., Curtis, P. & Morton, J., 1986. An Assessment of the Impact Performance of CFRP Reinforced with High-strain Carbon Fibres. *Composites Science and Technology,* Volume 25, pp. 133-148.

Cantwell, W. & Morton, J., 1989. Comparison of the low and high velocity impact repsonse of CFRP. *Composites,* 20(6).

Cantwell, W. & Morton, J., 1991. The impact resistance of composite materials - a review. *Composites,* 22(5).

Cao, Y., Liu, G., Brouwers, H. & QingliangYu, 2020. Enhancing the low-velocity impact resistance of ultra-high performance concrete by an optimized layered-structure concept. *Composites Part B,* Volume 200.

Cao, Y., Yu, Q., Li, P. & Brouwers, H., 2019. Effects of Fiber Content on Mechanical Properties of UPFRC with Coarse Aggregates. *International Interactive Symposium on Ultra-High Performance Concrete,* 2(1).

Carey, A. S. et al., 2020. Impact of Materials, Proportioning, and Curing on UltraHigh-Performance Concrete Properties. *ACI Materials Journal,* 117(1).

Chajes, M. J., Jr., W. W. F., Januszka, T. F. & Theodore A. Thomson, J., 1996. Bond and Force Transfer of Composite Material Plates. 93(2).

Cheng, J. & Teng, J., 2005. Experimental study on FRP-to-concrete bonded joints. *Composites-Part B: Engineering,* 36(2), pp. 99-113.

Dai, J., Ueda, T. & Sato, Y., 2005. Development of the Nonlinear Bond Stress-Slip Model of Fiber Reinforced Plastics Sheet-Concrete Interfaces with a Simple Method. *Journal of Composites for Construction,* pp. 52-62.

Dancygier, A. N., Yankelevsky, D. Z. & Jaegermann, C., 2007. Response of high performance concrete plates to impact of non-deforming projectiles. *International Journal of Impact Engineering,* Volume 34, pp. 1768-1779.

Dancygier, A. & Yankelevsky, D., 1996. High strength concrete response to hard projectile impact. *Int. J. Impact Engng,* 18(6), pp. 583-599.

Dingqiang, F. et al., 2021. Optimized design of steel fibres reinforced ultra-high performance concrete (UHPC) composites: Towards to dense structure and efficient fibre application. *Construction and Building Materials,* Volume 273.

Dong, K. & Hu, K., 2016. Development of bond strength model for CFRP-to-concrete joints at high temperatures. *Composites Part B,* Volume 95, pp. 264-271.

Entec, 2020. *Surlyn 8940 DuPont Packaging & Industrial Polymers - Ethylene Methacrylic Acid,* s.l.: s.n.

Fall, R., 2001. *Puncture Reversal of Ethylene Ionomers – Mechanistic Studies,* Blacksburg, Virginia: Virginia Polytechnic Institute and State University.

Farnam, Y., Mohammadi, S. & Shekarchi, M., 2010. Experimental and numerical investigations of low velocity impact behaviorof high-performance fiber-reinforced cement based composite. *International Journal of Impact Engineering,* Volume 37, pp. 220-229.

Feng, J. et al., 2020. Numerical and analytical investigations on projectile perforation on steel-concrete-steel sandwich panels. *Results in Engineering,* Volume 8.

Fladr, J. & Bily, P., 2018. Specimen size effect on compressive and flexural strength of high-strength fibre-reinforced concrete containing coards aggregate. *Composites Part B: Engineering,* Volume 138, pp. 77-86.

Franco, A. & Royer-Carfagni, G., 2014. Effective bond length of FRP stiffeners. *International Journal of Non-Linear Mechanics,* Volume 60, pp. 46-57.

Fujikake, K., Adhikary, S. D. & Li, B., 2013. Effects of high loading rate on reinforced concrete beams. *ACI Structural Journal,* 111(3).

Gartner, A., Douglas, E. P., Dolan, C. W. & Hamilton, H., 2011. Small Beam Bond Test Method for CFRP Composites Applied to Concrete. *Journal of Composites for Construction,* 15(1), pp. 52-61.

Gartner, A. L., 2007. *Development of a flexural bond strength test to determine environmental degradation of carbon fiber-reinforced polymer (CFRP) composites bonded to concrete,* s.l.: s.n.

Ghorbani, M., Mostofinejad, D. & Hosseini, A., 2017. Experimental investigation into bond behavior of FRP-to-concrete under mixed-mode I/II loading. Volume 132.

Gillis, R. S., 2018. Development of Thermoplastic Composite Reinforced Ultra-High Performance Concrete Panels for Impact Resistance. *The Universiy of Maine Electronic Theses and Disserations.*

Hadigheh, S., Gravina, R. & Setunge, S., 2012. *Shear debonding of FRP plates from concrete surface: using modified single lap shear test setup,* Melbourne: Composites and Nanocomposites in Civil, Offshore and Mining Infrastructure.

Harmon, T. G. et al., 2003. Bond of Surface-Mounted Fiber-Reinforced Polymer. 100(5).

Harries, K., Reeve, B. & Zorn, A., 2007. Experimental evaluation of factors affecting monotonic and fatigue behavior of fiber-reinforced polymer-to-concrete bond in reinforced concrete beams. *ACI Structural Journal.*

Hiremath, P. N. & Yaragal, S., 2017. Effect of different curing regimes and durations on early strength development of reactive powder concrete. *Construction and Building Materials,* Volume 154, pp. 72-87.

Hiroyuki, Y. & Wu, Z., 1997. Analysis of debonding fracture properties of CFS strengthened member subject to tension. *In: Proc. of 3rd international symposium on non-metallic (FRP) reinforcement for concrete structures,* Volume 1, pp. 284-294.

Hoang, A. L. & Fehling, E., 2017. Influence of steel fiber content and aspect ratio on the uniaxial tensile and compressive behavior of ultra high performance concrete. *Construction Building Materials,* Volume 153, pp. 790-806.

Hongkarnjanakul, N., Bouvet, C. & Rivallant, S., 2013. Validation of low velocity impact modelling on different stacking sequences of CFRP laminates and influence of fibre failure. *Composite Structures,* Volume 106, pp. 549-559.

Ibrahim, M. A., Farhat, M., Issa, M. A. & Hasse, J. A., 2017. Effect of Material Constituents on Mechanical and Fracture Mechanics Properties of Ultra-High Performance Concrete. *ACI Materials Journal,* 114(3).

J. Morton, E. G., 1989. Imapct Response of Tough Carbon Fibre Composites. *Composite Structures,* Volume 13, pp. 1-19.

Jalalvand, M. et al., 2016. Energy dissipation during delamination in composite materials - An experimental assessment of the cohesive law and the stress-strin field ahead of crack tip. *Composites Science and Technology,* Volume 134, pp. 115-124.

Jamnam, S. et al., 2020. Steel fiber reinforced concrete panels subjected to impact projectiles with different caliber sizes and muzzle energies. *Case Studies in Construction Materials,* Volume 13.

Jia, P., Wu, H., Wang, R. & Fang, Q., 2021. Dynamic responses of reinforced ultra-high performance concrete members under low-velocity impact. *International Journal of Impact Engineering,* Volume 150.

Karbhari, V. M. & Ghosh, K., 2009. Comparative durability evaluation of ambient temperature cured externallybonded CFRP and GFRP composite systems for repair of bridges.

Khshain, N. T., Al-Mahaidi, R. & K. A., 2015. Bond behaviour between NSM CFRP strips and concrete substrate using single-lap shear testing with epoxy adhesive. *Composite Structures,* Volume 132, pp. 205-214.

Kulpa, M. & Siwowski, T., 2019. Stiffness and strength evaluation of a novel FRP sandwich panel for bridgeredecking. *Composites Part B,* Volume 167, pp. 207-220.

Leissa, A., 1969. *Vibration of Plates,* Washington, D.C.: National Aeronautics and Space Administration.

Liu, D., 1988. Impact-Induced Delamination - A View of Bending Stiffness Mismatching. *Journal of Composite Materials,* 22(7), pp. 674-692.

Lo´pez-Puente, J., A. Arias, R. Z. & Navarro, C., 2005. The effect of the thickness of the adhesive layer on the ballistic limit of ceramic/metal armours. An experimental and numerical study. *International Journal of Impact Engineering,* Volume 32, pp. 321-336.

Lorenzis, L. D., Miller, B. & Nanni, A., 2001. Bond of Fiber-Reinforced Polymer Laminates to Concrete. *ACI Materials Journal,* 98(3).

Lu, L. & Li, G., 2016. One-Way Multishape-Memory Effect and Tunable Two-Way Shape Memory Effect of Ionomer Poly(ethylene-co-methacrylic acid). *ACS Applied Materials & Interfaces,* Volume 8, pp. 14812-14823.

Lu, X., Teng, J., Ye, L. & Jiang, J., 2005. Bond-slip models for FRP sheets/plates bonded to concrete. *Engineering Structures,* Volume 27, pp. 920-937.

Maeda, T. et al., 1997. A study on bond mechanism of carbon fiber sheet. *In: Proc. of 3rd international symposium on non-metallic (FRP) reinforcement for concrete structures,* Volume 1, pp. 279-285.

Ma, J., Dehn, F. & Ograss, M., 2004. Comparatie Invesigations on Ultra High Performance Concrete with and without Coarse Aggregates. *Proceedings of the International Symposium on Ultra High Performance Concrete,* pp. 205-212.

Ma, J. & Schneider, H., 2005. Properties of Ultra-High Performance Concrete. *LACER LEIPZIG Annual Civil Engineering Report,* Volume 7, pp. 25-32.

Manalo, A. et al., 2017. State-of-the-Art Review on FRP Sandwich Systems for Lightweight Civil Infrastructure. *Journal of Composites for Construction,* 21(1).

Mata, O. R. & Atadero, R. A., 2014. Evaluation of Pull-Off Tests as a FRP–Concrete Bond Testing Method in the Laboratory and Field. 19(2).

Mazzotti, C., Savoia, M. & Ferracuti, B., 2009. A new single-shear set-up for stable debonding of FRP–concrete joints. *Construction and Building Materials ,* Volume 23, pp. 1529-1537.

McGhee, K. H., 1970. *Water Bath Accelerated Curing of Concrete,* Charlottesville, Virginia: Virginia Highway Research Council.

McMaster-Carr, n.d. *Clear Easy-to-Form PETG Sheet Product Detail,* s.l.: McMaster-Carr.

Meng, W. & Khayat, K. H., 2018. Effect of hybrid fibers on fresh, mechanical properties, and autogenous shrinkage of cost effective UHPC. *Journal of Materials in Civil Engineering,* 30(4).

Miwa, Y., Kohbara, Y., Furukawa, H. & Kutsumizu, S., 2018. The effects of local glass transition temperatures of ionic core-shell structures on the tensile behavior of sodium-neutralized poly(ethylene-co-methacrylic acid) ionomer/lauric acid blends. *Polymer,* Volume 148, pp. 303-309.

Mohammadi, T., 2014. *Failure Mechanisms and Key Parameters of FRP Debonding from Cracked Concrete Beams,* s.l.: Marquette University.

Morton, J., 1989. Impact Response of Tough Carbon Fibre Composites. *Composite Structures,* Volume 13, pp. 1-19.

Mosallam, A. S., 2016. Structural evaluation and design procedure for wood beams repairedand retrofitted with FRP laminates and honeycomb sandwich panels. *Composites Part B,* Volume 87, pp. 196-213.

Mukhtar, F. M. & Faysal, R. M., 2018. A review of test methods for studying the FRP-concrete interfacial bond behavior. *Construction and Building Materials,* Volume 169, pp. 877-887.

Neubauer, U. & Rostasy, F., 1997. Design aspects of concrete structures strengthened with externally bonded CFRP plates. *In: Proc. of 7th international conference on structural faults and repair,* Volume 2, pp. 109-118.

O'Neil, E., Neeley, B. & Cargile, J., 1999. Tensile properties of very-high-strength concrete for penetration-resistant structures. *Shock and Vibration,* Volume 6, pp. 237-245.

Ong, K., Basheerkhan, M. & Paramasivam, P., 1999. Resistance of Æbre concrete slabs to low velocity projectile impact. *Cement & Concrete Composites,* Volume 21, pp. 391-401.

Othman, H. & Marzouk, H., 2016. *Performance of UHPFRC Plates under Repeated Impact Load,* Toronto, Ontario: Department of Civil Engineering, Ryerson University.

Ramakrishnan, V. & Dietz, J., 1975. *Accelerated methods of estimating the strength of concrete,* s.l.: Transportation Research Board.

Ranade, R., Li, V. C., Heard, W. F. & Williams, B. A., 2017. Impact resistance of high strength-high ductility concrete. *Cement and Concrete Research,* Volume 98, pp. 24-35.

Resnyansky, A. & Weckert, S., 2009. *Response of an ultra high performance concrete to shaped charge jet,* Adelaide, Australia: Shock & Impact Loads on Structures.

Reynolds, P. J., 2011. *A Surlyn® Ionomer as a Self-Healing,* s.l.: University of Birmingham.

Saadatmanesh, H. & Ehsani, M. R., 1990. Fiber Composite Plates Can Strengthen Beams. 12(3).

Safri, S., Sultan, M., Yidris, N. & Mustapha, F., 2014. Low Velocity and High Velocity Impact Test on Composite Materials - A Review. *The International Journal of Engineering and Science,* 3(9), pp. 50 - 60.

Santandrea, M., Imohamed, I. A. O. & Carloni, C., 2020. Width Effect in FRP–Concrete Debonding Mechanism: A New Formula. *Journal of Composites for Construction,* Volume 4, p. 24.

Sarva, S., Nemat-Nasser, S., McGee, J. & Isaacs, J., 2007. The effect of thin membrane restraint on the ballisticperformance of armor grade ceramic tiles. *International Journal of Impact Engineering,* Volume 34, pp. 277-302.

Shi, A., 2013. Order-Disorder and Order-Order Transitions. *Encyclopedia of Polymeric Nanomaterials.*

Shi, J.-W., Cao, W.-H. & Wu, Z.-S., 2019. Effect of adhesive properties on the bond behaviour of externally bonded FRP-to-concrete joints. *Composites Part B.*

Sierakowski, R. & Hughes, M., 2006. Force protection using composite sandwich structures. *Composites Science and Technology,* Volume 66, pp. 2500-2505.

Smith, S. & Teng, J., 2001. Interfacial stresses in plated beams. *Engineering Structures,* Volume 23, pp. 857-871.

Sohel, K. & Liew, J. R., 2014. Behavior of steel–concrete–steel sandwich slabs subject to impact load. *Journal of Constructional Steel Research,* Volume 100, pp. 163-175.

Stevanović, M., Kostić, M., Stecenko, T. & Briški, D., 1987. Impact Behaviour of CFRP Composites of Different Stacking Geometry. *Proceedings of the Second International Conference on Testing, Evaluation and Quality Control of Composites,* pp. 78-83.

Strait, L. H., Karasek, M. & Amateau, M., 1992. Effects of Stacking Sequence on the Impact Resistance of Carbon Fiber Reinforced Thermoplastic Toughened Epoxy Laminates. *Journal of Composite Materials,,* 26(12), pp. 1725-1740.

Sukontasukkul, P., Mindness, S. & Banthia, N., 2002. *Penetration resistance of hybrid fibre reinforced concrete under low-velocity impact loading,* Montreal, Quebec: Canadian Society for Civil Engineering.

Sya, B. L., Fawaz, Z. & Bougherara, H., 2018. Damage evolution in unidirectional and cross-ply flax/epoxy laminates. *Composites Part A,* Volume 112, pp. 452-467.

Tanaka, T., 1996. *Shear resisting mechanism of reinforced concrete beams with CFS as shear reinforcement. Graduation thesis.,* s.l.: Japan: Hokkaido University.

Teng, J., Zhang, J. & Smith, S., 2002. Interfacial stresses in reinforced concrete beams bonded with a soffit plate: a finite element study. *Construction and Building Materials,* Volume 16, pp. 1-14.

Toutanji, H. & Ortiz, G., 2001. The effect of surface preparation on the bond interface between FRP sheets and concrete members. *Composite Structures.*

University of Liverpool, 2009. *Science Daily.* [Online]
Available at: www.sciencedaily.com/releases/2009/01/090122080930.htm
[Accessed 19 February 2021].

van Gemert, D., 1980. Force transfer in epoxy-bonded steel–concrete joints. *International Journal of Adhesion and Adhesives,* Volume 1, pp. 67-72.

Verma, M., Prem, P. R., Rajasankar, J. & Bharatkumar, B., 2016. On low-energy impact response of ultra-high performance concrete (UHPC) panels. *Materials and Design,* Volume 92, pp. 853 - 865.

Vieille, B., Casado, V. & Bouvet, C., 2013. About the impact behavior of woven-ply carbon fiber-reinforcedthermoplastic- and thermosetting-composites: A comparative study. *Composite Structures,* Volume 101, pp. 9-21.

Villanueva, G. R. & Cantwell, W., 2004. The high velocity impact response of composite and FML-reinforced sandwich structures. *Composites Science and Technology,* Volume 64, pp. 35-54.

Wang, R. & Gao, X., 2016. Relationship between Flowability, Entrapped Air Content and Strength of UHPC Mixtures Containing Different Dosage of Steel Fiber. *Applied Sciences,* 216(6).

Wu, H., Hu, F. & Fang, Q., 2019. A comparative study for the impact performance of shaped charge JETon UHPC targets. *Defence Technology,* Volume 15, pp. 506-518.

Yang, h. & Li, J., 2019. Double shear test on bonding mechanical properties of sprayed FRP andconcrete substrate. *Composites Part B,* Volume 162, pp. 388-396.

Yao, Y. et al., 2021. Tensile and Flexural Behavior of Ultra-High Performance Concrete (UHPC) under Impact Loading. *International Journal of Impact Engineering,* Volume 153.

Yu, R., Spiesz, P. & Brouwers, H., 2016. Energy absorption capacity of a sustainable Ultra-High PerformanceFibre Reinforced Concrete (UHPFRC) in quasi-static mode and underhigh velocity projectile impact. *Cement and Concrete Composites,* Volume 68, pp. 109-122.

Zhang, P. et al., 2020. Experimental and numerical investigation of debonding process of the FRP plate-concrete interface. 235(28).

Zheng, X., Huang, P., Chen, G. & Tan, X., 2015. Fatigue behavior of FRP-concrete bond under hygrothermal environment. Volume 95.

Zhou, Y., Xing, F. & Sui, L., 2013. Refinement of an ultimate strain model for circular concrete columns retrofitted with FRP based on a most comprehensive test database. *Applied Mechanics and Materials,* Volume 275, pp. 1233-1238.

APPENDIX A: LOW-VELOCITY IMPACT TESTING DATA

This appendix consists of the data from the quasi-static and low-velocity impact testing, including maximum impact load, residual displacement, change in compliance, front face delamination area, back face delamination area, and failure interface. The specimen ID begins with P if the specimen was manufactured with PETG neat resin and begins with SUR if the specimen was manufactured with EAA. Debonding in the adhesive-concrete interface is denoted as A-C in the failure-interface column, and debonding in the thermoplastic-adhesive interface is denoted as T-A.

Table 14: Data Acquired from Quasi-Static Testing for All Specimens

Specimen ID	Consolidation Pressure (psi)	Residual Displacement (mm)	Change in Compliance (mm/kN)	Change in Compliance (%)
P1-6	100	2.45	1.14	96
P1-7	100	1.88	0.39	91
P1-8	100	2.2	1.25	94
P2-6	100	2.1	1.07	97
P2-8	100	3.17	0.74	95
P3-6	80	2.38	1.31	96
P3-7	80	2.13	0.4	87
P3-8	80	2.04	1	97
P4-6	80	2.43	1.19	97
P4-7	80	2.04	1.36	98
P4-8	80	2.06	0.92	97
SUR1-4	100	0.86	0.4	89
SUR1-5	100	0.68	0.33	87
SUR3-6	80	1.41	0.21	75
SUR3-8	80	1.26	0.19	73
SUR4-6	80	1.1	0.31	91
SUR4-7	80	0.1	0.01	22
SUR4-8	80	2.2	0.95	92
SUR5-7	80	0.13	0.01	26
SUR5-8	80	0.93	0.37	91
SUR7-6	100	0.26	0	0
SUR7-7	100	0.83	0.03	35

Table 14 Continued

SUR7-8	100	0.63	0.08	59
SUR8-4	100	data not acquirable	0.05	62
SUR8-5	100	0.1	0.01	21

Table 15: Data Acquired from Drop-Weight Testing for All Specimens

Specimen ID	Consolidation Pressure (psi)	Maximum Impact Load (kN)	Front Face Delamination Area (mm^2)	Rear Face Delamination Area (mm^2)	Failure Interface
P1-6	100	53.1	7.09E+03	2.11E+04	T-A
P1-7	100	56.8	6.36E+03	2.09E+04	T-A
P1-8	100	54.1	5.03E+03	7.25E+03	A-C
P2-6	100	47.5	5.03E+03	1.54E+04	A-C
P2-8	100	23.8	6.36E+03	1.33E+04	A-C
P3-6	80	47.5	6.36E+03	1.43E+04	T-A
P3-7	80	data not acquirable	7.85E+03	1.13E+04	none
P3-8	80	51.9	5.03E+03	1.54E+04	T-A
P4-6	80	50.6	7.85E+03	2.12E+04	A-C
P4-7	80	55.1	9.50E+03	2.10E+04	A-C
P4-8	80	53.4	6.36E+03	2.09E+04	A-C
SUR1-4	100	50.2	2.83E+03	1.65E+04	none
SUR1-5	100	59.9	7.85E+03	1.33E+04	none
SUR3-6	80	62	6.36E+03	1.65E+04	A-C
SUR3-8	80	37.9	3.85E+03	2.04E+04	T-A
SUR4-6	80	51	5.68E+03	1.65E+04	none
SUR4-7	80	63	7.85E+03	0.00E+00	none
SUR4-8	80	44.5	5.03E+03	1.33E+04	A-C
SUR5-7	80	61	7.07E+02	4.42E+03	none
SUR5-8	80	61.1	5.03E+03	1.13E+04	none
SUR7-6	100	61.3	6.36E+03	1.26E+03	none
SUR7-7	100	48.4	3.85E+03	1.13E+04	none
SUR7-8	100	48.4	5.03E+03	1.33E+04	none
SUR8-4	100	67.7	6.36E+03	0.00E+00	none
SUR8-5	100	68.1	6.36E+03	1.77E+02	none

APPENDIX B: THREE-POINT BENDING DATA

This appendix consists of the data from the three-point bending tests, including peak load, peak displacement, energy dissipated, failure mode, and debonding interface. The specimen ID begins with "P" if the specimen was manufactured with PETG neat resin, and it begins with "SUR" if the specimen was manufactured with EAA. Debonding in the adhesive-concrete interface is denoted as A-C in the failure-interface column, and debonding in the thermoplastic-adhesive interface is denoted as T-A.

Table 16: Three-Point Bending Data for PETG Neat Resin Specimens

Specimen ID	Consolidation Pressure (psi)	Peak Load (N)	Peak Displace-ment (mm)	Energy Dissipated (N-mm)	Bond Strength (MPa)	Failure Mode	Failure Interface
P1-1	100	1631	1.06	982	0.657	concrete shear	A-C
P1-2	100	1881	1.19	1245	0.758	concrete shear	A-C
P1-3	100	2030	1.37	1655	0.818	concrete shear	A-C
P1-4	100	1997	1.24	1516	0.805	concrete shear	A-C
P1-5	100	1917	1.21	1405	0.772	concrete shear	A-C
P2-1	100	1920	1.35	1644	0.691	concrete shear	A-C
P2-2	100	1684	1.04	1093	0.606	concrete shear	A-C
P2-3	100	1802	1.09	1243	0.648	concrete shear	A-C
P2-4	100	1478	1.00	921	0.531	concrete shear	A-C
P2-5	100	1104	0.75	400	0.397	concrete shear	A-C
P3-1	80	1413	0.94	824	0.541	concrete shear	A-C
P3-2	80	1586	0.90	839	0.607	concrete shear	A-C
P3-3	80	1751	0.95	964	0.671	concrete shear	A-C
P3-4	80	1836	1.05	1140	0.703	concrete shear	A-C
P3-5	80	1712	1.19	1333	0.656	concrete shear	A-C

Table 16 Continued

P4-1	80	1205	0.86	688	0.398	concrete shear	A-C
P4-2	80	1145	0.75	407	0.378	concrete shear	A-C
P4-3	80	1500	0.90	906	0.495	concrete shear	A-C
P4-4	80	1645	1.01	1003	0.543	concrete shear	A-C
P4-5	80	1648	0.96	1070	0.544	concrete shear	A-C

Table 17: Three-Point Bending Data for EAA Specimens

Specimen ID	Consolidation Pressure (psi)	Peak Load (N)	Peak Displace-ment (mm)	Energy Dissipated (N-mm)	Bond Strength (MPa)	Failure Mode	Failure Interface
SUR1-1	100	1322	1.12	570	0.621	concrete shear	A-C
SUR1-2	100	2745	3.26	5372	1.290	concrete shear	A-C
SUR1-3	100	1788	2.59	3212	0.840	concrete shear	A-C
SUR1-6	100	1987	1.68	1219	0.933	concrete shear	A-C
SUR1-7	100	1635	2.01	1085	0.768	concrete shear	none
SUR2-2	80	2104	1.72	1739	1.104	concrete shear	A-C
SUR2-3	80	1816	1.53	1163	0.952	concrete shear	A-C
SUR2-4	80	2202	2.08	2464	1.155	concrete shear	A-C
SUR3-1	80	1832	1.41	1587	0.680	concrete shear	A-C
SUR3-2	80	1921	1.52	1839	0.713	concrete shear	A-C
SUR3-3	80	1998	1.59	2000	0.742	concrete shear	A-C
SUR3-4	80	2007	1.36	1171	0.745	concrete shear	A-C
SUR3-5	80	1769	0.755	641	0.657	concrete shear	T-A
SUR4-1	80	1620	1.3	1422	0.601	concrete shear	A-C
SUR4-2	80	1563	1.4	1296	0.580	concrete shear	A-C
SUR4-3	80	1780	1.3	1468	0.661	concrete shear	A-C
SUR4-4	80	1792	1.14	1228	0.665	concrete shear	A-C
SUR4-5	80	1569	1.22	1277	0.583	concrete shear	A-C
SUR5-1	80	1375	0.807	495	0.510	concrete shear	A-C
SUR5-2	80	1684	0.887	762	0.625	laminate debonding	A-C
SUR5-3	80	1177	0.626	329	0.437	concrete shear	T-A
SUR5-4	80	983	1.34	567	0.365	laminate debonding	T-A
SUR5-5	80	987	0.817	311	0.366	laminate debonding	T-A

Table 17 Continued

SUR7-1	100	1856	1.68	1795	0.689	concrete shear	A-C
SUR7-2	100	1854	1.82	2217	0.689	concrete shear	A-C
SUR7-3	100	1834	1.43	1588	0.681	concrete shear	A-C
SUR7-4	100	1963	1.55	2065	0.729	concrete shear	A-C
SUR8-1	100	576	2.55	877	0.756	flexure	T-A
SUR8-2	100	2351	1.64	2229	0.241	concrete shear	T-A
SUR8-3	100	1853	1.21	1259	0.983	concrete shear	T-A
SUR8-6	100	2180	2.59	3817	0.775	concrete shear	T-A
SUR8-7	100	2156	1.36	1594	0.912	concrete shear	T-A
SUR8-8	100	1673	1.53	1040	0.902	concrete shear	T-A

APPENDIX C: SINGLE-LAP SHEAR TESTING DATA

This appendix consists of the data from the single-lap shear tests, including peak load and failure interface. The specimen ID begins with “P” if the specimen was manufactured with PETG neat resin, and it begins with “SUR” if the specimen was manufactured with EAA. Debonding in the adhesive-concrete interface is denoted as A-C in the failure interface column, and debonding in the thermoplastic-adhesive interface is denoted as T-A.

Table 18: Single-Lap Shear Data for All Specimens

Specimen ID	Consolidation Pressure (psi)	Peak Load (N)	Failure Interface
P1_100_1	100	2046	A-C
P1_100_2	100	4123	A-C
P1_100_3	100	4887	A-C
P2_80_1	80	6257	A-C
P2_80_2	80	5220	A-C
P2_80_3	80	9030	A-C
SUR1_100_1	100	10355	A-C
SUR1_100_2	100	11285	T-A
SUR1_100_3	100	10411	T-A
SUR2_100_1	100	7448	T-A
SUR2_100_2	100	8966	T-A
SUR2_100_3	100	7274	T-A
SUR1_80_1	80	6959	T-A
SUR1_80_2	80	8354	T-A
SUR1_80_3	80	1844	T-A
SUR2_80_1	80	12710	T-A
SUR2_80_2	80	8057	T-A

BIOGRAPHY OF THE AUTHOR

Alyssa Libby was born in Portland, Maine and grew up in Buxton, Maine. She developed a passion for building design and structural engineering in her middle school Gifted and Talented math program, where she drew the blueprint for her dream home and constructed it out of cardboard and other craft materials. She attended Bonny Eagle High School, and her love for math and science grew throughout her studies. She then chose to study civil engineering at the University of Maine. During her undergraduate studies, she worked as a structural design engineering intern at Kleinschmidt Associates which solidified her decision to work in the structural design discipline of civil engineering. Alyssa graduated with her Bachelor of Science degree in Civil & Environmental Engineering in May of 2019 with a concentration in structural design. She chose to further her education at the University of Maine by working towards a Master of Science degree in Civil Engineering with a concentration in Structural Engineering and Mechanics. She is a member of the engineering honor society, Tau Beta Pi, and the American Concrete Institute. Throughout her graduate studies, she worked closely with her advisor, Eric Landis, and the U.S. Army Corps of Engineers Engineer Research and Development Center to optimize a hybrid UHPC-thermoplastic system for increased resistance to impact loading. She is a candidate for the Master of Science degree in Civil Engineering from The University of Maine in May 2021.